UiT
THE ARCTIC UNIVERSITY OF NORWAY

Faculty of Science and Technology

Department of Geology

Paleoceanographic development in Leirdjupet, during *the last deglaciation.*

—

Lasse Aase Tønnessen

Master thesis in Marine Geology and Geophysics *[GEO-3900]*
June 2016

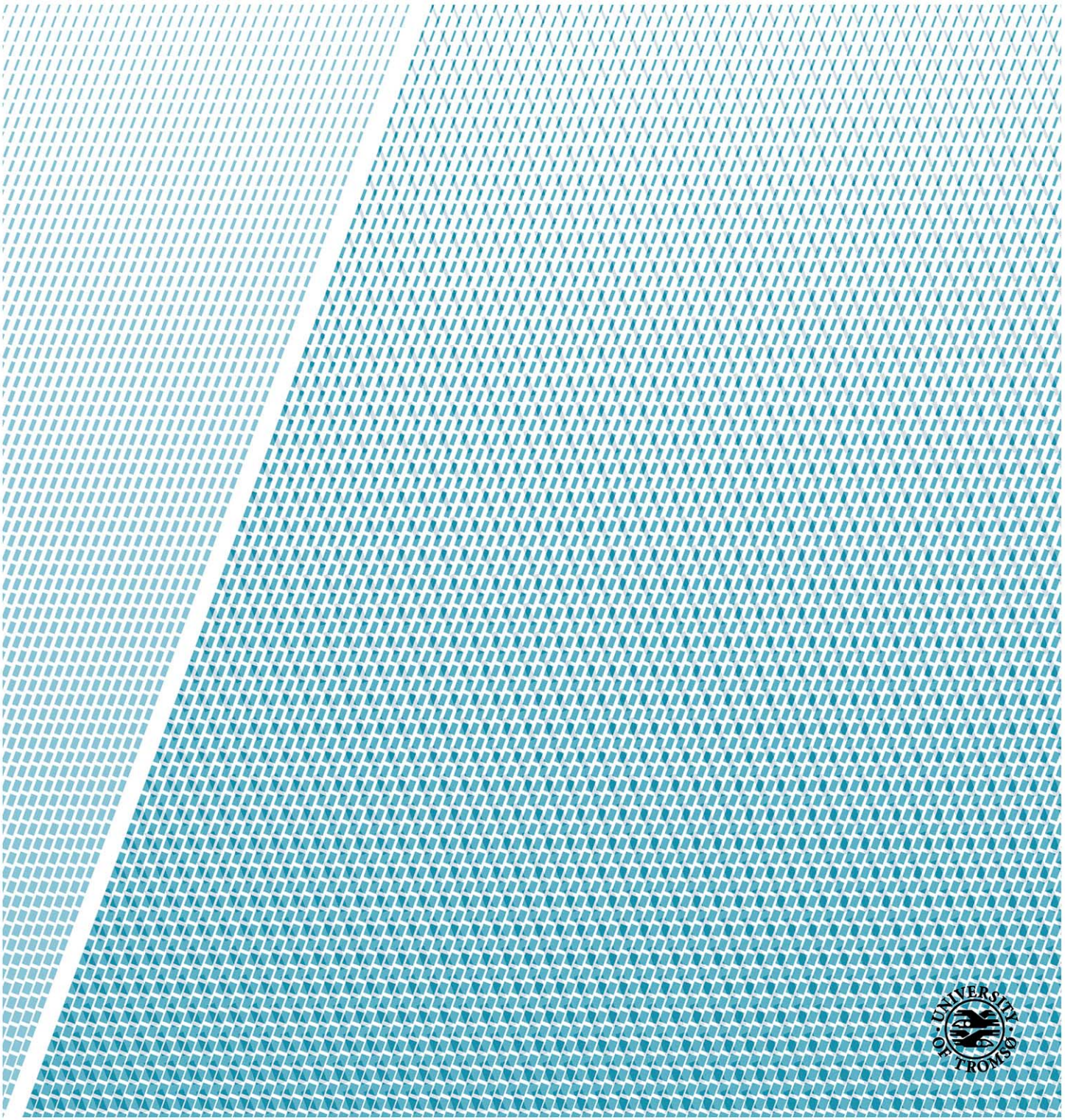

ABSTRACT

The focus of this master thesis is to investigate the paleoenvironmental and paleoceanography during the last deglaciation in Leirdjupet, a small submarine trough in the southwestern Barents Sea. The lower half of the piston corer HH15-1303PC has been investigated for the distribution pattern of benthic foraminifera faunas, ice rafted debris (IRD), lithology and oxygen and carbon isotopes covering; the Bølling, Allerød, the Younger Dryas, the Younger Dryas-Holocene transition and the early Holocene.

ACKNOWLEDGEMENTS

As I am sitting here getting ready to submit, reflecting on the year that has passed and the process I have been through!. From attending the core retrieval on R/V Helmer Hanssen back in August 15, a truly great experience, the subsequent laboratory work before attempting to solve the cores (HH15-1303PC) mysteries that is now this thesis. There is quite a few people I would like to thank, that has helped me along the way.

Firstly, I would like to thank my supervisor Tine L. Rasmussen for all the help, guiding and the unique opportunity she gave me.

I would like to thank Trine Dahl, Ingvild Hald and Karina Monsen for all the help in the laboratory and Erna Osk Arnardottir for the help with the GEOTEK Multi Sensor Core logger. The taxonomic work at the micropaleontology laboratory was especially initially frustrating and confusing at times. However, it was never any problem to ask for some much appreciated identification help, thanks to Teena Chauhan, Kari Skirbekk, Mohamed M Ezat, Ida K Danielsen and Boriss Kovalenko who worked on the Holocene part of Leirdjupet letting me rent his species identification slides and providing me with reading material.

Further, I would like to thank the staff, crew and students of R/V Helmer Hanssen for a memorable cruise the summer of 2015, and Steinar Iversen supplying the chirp.

Lasse Tønnessen

June 2016

CONTENTS

1 INTRODUCTION……..……..1

1.2 Background……...1

1.2.1 The Barents Sea…….1

1.2.2 Barents Sea oceanography…….3

1.2.3 Ice Streams…….7

1.2.4 Glacial history of the Barents Sea region . ……8

2 STUDY AREA……...……...12

3 MATERIAL AND METHODS…….14

3.1 Field work……...14

3.2 Chirp Sonar…….14

3.3 Coring …….15

3.4 CTD…….16

3.5 Laboratory work……..17

3.6 Physical properties …….17

3.7 X-ray photography……..19

3.8 Core description……..19

3.9 Sediment sampling procedure ……20

3.10 IRD……21

3.1

3.11 Foraminiferal analysis……..22

3.12 Foraminifera data……..24

3.13 Radiocarbon dating……...…27

4 BENTHIC FORAMINIFERA……...30

4.1 Ecological preferences for the cores most abundant species……..31

4.1.1 *Cassidulina reniforme*……..31

4.1.2 *Cibicides lobatulus*……...31

4.1.3 *Elphidium excavatum*……..32

4.1.4 *Islandiella norcrossi* …...……32

4.2 Ecological preferences of the secondary species……33

4.2.1 *Cassidulina neoteretis*……..33

4.2.2 *Buccella spp.* ……...34

4.2.3 *Melonis barleeanus*……..35

4.2.4 *Elphidium subarticum*……..35

4.2.5 *Nonionellina labradoricum*……..36

4.2.6 *Stainforthia loeblichi*……..…….36

4.2.7 *Astronion gallowayi*……36

4.2.8 *Islandiella islandica*……..……..36

5 RESULTS……..38

5.1 Radiocarbon dating…….38

5.2 Lithological units……41

5.2.1 Unit 1……41

5.2.2 Unit 2……....42

5.2.3 Unit 3……42

5.2.4 Unit 4……42

5.2.5 Unit 5……43

5.2.6 Unit 6……43

5.2.7 Unit 7……44

5.3 Foraminiferal results……...46

5.4 Biozones …….49

5.4.1 Assemblage zone A……..49

5.4.2 Assemblage zone B……..50

5.4.3 Assemblage zone C……..51

5.4.4 Assemblage zone D……..51

5.4.5 Assemblage zone E……..52

5.4.6 Assemblage zone F……..…52

5.4.7 Assemblage zone G……..53

5.5 Stable isotope analysis……..……...54

5.6 CTD…….57

6 CHRONOLOGY……58

7 INTERPRETATION……..60

7.1 Time prior to the Leirdjupet deglaciation >14,800 cal yr BP…….64

7.2 Bølling interstadial 14,800-14,000 cal yr BP……..……64

7.3 Allerød interstadial 14,000-13,000 cal yr BP…….68

7.4 Younger Dryas 13,000-12,300 cal yr BP……69

7.5 Younger Dryas-Holocene transition 12,300-11,800 cal yr BP…….…….……70

7.6 Early Holocene 11,300-10,200 cal yr BP……...71

8 DISCUSSION ……...73

9 SUMMARY……...82

10 REFRENCES……...83

1 INTRODUCTION

1.1 Objectives

The primary objective of this study is to reconstruct the paleoenviroment and paleoceanography in Leirdjupet trough during the deglaciation towards the transition into early Holocene, based on foraminiferal, sedimentological and stable isotope records. The submarine trough has acted as a natural sediment trap through time, which provide high-resolution records of the past environment.

1.2 Background

1.2.1 The Barents Sea

The Barents Sea is an epicontinental sea covering an estimated area of 1.4 mill km² (Smedsrud et al., 2013), ultimately covering one of the widest continental shelves in the world (Fig. 1.1). Bordered by a continental slope to the Norwegian-Greenland Sea in the west, Novaya Zemlya to the east by a continental slope to the Arctic Ocean in the north, the Kola Peninsula and northern Norway to the south.

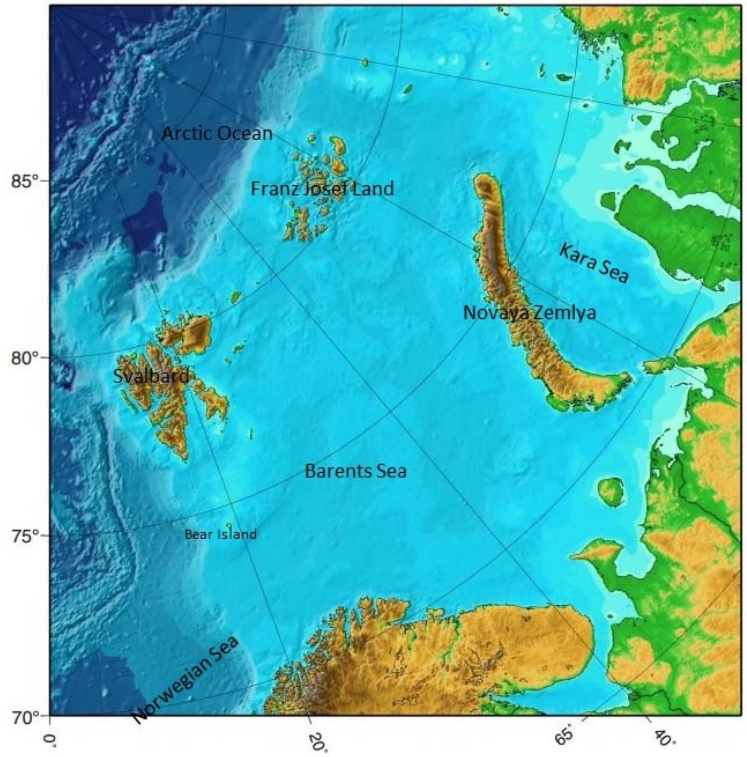

Figure 1.1: IBCAO Bathymetry map of the Barents Sea, and its surrounding seas. Modified from Jakobsson et al. (2012).

The average depth is modest, 230 m (Loeng et al., 1991). Late Cenozoic glacial erosion and deposition has strongly influenced and modified the present topography of the Barents Sea and has remained intact perseveration vice since the following last deglaciation. The bathymetry of the ocean floor is relatively uneven

characterized by a number of shallow banks and plateaus separated by smaller and larger scale deeper transverse submarine-troughs. The larger submarine-troughs in the SW Barents Sea opens to the Arctic Basin and the Norwegian Sea, and are the result of several glacial erosion episodes in Barents Sea (e.g. Elverhøi et al., 1998; Wilson et al., 2011). Prime examples of the overdeepened large scale submarine-troughs on the western margin are the two prominent Bjørnøyrenna and Storfjordrenna, both extending out to the southwestern Barents Sea continental break. Contrasting the deep troughs are the shallower banks, typically at water depths <100m north of Bjørnøyrenna, but somewhat deeper 200-300 m water depths south of Bjørnøyrenna. Characteristic for the banks are the superimposed large and small morainic ridges diagnostic of slow ice retreat (e.g. Elverhøi and Solheim, 1983; Ottesen and Dowdeswell, 2009; Bjarnadottir et al., 2013).

The Barents Sea is an area of intense heat exchange between ocean and atmosphere, mainly facilitated by warm northward flowing Atlantic Water, that maintains the Barents Sea marine climate though latent heat release during sea ice formation, as first suggested by Helland-Hansen and Nansen [1909] (e.g. Risebrobakken et al., 2010; Smedsrud et al., 2013). The atmospheric circulation also contribute to Barents Sea Climates, to what extent is still an ongoing debate (Smedsrud et al., 2013).

1.2.2 Barents Sea oceanography

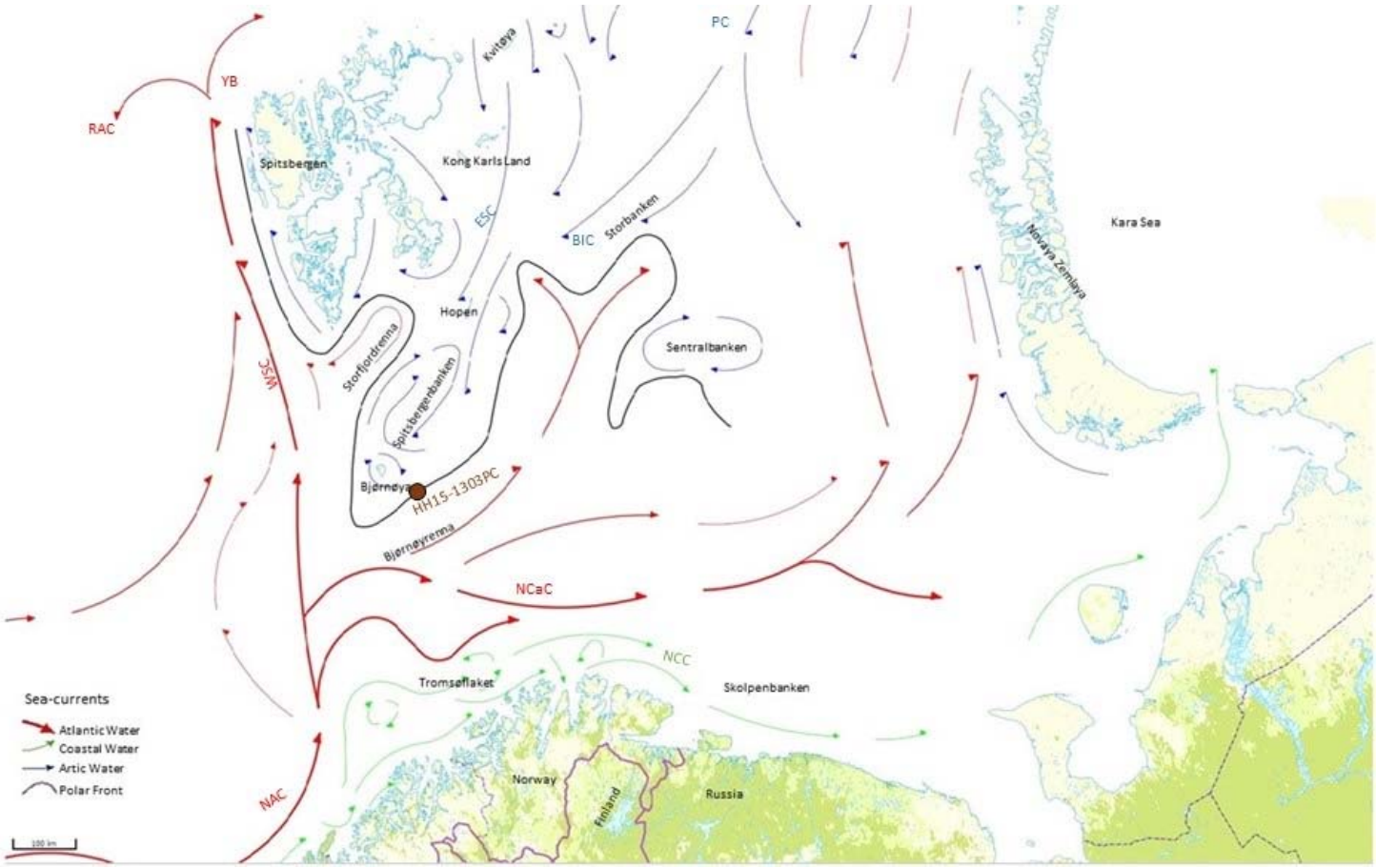

Figure 1.2: The main currents in the Barents Sea. NAC- Norwegian Atlantic Current; NCaC- North Cape Current; NCC- Norwegian Coastal Current; WSC- West Spitsbergen Current; RAC- Returning Atlantic Current; YB- Yermak Branch; ESC- East Spitsbergen Current; BIC- Bear Island Current. Map modified from www.mareano.no

The bathymetry of the Barents Sea significantly influence and complicates the current circulation pattern within the Barents Sea, bathymetric reliefs guide waters while the shallower bank areas may pose as obstacles, generating eddies (Pfirman et al., 1994). There are presently considered three main and six less significant water masses in the Barents Sea defined by their specific water properties (Table 1.1). The North Atlantic Water as a major component in controlling the climate, due to its high heat release, nutrient and salinity supplier was first defined by Helland-Hansen and Nansen back in [1909]. The warm and

saline Atlantic Water is carried as a jet northwards through the Norwegian sea by the Norwegian Atlantic Current (NwAC). The warm saline Norwegian Atlantic Current splits into two major branches ~72°, a branch that flows eastward into the southern Barents Sea as the "North Cape Current" (NCaC) through the southern Barents Sea opening (BSO)/Bjørnøyrenna, which is the main Atlantic Water inflow into the Barents Sea (Loeng, 1991; Ingvaldsen et al., 2004). The North Cape Current further bifurcates into two branches inside Bjørnøyrenna, one flowing northwards towards the southern flank Hopen Trench, where some water will recirculate and eventually leave the Barents Sea (Ingvaldsen, 2005). The other North Cape branch continues eastward into the central basin (Ingvaldsen, 2005). While the other Norwegian Atlantic Current branch the West Spitsbergen Current (WSC), continues northwards along the western Barents Sea slope-western Svalbard margin (Aagaard et al., 1987). A smaller portion of the West Spitsbergen Current branches off into Storfjorden (Maslowski et al., 2004). The West Spitsbergen Current further splits, with one branch flowing west eventually southward, while the other flows eastwards into the Arctic Ocean as a subsurface current. Some of the Atlantic Water than reenters the Barents Sea as a diluted subsurface flow between Kvitøya and Victoria Island and the Franz Victoria trough (Parsons et al., 1996).The Atlantic will also mix with Polar Water from the Arctic Ocean forming the cold fresh Arctic Water mass (Hald et al., 2007). The Arctic Water enters the Barents Sea between Spitsbergen and Franz Josef Land as the East Spitsbergen Current (ESC), and between Franz Josef Land Novaya Zemlya as Persey Current (Loeng, 1991). The surface, near surface East Spitsbergen Current flows southward along the coast of Spitsbergen (Loeng, 1991). The Arctic Water mass is typically seasonally covered by sea ice. A sharp water mass boundary "oceanic front" called the Barents Sea Polar Front, forms where the deeper warm saline Atlantic Water encounters the shallower colder, low saline Arctic Water (Pfirman 1994; Gawarkiewicz and Plueddemann, 1995). The warm dense Atlantic Water converges and

descends under the Artic Water, subsequently flowing as an intermediate current below the Artic Water, some will mix with the Arctic Water to form the Polar Front Water (Vogt and Knies, 2009). The Barents Sea Artic Front function as an important high biological productivity region ("carbonate factory") during the spring-summer months due to highly concentrated nutrient levels within melting sea ice, encouraging high primary production as the sea ice retreats along the ice edge (Wright, 1974; Berben et al., 2014). The sea ice edge (MIZ) tend to move in accordance to the front (Ådlandsvik and Loeng 1991). Leirdjupet is presently situated close to-beneath the Barents Sea Arctic Front, which follows the Spitsbergenbanken margin, possibly indicating that the front is topographically trapped (Henrich, 1997; Harris et al., 1998).

The third main water mass in the Barents Sea is the Norwegian Coastal Current that carries water of relatively low salinity and high temperature, flowing into the Barents Sea along the Norwegian Coast and further eastward along Russian coast (Loeng, 1991).

Dense Bottom Water Masses are formed various places by several different processes, Helland-Hansen and Nansen already theorized this back in [1909] (Loeng, 1991) (Fig 1.3). This dense corrosive cold highly saline CO^2 and oxygen-enriched water mass, forms as Atlantic Water cools, subsequently leading to brine rejection during sea ice formation (Pfirman 1994). This bottom water formation particularly occurs on the shelf of Novaya Zemlya, Sentralbanken and along the Barents Sea Arctic Front (Midttun, 1989). Most of the dense water descends down into depressions and troughs, whereby much will leave the Barents Sea along the sea floor through in the strait between Novaya Zemlya and Franz Josef Land into the Arctic Ocean, consequently ventilating the Arctic Ocean (Smedsrud et al., 2013). One such trough is presently Leirdjupet that episodically drains cascading dense brine water formed over the shallow Spitsbergenbanken, which is highly related to the proximity to

the sea ice margin and Barents Sea Arctic Front (Henrich, 1997). The production of this dense water masses vary from year to year (Loeng, 1997)

Water masses		Water mass charateristics	
		T, °C	S, PSU
Atlantic Water	NAW	>3.0	>35.0
Artic Water	AW	<0.0	34.3-34.8
Coastal Water	CW	>2.0	<34.7
Locally formed water masses			
Barents Sea Water	BSW	-1.5-2.0	34.7-35.0
Bottom Water	BW	<-1.5	>35
Polar Front Water	PW	-0.5-2.0	34.8-35.0
Spitsbergenbanken Water	SBW	1.0-3.0	<34.4
Melt Water	MW	>0.0	<34.2

Table 1.1: Characteristics of the water masses in the Barents Sea after Loeng. (1991).

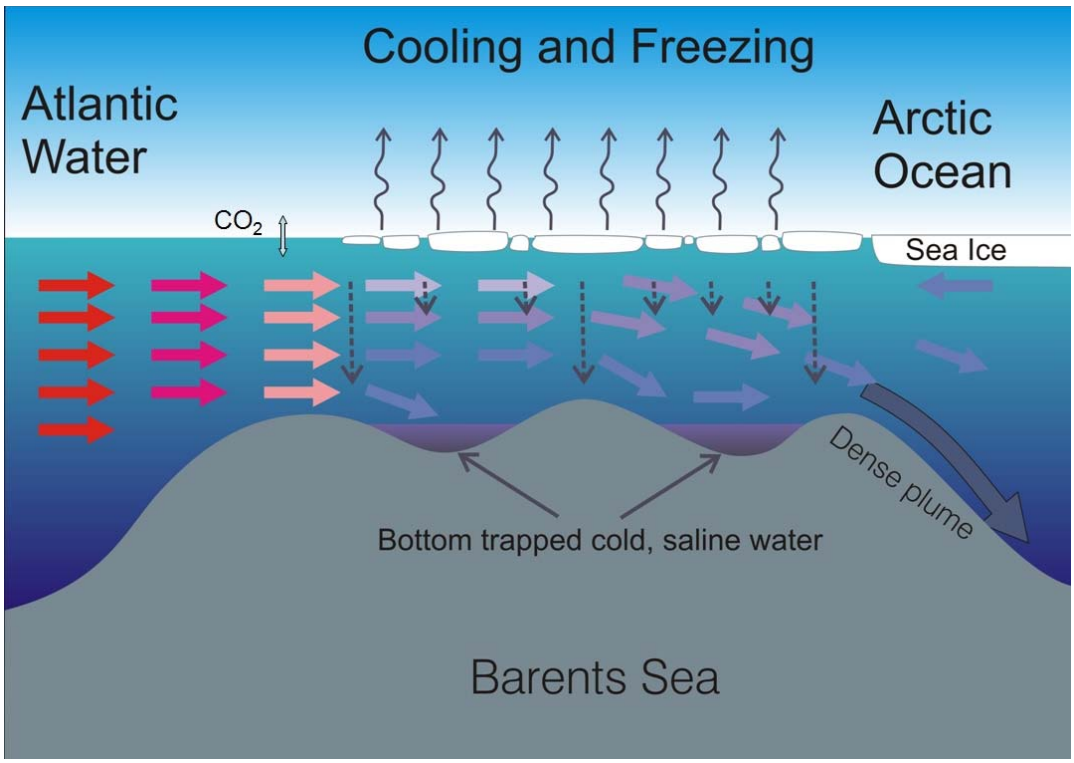

Figure1.3: Illustrates the Barents Sea water mass modification, as water warm Atlantic Water flows over the shallow Barents Sea, during the sea ice formation the water mass loses heat and brine rejection, increase the density of the water masses. The modified cold, saline water than continues towards the Arctic Ocean. Figure from Geophysical Institute of the University of Bergen.

1.2.3 Ice Streams

Ice streams are narrow dynamic fast flowing ice masses, that can drain large portions (up to over 90%) of the ice within the larger slower moving ice sheet domes (Bennett, 2003). Ice streams are consequently critical for the stability, mass balance and dynamics of the ice sheets as they dominate the ice mass transfer and ice mass loss within them (Bennet, 2003). The rate of erosion in the ice streams are believed to be controlled by the glaciation duration and the velocity of the ice stream, in addition to for the Barents Sea in particular the geology concerning the weak sedimentary bedrock and its structural trends, size of drainage area and basal thermal regime (Laberg et al., 2012; Batchelor and Dowdeswell, 2014). Ice streams transport basal deforming sediments along the direction of the ice flow towards their margins called grounding line (Vorren and Laberg 1997). The ice sheets grounding line is defined as the point the in which the ice starts to float forming an ice shelf i.e. the point of no basal contact, where calving is predominant (Patton et al., 2015). Changes in the grounding line affects the stability of the ice streams, and can consequently escalate in rapid changes in order for the ice streams to adapt as the grounding line retreats to shallower waters or thicker ice (Bjarnadottir, 2012; Patton et al., 2015). Their dynamic behavior of the ice streams are complex, some of the controlling factors probably include e.g. oceanic temperatures, sea level changes, air temperatures, oceanic tides and subglacial bathymetry.

1.2.4 Glacial history of the Barents Sea

During the Pleistocene as much as 1000-1200 m of sedimentary rock was eroded in the troughs on the south western Barents Sea shelf, 500-650 m in the shallower bank areas (Laberg et al., 2012). A pronounced seismic reflector "The Upper Regional Unconformity" (URU) on the continental shelf constitute an erosional boundary between the pre-glacial lithified seaward dipping sedimentary bedrock from the overlaying unlithified glacial deposits (Vorren et al., 1986). Representing the shift from an erosional regime to depositional regime (e.g. Larsen et al., 2003). The varying morphology of the URU suggest that some areas have experienced larger glacial erosion compared to others. The superimposed glacigenic sediment cover are unevenly distributed even over short areas, depending on the location in relation to ice streams, but it's generally thin <100 m (Larsen et al., 2003; Rüther et al., 2011).

The first signs of a Pleistocene glacial expansion beyond the coastline in the Barents Sea first occurs ~2.7 Ma (Knies et al., 2009). During the following time "transitional growth phase" 2.4-.1.0 Ma, the ice sheets grew, starting their expansions, developing from a land-based ice mass towards a fully developed ice sheets (Knies et al., 2009). The first of a minimum of eight major Barents Sea Ice Sheet advances reaching the western continental shelf break occurred ~1.5 Ma (Andreassen et al., 2004; Andreassen et al., 2007). According to isostatic modelling by Butt et al. (2002) the Barents Sea Ice Sheet underwent a transformation ~1 Ma, from a mainly subaerial (totally subaerial from 2.3 Ma) towards a marine based ice sheet as significant parts now became submarine, further marking the time of large scale glacial intensification. Marine based ice sheets meaning ice sheets grounded below sea level, vulnerable to destabilization, resulting from e.g. climate change, sea level change, subsurface warming (e.g. Siegert and Dowdeswell, 2004; Hormes et al., 2013). During the last 0.7 Ma the glacial erosion have mainly occurred beneath large fast flowing ice streams that occupied the bathymetric troughs (e.g. Laberg et al., 2012). Their topographically confinement

influence gradually increased through time as the erosional carving within the trough progressed, implying an adjustment from a wide scale towards a focused erosional domain (Laberg et al., 2010). The ice streams, transported large amounts of sediments along the direction of the ice flow towards their margins, which for the larger ice streams is the western and northern Barents Sea shelf breaks (Vorren and Laberg 1997). Where the sediment accumulations forms series large fan shaped sediment accumulations called trough mouth fans (Vorren and Laberg, 1997). The largest on the north western margin the Bjørnøya Trough Mouth Fan cover an area of 215 000 km^2, holding a volume of 650 560 km^2 reflecting the exceptional sediment discharge resulting from erosion in the south western Barents Sea from Bjørnøyrenna and its corresponding drainage area (Vorren and Laberg, 1997).

The ice sheet extent during the Late Weichselian has been much debated over the decades. The Svalbard-Barents Sea Ice Sheet probably started to grow ~32 ka years ago reaching the outermost barriers the shelf beaks i.e. full Barents Sea continental shelf glaciation western ~24-23 ka years ago, where it remained to ~20 years ago a time referred to as the Last Glacial Maximum (LGM) (Jessen et al., 2010; Patton et al., 2015). A time which the Barents Sea Ice Sheet (BSIS) were confluent with the Fennoscandian Ice Sheet (FIS), an ice sheet covering the terrestrial and marine parts of Scandinavia (Winsborrow et al., 2010). Whereby the cross shelf trough Bjørnøyrenna functioned as the main drainage

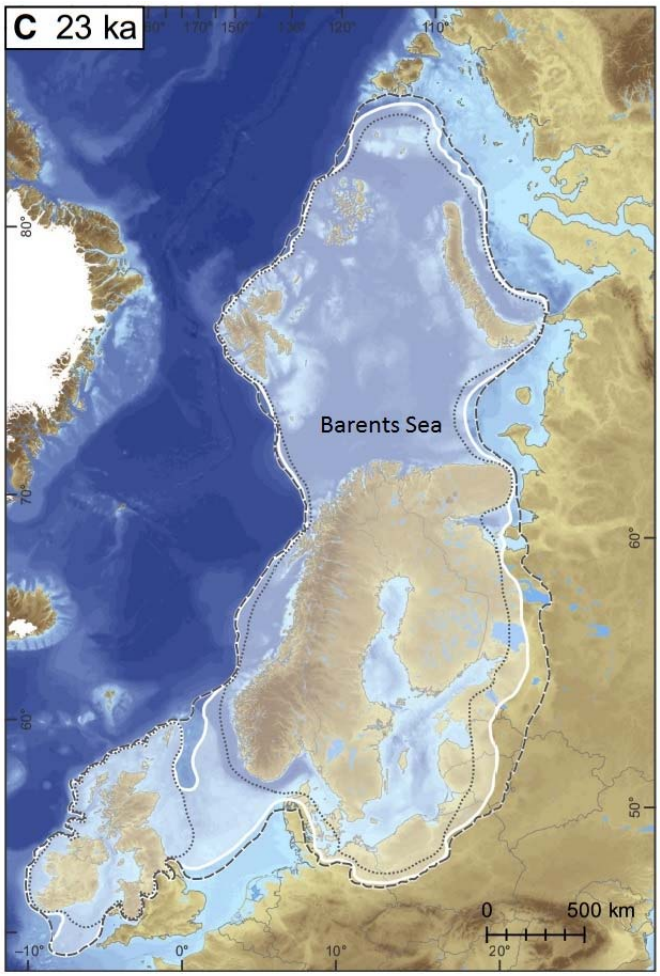

Figure 1.4: Figure showing the Eurasian ice extent 23ka years ago. Figure modified from Hughes et al. (2016).

pathway, it was consequently important for the overall mass balance of the ice sheet, with two main southerly branches Ingøydjupet while the other operated at the present day Nordkappbanken (Winsborrow et al., 2010). Likewise, it was also fundamental for a rapid disintegration of ice in the central Barents Sea during retreat stages (Larsen et al., 2003).

Rising eustatic sea level is usually cited as the main initial deglaciation trigger (e.g. Elverhøi et al., 1993; Winsborrow et al., 2010), however its complicated to certify due to the complex interplay between eustatic isostatic effects on sea level (Winsborrow et al., 2010). Rising sea level would have destabilizing effects, increased water depth causes enhanced calving on the assumption it were grounded at the seafloor (Siegert and Dowdeswell, 2002). A sea level rise, would further cause a reduction in the ice sheet effective weight resulting in a reduced basal drag which would enable a faster more rapid transfer of mass from the interior e.g. Spitsbergenbanken for Leirdjupet (Siegert and Dowdeswell, 2002). Hormes et al. (2013) was not convinced that a sea level rise was one of the initial initiation BSIS disintegration triggers, considering no sea level rise correspond to Jessen et al. (2010) 20,5 ka cal yr BP onset age. The age discrepancy between the Storfjorden and Bjørnøya system are somewhat contradictory, concerning a sea level change that would initiate higher calving fluxes within the same time frame (Bjarnadottir et al., 2012). A meltwater pulse (a short lived global acceleration in sea level) is recognized ~19 ka the MWP-19 ka (mwp-1a0), such a rise would cause marine based ice masses in the Antarctic to collapse injecting meltwater into the thermohaline system thereby strengthening the Atlantic Water circulation consequently accelerating the climate warming in the North Atlantic region leading up to the Bølling interstadial (Weaver et al., 2003; Lucchi et al., 2015). Hormes et al. (2013) rather suggested a combination of increasing solar insolation during summer season and a generally drier warmer climate inflicted by a change in atmosphere circulation as the initial triggers pre Bølling in Barents Sea. Hormes et al. (2013) viewed the sea level rise and ~10% increased

solar radiation as important attributing factors on a later stage during the deglaciation correspondent to Bølling interstadial. The eustatic sea level rise was caused by a more dramatic and prominent meltwater pulse called mwp-1A (~14,6-14,3 ka cal yr BP) that raised sea level by ~20 m in less than 500 years, causing an escalating destabilization of the BSIS (e.g. Fairbanks, 1989; Aagaard-Sørensen et al., 2010; Deschamps et al., 2012). Climate warming induces melting consequently thinning of the streams inflicting acceleration and subglacial melting (Zwally et al., 2002; Lucchi et al., 2013). Additionally has warm subsurface Atlantic Water beneath cold fresh polar surface water been proposed to inflict basal glacial melting, causing increasing melting and calving rates (e.g. Flückiger et al., 2006; Rasmussen et al., 2007; Rüther et al., 2012; Hormes et al., 2013). The time span between LGM and Bølling is known as the Heinrich Stadial 1 (HS1) (Bond et al., 1993; Rasmussen et al., 2007).

2 STUDY AREA

The study area affiliated with the core is located in the southwestern Barents Sea, south east of Bjørnøya (fig. 2.1). The core HH15-1303PC was retrieved from 340.5 m water depth at the coordinates Longitude 21 05'N; Latitude 74 08'E, presently centered beneath the Barents Sea Arctic Front (Elverhøi and Kristoffersen, 1977a; Henrich, 1997)

Figure 2.1: IBCAO Bathymetry map of Barents Sea, with highlighted study area. Modified from Jakobsson et al. (2012).

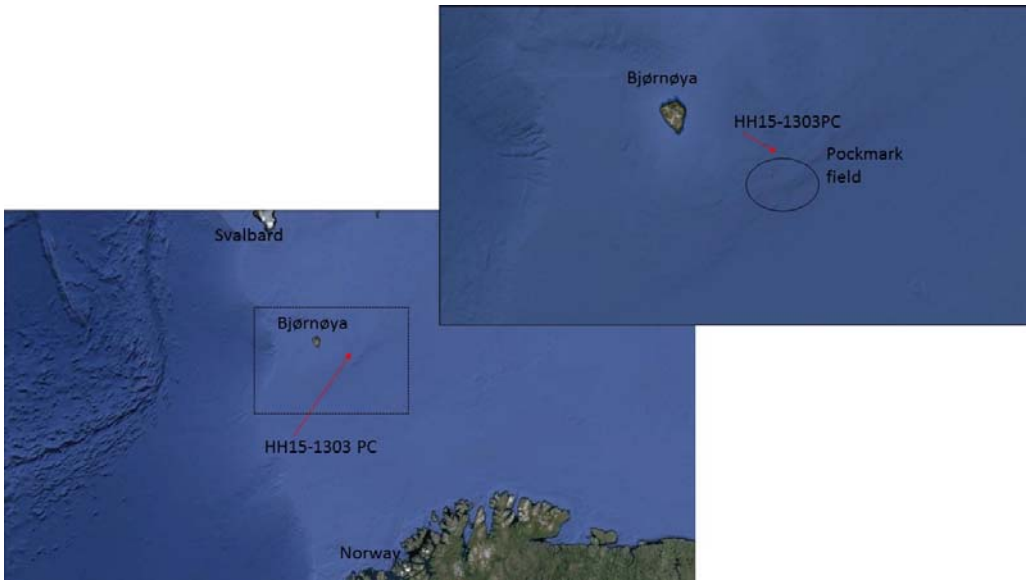

Figure 2.2: Satellite images of the study area. Modified from Google Earth.

Leirdjupet is a 40 km long and 16 km wide southward oriented submarine trough on the northern end of the Leirdjupet fault complex (Elverhøi and Kristoffersen, 1977b; Faleide et al., 1993). An asymmetric 150 m thick, 12-15 km long east-west striking ridge with steepest

slope facing southwards at 300-350 m water depth, separates Leirdjupet trough from the 220 m deeper Bjørnøyrenna (Fig. 2.3) (Elverhøi and Kristoffersen, 1977b; Elverhøi and Solheim, 1983). A smaller transverse ridge is situated in a more central position in the Leirdjupet trough at 150-200 m water depth (Fig. 2.3) (Elverhøi and Kristoffersen, 1977b). The bathymetry of the trough are irregular/hummocky (Elverhøi and Kristoffersen, 1977a). Leirdjupet trough is separated from Fingerdjupet trough by a thin parallel ridge narrowing in the dipping direction.

Leirdjupet trough presently acts as a sediment trap basin, supplied by winnowed sediments from the adjacent elevated areas that includes Spitsbergenbanken that are subjected to reworking by oceanic currents (Elverhøi and Kristoffersen, 1977a; Henrich, 1997). Corrosive waters originating from sea-ice brine rejection are known to episodically cascade down Leirdjupet (Henrich, 1997).

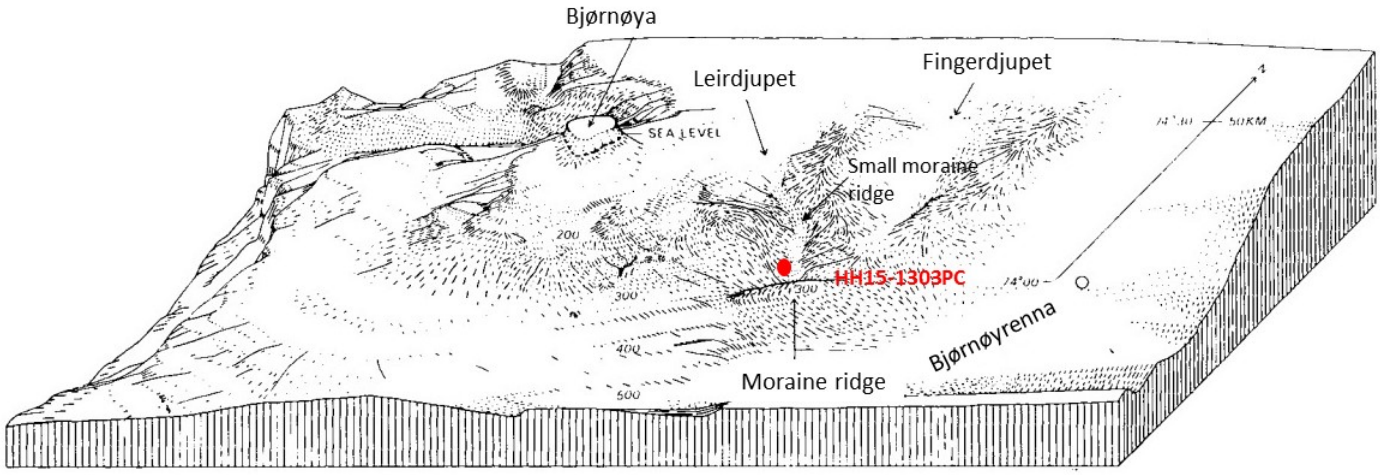

Figure 2.3: Figure illustrating the seafloor morphology in the study area with the coring position. Figure modified from Elverhøi and Kristoffersen (1977a).

3 MATERIAL AND METHODS

3.1 Field work

The basis of the master project work is the marine core HH15-1303PC a piston corer collected during the scientific and educational AMGG research school cruise, focusing on greenhouses gases in the ocean (Table . 3.1). The core was retrieved from Leirdjupet SW Barents Sea, SE of Bjørnøya, on the research vessel RV Helmer Hansen July-August 2015. This work particularly concerns the core sections 4-6, and to some extent 7-8. The three uppermost sections 1-3, was not examined during this work, as the interval correlate to the Holocene, an epoch that will not be given much attention in this master thesis. Leirdjupets paleoceanographic development during the Holocene was covered by Boriss Kovalenko (2015) during his MSc dissertation, this master thesis can be regarded as a continuation of his dissertation.

Core:	Position	Water depth (m)	Core length	Collecting date:
HH15-1303PC	74°08,28'N 21°06,0'E	340.52 m	765.5 cm	01.08.2015

Table 3.1: position, water depth, core length and recovery date of the studied core HH15-1303PC.

3.2 Chirp sonar

Deeper penetrating echosounder "Chirp" profiles was recorded/collected at the location and area in association with the coring on 1 August 2015, using the vessels installed chirp EdgeTech 3300-HM hull mounted sub-bottom profiler 4*4 arrays (Fig. 3.1). To gain deeper vertical penetration of the sub-surface seafloor, the Edge Tech chirp ran on lower frequencies 1.5-8 kHz to locate suitable sampling positions for retrieving deglacial sediments, penetrating >10 m in unconsolidated soft sediments.

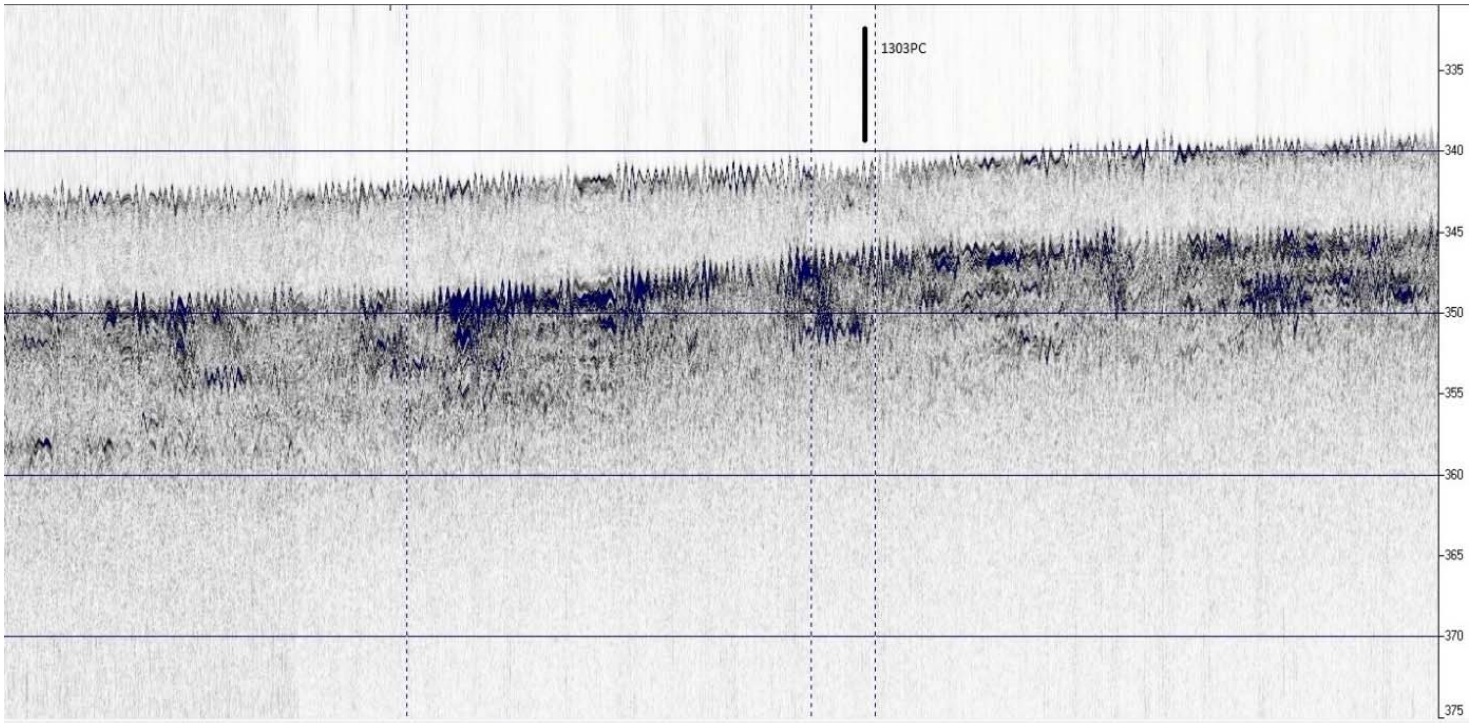

Figure 3.2: Chirp from coring position inside Leirdjupet, the transparent upper layer is Holocene sediments, overlaying deglacial sediments. Showing the HH15-1303PC coring position. Depth (m) on the right scale. ..

3.3 CORING

The piston corer installed at Helmer Hanssen consist of a 12 m long x 110 mm diameter steel barrel with a 1.5 ton weight at the top. Two 6 m long x 100 mm diameter plastic liners were rigged into the piston corers steel barrel. Eventually the gear is fitted with a conical shaped core cutter that enables deeper penetration and a conical shaped core catcher that closes the system keeping the sediments trapped in situ in the device. The piston corer penetrates into the sediments on the seafloor by the force of gravity in addition to a piston system. Once the core was on deck, the plastic liner was divided into eight ~1 m long sections, properly capped at the respective ends and labelled with core-, section number, length and person of reference. Some water rich intervals caused some initial problems during the cutting and labelling procedure, possibly due to suction or disturbance upon impact with firm stiff lowermost sediments. Suction may occur from unsteady coring penetration, improper placement, wire

vibration or elastic rebound upon the corer weight release (Buckley et al., 1994; Lunne and Long, 2006). Plastic liners occasionally implode when high suction pressure develops beneath the piston corer, and can consequently cause implosion in mid core regions (Lunne and Long, 2006). The section was subsequently brought to the vessels lab for measurements of magnetic susceptibility (Loop sensor), for a quick interpretation regarding the lithostratigraphy as a part of the scientific cruise teaching purposes. After the recordings the sections was stored in a cooling room holding a temperature close to 4°C awaiting further work.

Picture 3.1: Picture from the retrieval of the HH15-1303PC.

3.4 Conductivity, temperature and depth (CTD) rigged with water sampler

The CTD (HH15-1304CTD) (Fig.5.12) recordings was collected close to the core site, shortly after the piston corer retrieval at the coordinates ~74°08,25N 21°06,14E by the CTD instrument type Seabird 911 Plus rigged with water samplers. The CTD was lowered/retrieved at a specified speed (c. 1m/s) through the water column continuously obtaining data on various oceanographic parameters; depth, temperature and conductivity. Based on these direct measurements in addition to pressure the instrument calculate the salinity. The collected data thus provide the oceanographic conditions through the water column, data that further will used to calibrate the acoustic equipment.

3.5 Laboratory work

The laboratory work was conducted at the Department of Geology, University of Tromsø (UiT) laboratory between August 2015 until March 2016. 61 foraminifera samples throughout the core was analyzed for stable isotopes at the Department of Earth Science and Bjerknes Centre for Climate Research at the University of Bergen, Norway Accelerator Mass Spectrometry (AMS) measurements were employed on selected shell fragment samples in addition to one foraminifera sample at the 14 CHRONO Centre, Queen's University Belfast in the Northern Ireland radiocarbon laboratory**.**

3.6 Physical properties

Physical properties of the core sections were measured every consecutive centimeter using the GEOTEK Multi Sensor Core Logger (MSCL) (Fig. 3.2) instrument installed at the Department of Geology, University of Tromsø laboratory September 2015. The sections were stored in room temperature in the lab through the night in advance, in order for the sections to adapt a core temperature closer to room temperature, for more accurate recordings particularly concerning P-wave velocity (Weber et al., 1997)**.** The GEOTEK Multi Sensor Core Logger (MSCL) measured data on the following parameters: wet bulk density, P-wave velocity, the magnetic susceptibility, core length, core width and current temperature of the 8 sections. By the obtained data, it was further possible to calculate the porosity and acoustic impedance. Knowing the wet bulk density and porosity, it was possible to calculate the dry bulk density by the following equation:

Dry bulk density = Wet bulk density – ((1.026)(Porosity/100))*

Magnetic susceptibility (MS): MS is the measurement of the magnetization of the sediments. Where continental derived ferromagnetic minerals like magnetite produce a peaking MS signal, while e.g. biological carbonate dilute the signal (e.g. Jessen et al., 2010). The

fluctuating MS responses depend on the sediment minerology, concentration and the grain size distribution. The coarser fraction e.g. sand and gravel would commonly contain minerals with higher MS than the minerals composing clay (e.g. Pau et al., 2014). The grain size of oceanic sediments are controlled by e.g. the current regime and glacial activity (Robinson, 1986; Jessen et al., 2010). Thus, MS respond to environmental conditions giving rise to characteristics patterns, further enabling it as a regional-local correlation tool (e.g. Jessen et al., 2010) and during logging processes concerning stratigraphic changes. MS recordings was also performed on the respective scientific cruise, performed on 3cm spacing intervals manually by a Bartington MS2C Core Logger soon after core retrieval. The obtained data will not be considered for this work. Wet bulk density (gamma density) is the wet weight per unit of volume, describing the degree of compaction of the substance, dry bulk density is the dry weight per unit of volume the degree of compaction excluding the moisture saturation. P-wave velocity is a function of sedimentological and geotechnical properties.

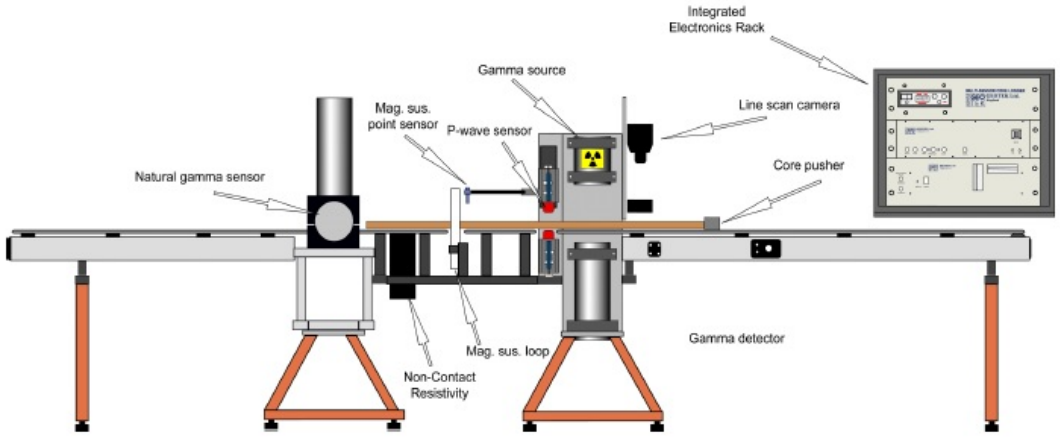

Figure 3.2: Schematic illustration of the Multi Sensor Core Logger system (MSGL).Figure from www.GEOTEK.no.uk.

3.7 X-ray photography

Whole sections were scanned by GEOTEK X-ray imaging system instrument (MSCL-XCT) (Fig. 3.3) at Department of Geology, University of Tromsø laboratory September 2015, providing digital x-ray images of the sectioned core. The Quick View software by Geotek allow you to adjust the image shadow after density preferences. Light objects having high densities while dark objects are of a lower densities. X-ray photography is a very useful tool for identifying features within the core e.g. structures, bioturbation, shell (fragments), IRDs, gaps, texture, mineral composition etc.

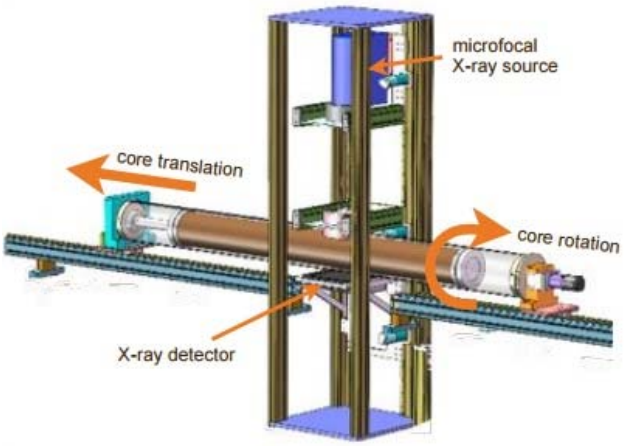

Figure 3.3: Schematic illustration of the X-ray Core Imaging with CT. Figure from www.GEOTEK.no.uk.

3.8 Core description

The core sections plastic tubes was subsequently opened September-October 2015, divided into two halves by the aid of a circular saw and a steal string. One “archive” half that was labelled, properly wrapped and sealed in plastic, eventually stored in the cooler at 4 °C, the other half “work” was to be processed as the fundament of this dissertation. The sediment surface of the single sections was in turn carefully scraped clean in order to reveal any structures before a photoshoot session by a regular camera. The archive half sections was on a later stage (April 2016) scanned by an Avaatech XRF core scanner for high resolution pictures, at the University of Tromsø. Following the scraping treatment, core sections was

visually logged and described. Coloration codes was applied according to the well established Munsell's soil color chart Munsell [1973]. The constructed log is established on visual inspection supplemented by the X-ray photography, pictures and obtained grain size data.

3.9 Sediment sampling procedure

The sampling spacing intervals remained approximately every 1cm throughout the selected sections (sections 3- 8). 1 cm thick slices were cut with a spatula, inserted into a labelled folded plastic zip bag, eventually taking a measure of the weight on a two decimal certified scale (Sartorius AG ED2202S-CW). The collected samples from the sections 3-7 was stored in the freezer, awaiting to be dried in the freeze drier. All the respective samples from section 8 was rather put directly into the oven for a couple of days of drying at ~40°C as they allegedly appeared to be of till origin. Which in terms of a foraminifera study perspective is anticipated to be of limited interest. The freeze drier used was the newly arrived and installed CHRIST ALPHA 1-4 LSC plus. It will vaporize the water from ice to water vapor without any melting in between, processes known to be less destructive on the fragile microfossils.

After processed by the freeze drier/oven, the samples were in turn weighted again in order to obtain the % water content. Samples for further inspection were selected from a 5 cm spacing interval (foraminifera, IRD and grain size distribution) and subsequently wet sieved, in the process the weight of the plastic zip bag containing the selected samples was measured on the scale in order to calculate a more precise dry weights and wet weight of the samples. The wet sieving was performed on the specified stacked mesh sizes; 63-100 μm, 100-500 μm, 0.5-1 mm and >1 mm. As the samples appeared to be sufficiently clean, the residues were flushed by distilled water into the associated labelled special filter paper. The sorted samples were subsequently inserted into the oven holding 40°C for a minimum of 48 hours. The sieves were carefully cleaned in-between each sieved sample, the two finest sieve fractions were additionally washed in a Branson 5510 ultrasonic cleaner. After the initial >48 hours had

passed, the sorted size fraction samples was weighted once more on a 4 decimal certified scale (Mettler AE160 and a Seartorious CP64), subsequently carefully guided into small labelled dram storage glasses. Based on the weight of the relative grain sizes, the grains size distribution was calculated expressed as percentages. The relative percentage of the two finest fractions was further combined, similarly with the two coarsest fractions to calculate their respective flux according to the following formula:

*Flux specified fraction (weight%/cm^2*1000 yr) = Specified fraction x sedimentation rate pr. 1000 years.*

Sedimentation rate pr. 1000 years are commonly referred to Mass accumulation rate (MAR) (g cm-2 ka-1). Which is the linear sedimentation rate pr. 1000 years for specific interval x dry bulk density. 1000 years are referred to as "ka".

The grain sizes will according to the context be referred to by its classification name after the Udden-Wentworth scale classification scheme (1922) (Table 3.2). The fraction finer than 63 µm are referred to as mud.

Grain size fraction	Diameter
Clay	<0.004 mm
Silt	0.004-0.0625 mm
Very fine sand	0.0625-0.125 mm
Fine sand	0.125-0.25 mm
Medium sand	0.25-0.50 mm
Coarse sand	0.50-1.00 mm
Very coarse sand	1.00-2.00 mm
Pebble	2.00-64.00 mm
Cobble	64.00-256 mm
Boulder	>256 mm

Table 3.2: The Udden-Wentworth grain size classification scale.

3.10 Ice rafted detrious/debris (IRD)

A minimum of 200-300 IRD grains was counted for the size fractions 0.5-1 mm and >1 mm every 5 cm in selected sections 3-8 in order to calculate numbers of IRD grains per gram dry

weight sediment distribution between 302-762 cm (93 samples). Large samples especially associated with core depth >~590 cm were randomly spread evenly over the picking tray 4with 45 squares, subsequently counted on a x-number of randomly selected squares until a total number of (200)-300 were reached. The counting procedure follow through with the counting until the current square had been fully counted. Samples above ~590 cm were generally smaller and often all grains were counted. Clay "lumps", gypsum crystals, pyrite crystals and other authigenous components not considered IRD was by best efforts excluded during the counting process. The counting process was performed under the Leica CLS 150X-MZ12.5 binocular microscope, at the geology lab at University of Tromsø.

IRD density and IRD flux were calculated using the following equations:

IRD density (number IRD/gram dry weight sediment) = (45/number of counted squares)(1/total weight)*(weight selected fraction/weight on picking tray)*

*IRD flux (number/cm^2*ka yr) = IRD density*dry weight*sedimentation rate/ka yr.*

3.11 Foraminiferal analysis

The >100µm size fraction anticipated to hold the higher portion of the foraminifera's was subsequently used for the picking and counting of benthic and planktonic foraminifera. Although former studies have found that small specimens could be overlooked, simply being too fine for the >100µm fraction, applying particularly to the species *Epistominella pusilla* (Pau and Hammer, 2016). The residue was evenly distributed by best efforts over a picking tray containing 45 squares. In circumstances where the residue was larger than the desired amount, a sediment sample splitter tool by Soiltest INC was used to split a credible 50/50 split until a manageable amount was reached. The Microscope used was a Leica CLS 150X-MZ12.5, at the geology lab at University of Tromsø. Ideally, a total number of >300 benthic foraminifera and >200 planktic foraminifera's for every consecutive 5 cm throughout the

selected interval should be picked. The paper "Ecology and distribution of recent foraminifera" by Fred B. Phleger (1960) suggested that counting a minimum of 300 specimens should provide sufficient accuracy for scientific quantitative examinations. In the intervals of high foraminifera concentration it would be sufficient to pick a limited amount of squares to achieve a number of >300 benthic foraminiferas, where each square where completely emptied for foraminiferas.

The selected interval was modified over time, in order to manage an overlap with the Holocene work of Kovalenko (2015). The interval was eventually 302-597cm implying a total number of 60 samples. Benthic foraminiferas were counted and identified to species level, occasionally genus. Heavily broken, worn, etched and foraminiferal fragments were if achievable identified to species or genus level, alternatively labelled "others". However, in circumstances concerning fragments, three identifiable fragments were considered equal of one theorized foraminifera. Due to their low abundance, planktic foraminiferas were exclusively counted, thus labelled planktic foraminifera. The picking session was over when >300 benthic foraminifera was reached, exclusively picking the planktonic foraminifera one came across in the benthic foraminifera processes. The overall preservation state was generally moderate, which is characteristic for late Quaternary period and at present in the southwestern Barents Sea (Hald et al., 1990). Scanning electron microscopes are frequently used as a tool in the search for evidence concerning carbonate dissolution.

The total concentration of the calcareous and agglutinated forms was calculated respectively (number foraminiferas per gram sediment). The estimated foraminiferal density and flux was calculated using the equations also applied to the IRD concentration:

Foraminifera density (number foraminifera/gram dry weight sediment) = (45/number of counted squares)(1/total weight)*(weight selected fraction/weight on picking tray)*

*Foraminifera flux (number/cm^2*ka yr) = foraminifera density*dry weight*sedimentation rate/ka yr.*

The relative abundance of each species was calculated relative to the total number of benthic specimens (calcareous + agglutinated).

3.12 FORAMINIFERA DATA

$^{18}O/^{16}O$ and $^{13}C/^{12}C$ isotope analyses of benthic foraminifera

61 foraminiferal samples (with occasional gaps) on a 5 cm spacing was picked throughout the core for analytical isotope measurements, specimens were counted and labelled (not weighted) and finally sent for isotope analysis at the Bjerknes Centre for Climate Change, University of Bergen. Measurements were performed on a Finnigan MAT 253 mass spectrometer instrument coupled with a Kiel IV device, with a relative laboratory reproducibility of +/- 0.05‰ and a 0.02‰ for the $\delta^{18}O$ and $\delta^{13}C$, respectively versus PeeDee Belemnite (PDB). The preservation state, species distribution and abundance made it difficult to achieve and obtain a species consistency. Well-preserved foraminifera of the same species of similar size are highly preferred, meaning no visible damage or contamination on the test. Further the specimens should have lived in situ in the environment implying that it is not transported or reworked in and fresh-food eaters are also preferable.

Several different species had to be picked as a result; *Islandiella norcrossi* (302-327+337-362+422+532-547+577 cm), *E. excavatum* (367-372+407 cm), *C. reniforme* (392-402+447+482-522+527+552-572+582-587+592 cm), *M. barleeanus* (412-417+432+447 cm), *C. lobatulus* (427+437-442+452-477+522+572+582+592 cm) and finally one with *N. labradoricum* (412 cm). Based on the overall general distribution the preferred species for selection was considered to be *C. reniforme*, *I. norcrossi* and *C. lobatulus*. The anticipated required quantity of each species was; 10-20 *I. norcrossi*, 40-50 *C. reniforme*, 5-10 *C.*

lobatulus, 20-30 and the supporting *E. excavatum*, 5-10 *M. barleeanus* and *N. labradoricum* 5-10 all numbers respectively size dependent.

Foraminiferal isotope analysis explores the concept of carbonate test construction development by abstracting elements from the ocean consequently reflecting the water mass isotope composition of the ambient prevailing surface or bottom seawater for planktic or benthic respectively at the time in which it develops. The general concept of utilizing stable isotopes in natural science was first described by Urey's ground-breaking paper back in [1946].

Three oxygen isotopes are known ^{16}O ^{17}O and ^{18}O, whereby the stable ^{18}O and ^{16}O ratio are exploited in isotope analysis, with an average ratio of 1:500. The concept of oxygen isotope analyses is to measure this ratio as a relative deviation from the PDB belemnite (concerning carbonates) or SMOW (concerning water, ice or snow) (Lowe and Walker, 1997). ^{16}O is lighter than the heavier ^{18}O oxygen isotope a phenomena which during fractionation processes due to e.g. evaporation leads to consequently a larger exchange of $H_2{}^{16}O$ towards the atmosphere over $H_2{}^{18}O$. This preference involves implications, in that ^{16}O is typically removed in higher concentrations than ^{18}O from the oceans and will there typically be the isotope more susceptible for a potential glacial storage during glacials, leaving the oceans relatively enriched in ^{18}O (Lowe and Walker, 1997). In short, ^{16}O is enriched during times of warm waters interglacials/interstadials resulting in low ^{18}O values, while ^{16}O is depletion during glacials/stadials resulting higher ^{18}O values i.e. ratio varies with ocean temperature, advection and mixing, global ice volumes, glacio-isostatic oscillations at sea level, salinity and vital effects (Lowe and Walker, 1997). The $\delta^{18}O$ variability should thus reflect temperature, salinity or a combination (e.g. Risebrobakken et al., 2010). Modern benthic and planktic $\delta\ ^{18}O$ values in the Barents Sea are more related to the temperature than salinity (Lubinski et al., 2001).

The stable ^{12}C isotope constitute 99% of all carbon, while the stable ^{13}C isotope makes up roughly 1% and finally the unstable isotope form ^{14}C constituting some minor fractions. Stable Carbon isotope analysis looks at the ^{13}C /^{12}C ratio ($\delta^{13}C$), a ratio/signal with a cyclic behavior due to various fractionation processes. Planktonic foraminiferas reflects productivity changes and ^{12}C flux in the upper water column (Shackleton and Pisias, 1985; Lowe and Walker, 1997), while benthic foraminifera are poorly understood, but appear to monitor the ventilation the passage of oxygen in the deep system (epifaunal species only), which have consequences for the preservation due to decaying implications associated with presence of oxygen, which further have implications for the nutrient availability. This ventilation is again a result of mixing of the deeper waters i.e. reflecting the deep water circulation (Berger and Vincent, 1986; Lowe and Walker, 1997). The benthic $\delta^{13}C$ tend to be lower during glacials.

Applying corrections known as "vital effects" are probably necessary for the majority of the sampled species, as not all species secrete their carbonate test in equilibrium with ambient sea water. Something Grossmann (1987) mainly though resulted from incorporation of metabolic CO2 compounds into the test. The effect has varied through time particularly during the deglaciation as it depends on the amounts of melting ice (e.g. Ebbesen et al., 2007).

The $\delta^{18}O$ *and* $\delta^{13}C$ values were corrected for vital effects. *Cibicides lobatulus* was corrected for vital effect offset $\delta^{18}O$ of +0.64‰, a value Duplessy (1980) suggested applied to the Cibicides genus. *Melonis barleeanus* was corrected for its disequilibrium with water of +0.4‰ (Duplessy et al., 1980; Rasmussen et al., 2007). +1.4‰ was applied to the inconsistent *E. excavatum* (Slubowska-Woldengen et al., 2007; Rasmussen et al., 2007). Another uncertain species *I. norcrossi* was corrected for +0.4‰ (Slubowska-Woldengen et al., 2007). *Cassidulina neoteretis* was corrected a disequilibrium of + 0.16‰ (Rasmussen et al., 2007), Klitgaard-Kristiansen et al. (2013) chose not to correct for vital effects on the species. Another species in the Cassidulina genus the *C. reniforme* was corrected for +0.27‰

(Aagaard-Sørensen et al., 2004) although some would argue that no correction for the species are necessary (Hald et al., 2004). A disequilibrium correction of -0.2‰ was applied for the *N. labradoricum* (Duplessy et al., 2005).

$\delta^{18}O$ was additionally corrected for ice volume effects based on the sea level calibration curve from Fairbanks (1989), where 10 m sea level correspond to 0.11 ‰ $\delta^{18}O$.

All results are reported in ‰ Vienna Pee Dee Belemnite (VPDB).

3.13 Radiocarbon dating

Five samples, 4 shell-fragments samples not identified due to their fragmentary state and one foraminiferal sample comprised of ~1000 various better preserved specimens of various species collected over an range-interval was sent to the 14 Chrono Centre lab in the Queen's University, Belfast, Northern Ireland for an analytical accelerator mass spectrometry (AMS) dating. The objectives over which depths to select was primarily; strategic positioning and the presence of material suitable for dating from samples generally low in carbonate content, preservation- and weight wise.

The AMS measures the number of ^{14}C atoms, relative to ^{12}C and ^{13}C. The principle behind the AMS method is in short: In the accelerator high speed electric charged particles is exposed to a magnetic field, the resulting deflection depends on the atom mass of the particle where heavier particles deflects less, which enables mass spectrometers to recognize/detects the numbers of atoms by specific weights, based on the deflection angle (Bowman, 1990). Criteria's are sufficient amounts of material and a upper limitation 50 000-60 000 (75 000) years depending on the laboratory.

Corrections for the attained results were applied in order to obtain calibrated calendar years BP (before present, conventionally 1950 AD) rather than the initially received raw radiocarbon ages. The isotope radioactively decays at a half-life (time for radioactive material

to decay to half its original amount) rate of 5570+/-30 yr (Libby half-life) following an organisms death (Godwin, 1962). The calibration issue is due to the fact that the ^{14}C production in the stratosphere is partly inconsistent through time, influencing the length of the ^{14}C years accordingly, consequently differ from calendar years. Another complicating factor is the reservoir effect, which in short is the phenomena of water masses of "different ages" encircling within the oceans. The marine reservoir age is defined as the difference between the ^{14}C age of the sea to that of the ^{14}C age in the atmosphere to any given time (Stuiver, 1986) (M_{res}=^{14}C age of a marine water – ^{14}C age of a contemparous terrestrial plants). The atmosphere expel ^{14}C to the oceans, while the ^{14}C levels at the ocean atmosphere-interface remains relatively constant (^{14}C levels is not consistent with time), the submerging water masses immediately starts the decay clock becoming progressively older due to radioactive decay with the absence of ventilation. A further complication is the dilution effect, contribution of older deeper water in upwelling processes. Marine organisms will further incorporate the ^{14}C into marine carbonate with the apparent age from the surrounding water masses, which essentially is older than true age (Bowmann, 1990; Mangerud et al., 2006). Adapting a correction is therefore a highly favorable in order to obtain the true age, an age that can be applied in order to compare it to terrestrial or ice core records.

Due to the many and wide range complexities of the ocean like upwelling, ocean currents and inter-hemispheric atmospheric ^{14}C, regional differences are inevitable. The difference between the global and the local marine reservoir age is expressed as ΔR, in which is considered constant within a region. The international marine reservoir correction network database "CHRONO Marine Reservoir Database" (www.calib.qub.ac.uk/marine/) gathers worldwide marine reservoir ages and ΔR values.

The radiocarbon dates was calibrated to calendar years BP using the CALIB Radiocarbon Calibration version 7.0.4 software (Stuiver and Reimer, 1993), which calculates the

probability distribution of the samples true age (calendar years age). The Marine13 calibration curve was selected (Reimer et al., 2013), operating with a standard reservoir correction of 400 years, often considered suitable for surface-water marine samples (Mangerud et al., 2006). The marine reservoir age ΔR was set according to Bondevik and Guilliksens reservoir age for the Northern Norway-Barents Sea to 71 +/-21 (Mangerud et al., 2006) after some consideration. A number also applied for Kveithola by Rüther et al. (2012). Awareness should be made that the reservoir effect have fluctuated through time, Younger Dryas has been shown to offset by as much of 200-600 additional years compared to the 415 years of Marine 13 (Bard et al., 1994; Bondevik et al., 2006; Reimer et al., 2013). When the record extends back to the LGM and Heinrich Stage (H1) Sarntheim (2011) suggested averagely, higher reservoir ages of 1000-2000 for the deep water masses. The reasons for an increased Younger Dryas reservoir ages is suggested to be a combination of increased sea ice cover and reduced advection rates of the surface water (Bard et al., 1994).

4 BENTHIC FORAMINIFERA

Benthic foraminifera are single celled organisms (protists) living as epifauna (on) or infauna (in) on the sea floor. They construct organic (theca), calcium carbonate (and aragonite) or agglutinated protective shells/tests composed of one or several chambers that subsequent to the organism's death potentially could be preserved as a microfossil within the sediments. Preserved tests could provide valuable assets in bio stratigraphy, paleo environmental, paleo oceanographical, paleo glacigenic, and paleo climatological applications in addition to in petroleum explorations and radiocarbon dating. Advantages for foraminifera adaptation are their relatively short life spans, sensitivity to external changes and generally worldwide presence making them a rapid responding faunal group concerning environmental changes and fluctuations. Some foraminiferal species are very particular about their habitat, some live more complicated life cycles where they are able to descend and ascend to and from the ocean floor during cycles, several species are known to exist in similar climatic zones in all oceans. Influential parameters on the foraminiferal fauna and mode of living includes e.g. temperature, salinity, alkalinity, oxygen levels, organic- inorganic substances, water depths/pressure, light levels, currents, turbidity, nutrition and food supply and preadaptation (Armstrong and Braiser, 2009). The rough Arctic winters with thick sea-ice cover and seasonal darkness highly limits the biological production in surface waters, further restricting food supply towards the sea bottom. The Arctic summers stand in stark contrast by 24 hours of daylight and open waters, allowing spring to-early summer blooms. Both benthic epifaunal and infaunal foraminifera absolute abundance are controlled by food (organic flux) and oxygen (Jorissen et al., 1995; Van der Zwaan et al., 1999), and further restrained by sea ice (e.g. Ivanova et al., 2008).

Application complications may arise if exposed to redistribution or reworking processes, essentially leading to misinterpretation of data unless acting under cautious procedures.

Resedimentation of various origins, bioturbations and diagenesis are processes known to misguide.

4.1 Ecological preferences for the cores most abundant species.

Four species were considered due to their high respective collective presence in the core HH15-1303PC as the dominating species and will be shortly presented in the following section in terms of ecological preferences and their modern distribution. Nine less abundant species are additionally briefly described, as they can be very much present at certain depths or intervals of depth i.e. very variable in that respect.

4.1.1 *Cassidulina reniforme* (Nørvang, 1945)

Cassidulina reniforme is an Arctic shallow-infaunal (endobenthic) opportunistic species, that tolerates oxygen depletion and thrives in cold water (<2°C) (e.g. Holtedahl and Bjerkli, 1982; Mackensen et al., 1985; Hald and Vorren, 1987; Steinsund, 1994). The species often dominates the foraminiferal assemblages in glaciomarine environments proximal to glaciers, stressed and unstable environments <100m water depth on the arctic shelves (Hald and Vorren, 1987; Korsun et al., 1995; Hald and Korsun, 1997; Polyak et al., 2002).

4.1.2 *Cibicides lobatulus* (Walker and Jacob, 1798)

Cibicides lobatulus is considered as an epifaunal (epibenthic) species, living preferably on coarser sediments where it can to cling onto gravels, grains, shells or algae being a suspension-filterfeeder feeding on the vigorous water set up by the stronger currents on fairly shallow but open marine glacier distal environments (e.g. Sejrup et al., 1981; Mackensen et al., 1985; Hald and Korsun, 1997; Polyak et al., 2002; Ivanova et al., 2008; Zajączkowski et al., 2010; Kubischta et al., 2010). Registrations of living infaunal *C. lobatulus* has been reported, Ivanova et al. (2008) regarded it as a epifaunal species that under circumstances concerning detachment potentially could infiltrate sediments by the search for food and/or

protection or simply by bioturbation processes (Zajaczkowski et al., 2010). In addition, according to Sejrup et al. (1981) on the basis of Jarke (1960) recognized them in association with the warm-cold water mixing zones (oceanic fronts) between the Atlantic-Arctic water occurring in the Barents Sea (Hald and Vorren, 1987). Thus, *C. lobatulus* is primarily useful for indicating presence of strong bottom currents (Mackensen et al., 1985).

4.1.3 *Elphidium excavatum* (Terquem, 1875)

Subspecies of *E. excavatum* have been scientifically proven trough time (Feyling-Hanssen, 1972), but overlooked and simply considered *Elphidium excavatum* for the simplicity of the dissertation. Worth noting however, is the widespread appearance of the cold-water thriving *E. excavatum forma clavata* (Cushman, 1944) in shallow polar waters (Hald and Vorren, 1987). *Elphidium excavatum* is an estuary and glacier proximal species (Linke and Lutze, 1993; Steinsund, 1994; Hald and Korsun, 1997; Korsun and Hald, 2000; Sejrup et al., 2004). Linke and Lutze (1993) consider them highly adaptable as both infaunal and epifaunal, adapting according to the nutritional levels and/or environmental changes i.e. very opportunistic. The species further features a great toleration concerning temperature, salinity and water depth, i.e. polar conditions where waters are of low salinities, low productivity, high turbidity and the ice cover extensive (e.g. Hald and Vorren, 1987; Linke and Lutze, 1993; Polyak et al., 2002). Hence, the species is regarded as a highly opportunistic polar species (Steinsund, 1994). In the Barents Sea its distribution are almost exclusively according to Steinsund (1994) confined to the realm of winter sea-ice covered Arctic waters.

4.1.4 *Islandiella norcrossi* (Cushman, 1933)

Islandiella norcrossi is an epifaunal/shallow-infaunal Arctic species associated with relatively deeper depths of approx. 200-400 m (Steinsund, 1994; Polyak et al., 2002; Jennings et al., 2004; Ivanova et al., 2008). The species appear to prefer finer sediment, found in deeper the

central Barents Sea where the fine concentration is at its highest (Steinsund, 1994). The areas are characterized by low sedimentation rates and presence of winter bottom water (Steinsund, 1994). The species seemingly prefers stable high bottom salinities, commonly associated with Atlantic water (e.g. Slubowska et al., 2005; Rasmussen et al., 2013). *Islandiella norcrossi* is usually found in areas with seasonal sea ice cover, often proximal to the sea ice edge, areas of high seasonal nutrient availability as they feed on fresh phytodetritus (Korsun and Polyak, 1989; Polyak et al., 2002; Zajączkowski et al., 2010).

While *I. norcrossi* is quite similar to the genus relative *I. helenae.* However, this species prefers shallower and less stable water (Steinsund, 1994). The two intergrading species can be difficult to distinguish and commonly combined, counted as one species (Korsun and Hald, 1998; Polyak et al., 2002).

4.2. Ecological preferences of the secondary species:

4.2.1 *Cassidulina neoteretis* (Seidenkrantz, 1995)

Cassidulina neoteretis is an epifaunal or shallow-infaunal subarctic species (Steinsund, 1994; Wollenburg and Mackensen, 1998; Jennings et al., 2004). The species is commonly associated with chilled slightly modified nutritious salty Atlantic Intermediate Water, submerged below colder fresher Arctic surface water in the deeper parts of the shelf including troughs, or the upper parts of the slope (e.g. Steinsund, 1994; Jennings and Helgadottir, 1994; Polyak and Mikhailov, 1996; Wollenburg and Mackensen, 1998; Lubinski et al., 2001; Jennings et al., 2004; Slubowska et al., 2005; Slubowska-Woldengen et al., 2008). Consequently this suggests a preference for low temperatures and saline conditions, accommodating finer sediments in connection with phytodetrial deposition (Mackensen et al., 1985; Mackensen and Hald, 1988; Steinsund, 1994; Wollenburg and Mackensen, 1998; Lubinski et al., 2001; Slubowska et al., 2005; Slubowska-Woldengen et al., 2008).

It is commonly found along with high concentrations of planktic foraminifera, suggesting a tendency towards the common traits suggested by Slubowska et al. (2005) to be the pursuing of phytoplankton blooms (Polyak and Mikhailov et al., 1996; Slubowska-Woldengen et al., 2008), possibly there are also a link to stratified water masses (Rasmussen et al., 2012). In the Barents Sea they occur almost exclusively in Bear Island, Franz-Victoria and St. Anna troughs acting as passageways for Atlantic Water (Lubinski et al., 2001). They do not appear where Atlantic Water has been strongly modified (Lubinski et al., 2001).

4.2.2 *Buccella* spp.

Buccella spp. are due to simplicity identified to genus level, assuming a predominance *Buccella frigida* (Slubowska et al., 2005). Although they show a wide range of distributions, some overall general traits seems consistent for the Barents Sea epifaunal shallow-infaunal genus including; moderate-low temperatures and relatively high salinities affiliated with Atlantic Water, 100-200 m water depths often in proximity to rivers (Steinsund, 1994; Polyak et al., 2002 Slubowska et al., 2005). Their presence further mainly respond to food availability, irrespective the cause (Seidenkrantz, 2013). Thus they are often numerous in high biological productivity areas as they feed on fresh phytodetritus, associated with proximity to seasonal sea-ice edge and/or oceanic fronts (Steinsund, 1994; Polyak et al., 2002; Slubowska et al., 2005). *Buccella frigida* is commonly found in sandy sediment (Kubischta et al., 2010). *Buccella* spp. shows similar distribution to that of *I. norcrossi* but appear to prefer shallower water and coarser sediments (Steinsund, 1994). Similarly to *I. norcrossi*, *Buccella* spp. are not tolerant under circumstances where high sedimentation rates causes turbid water (Zajaczkowski et al., 2010).

4.2.3 *Melonis barleeanus* (Williamson, 1858)

Melonis barleeanus is arctic-boreal and primarily an infaunal species, nourishing on buried organic matter within fine grained sediments (Caralp, 1989; Polyak et al., 2002; Jennings et al., 2004; Slubowska et al., 2005; Ivanova et al., 2008). Linke and Lutze (1993) reported based on behavioral observations of an adaptable *M. barleeanus* interchanging between infaunal and epifaunal according to food supply and environmental conditions. Furthermore, its appearance has been considered higher in finer organic-rich sediments that exhibit some degree of degradation often associated with cascading water masses enriched with food and nutrients, originating from shallower productive banks (Caralp, 1989; Steinsund, 1994; Polyak and Mikhailov, 1996; Polyak et al., 2002; Slubowska et al., 2005).

Melonis barleeanus is considered indicative of increased inflow of nutritious cold saline Atlantic intermediate water and high stable organic matter and sediment supply commonly occurring in shelf depressions and the continental slopes (Polyak and Mikhailov, 1996; Polyak et al., 2002; Jennings et al., 2004; Slubowska et al., 2005).

4.2.4 *Elphidium subarticum* (Cushman, 1944)

Elphidium subarticum is an epifaunal species, often associated with coarser sediments in e.g. the continental shelf or slope (e.g. Steinsund, 1994; Polyak et al., 2002). At present it has been reported occurring throughout the high and temperate- latitude shelves, a pattern, which from a critical point of view possibly reflects inconsistent taxonomic approaches (Polyak et al., 2002). Further, it has been set in association with sea ice (e.g. Steinsund, 1994). The species show a greater preference towards shallower water (Feyling-Hanssen et al., 1971) and lowered salinities (Steinsund, 1994; Skirbekk et al., 2010).

4.2.5 *Nonionellina labradoricum* (Dawson, 1860)

Nonionellina labradoricum is an infaunal Arctic-Polar species feeding on organic matter and fresh phytodetritus, i.e. found in cold saline bottom waters with high biological surface productivity, areas proximal to frontal zones, ice margins or bank slopes (e.g. Steinsund, 1994; Polyak and Mikhailov, 1996). Considered a glaciomarine, high seasonal (spring-early summer) biological productivity indicator associated with presence of Atlantic Water (e.g. Steinsund, 1994; Wilson et al., 2011; Rasmussen et al., 2013)

4.2.6 *Stainforthia loeblichi* (Feyling-Hanssen, 1954)

Stainforthia loeblichi is a highly opportunistic species that thrives in cold waters (0°C) in areas with algal blooms, seasonally covered by seasonal sea ice or sea ice margins, at present rapidly multiplying during the winter months (e.g. Steinsund, 1994; Slubowska et al., 2005; Rasmussen and Thomsen, 2015). Hence considered an indicator of increased sea ice cover (Polyak et al., 2002)

4.2.7 *Astrononion gallowayi* (Loeblichi and Tappan, 1953)

Astronion gallowayi is an epifaunal species known to particularly thrive in shallow cold saline productive waters with coarse sediments and currents (e.g. Steinsund, 1994; Polyak et al., 2002; Wilson et al., 2011) and associated with warm Atlantic Water (Hald and Aspeli, 1997). Sharing a similar distribution pattern to that of *C. lobatulus*, but prefer higher steadier food supply (e.g. Rasmussen et al., 2013).

4.2.8 *Islandiella islandica* (Nørvang, 1945)

This is an Arctic species quite similar to *I. californica,* often confused with and identified as *C. reniforme* (Rodriguez et al., 1980). In Nova Scotia, Canada the species was reported to

correlate strongly to salinity and coarser substrate and located in isolated outer banks and shallow depressions on the shelf (Williamson et al., 1984).

5 RESULTS

The following chapter will present the various results obtained during the processing of the core HH15-1303PC, five lower sections (section 4-8) (290-765 cm). Sedimentological, chronological and grain size distribution results concerns the complete selected interval, while the focused interval for the foraminiferal results are 302-597 cm.

The general idea of this master thesis is to be a continuation of the master thesis of Boriss Kovalenko (2015) which focused on the Holocene development in Leirdjupet trough, based on core HH14-012GC from Leirdjupet.

5.1 Radiocarbon dating

A total number of 5 samples were AMS ^{14}C dated (Table 5.1). The radiocarbon dates were calibrated to calendar BP years.

The sample at 487 cm shows an age older than the age of the 575 cm, i.e. “age reversal” (table 5.1). The higher age was therefore discarded. Some glacial reworking (iceberg rafting, iceberg ploughing/erosion, downward burrowing or coring disturbances are plausible explanations, where older material are incorporated into younger sediments. The 593-599 cm age is ostensibly too old, and therefore discarded. The abnormally high age (infinite age) of the 605-610 cm is in all likelihood also too old, presumably related to glacial reworking of older marine sediments. Radiocarbon dating of deglacial sediments are known to be problematic, due to the uncertainties related to factors that includes poorly constrained variations in the reservoir effect, contamination problems with older radiocarbon in circulation, glacial reworking, bioturbation and radiocarbon age calibration difficulties. Thus the calibrated dates should be considered as a minimum age.

Lab reference	Depth	Dating material	Δ R (year)	^{14}C uncalibrated yr	Cal. yr BP 2 2σ mean
UBA-31640	330 cm	Shell fragments	71+/-21	10,726 +/- 50	12,023+/-270
UBA-31639	487 cm	Shell fragments	71+/-21	13,216 +/- 63	15,158+/-256
UBA-30465	575 cm	Bivalve	71+/-21	12,980 +/- 54	14,693+/-380
UBA-31753	593-599 cm	Foraminifera collection	71+/21	17,804+/-80	20,908+/-270
UBA-30466	604-610 cm	Bivalve fragments	71+/-21	45,040 +/- 2320	47,090+/-2909

Table 5.1: Results from radiocarbon dating.

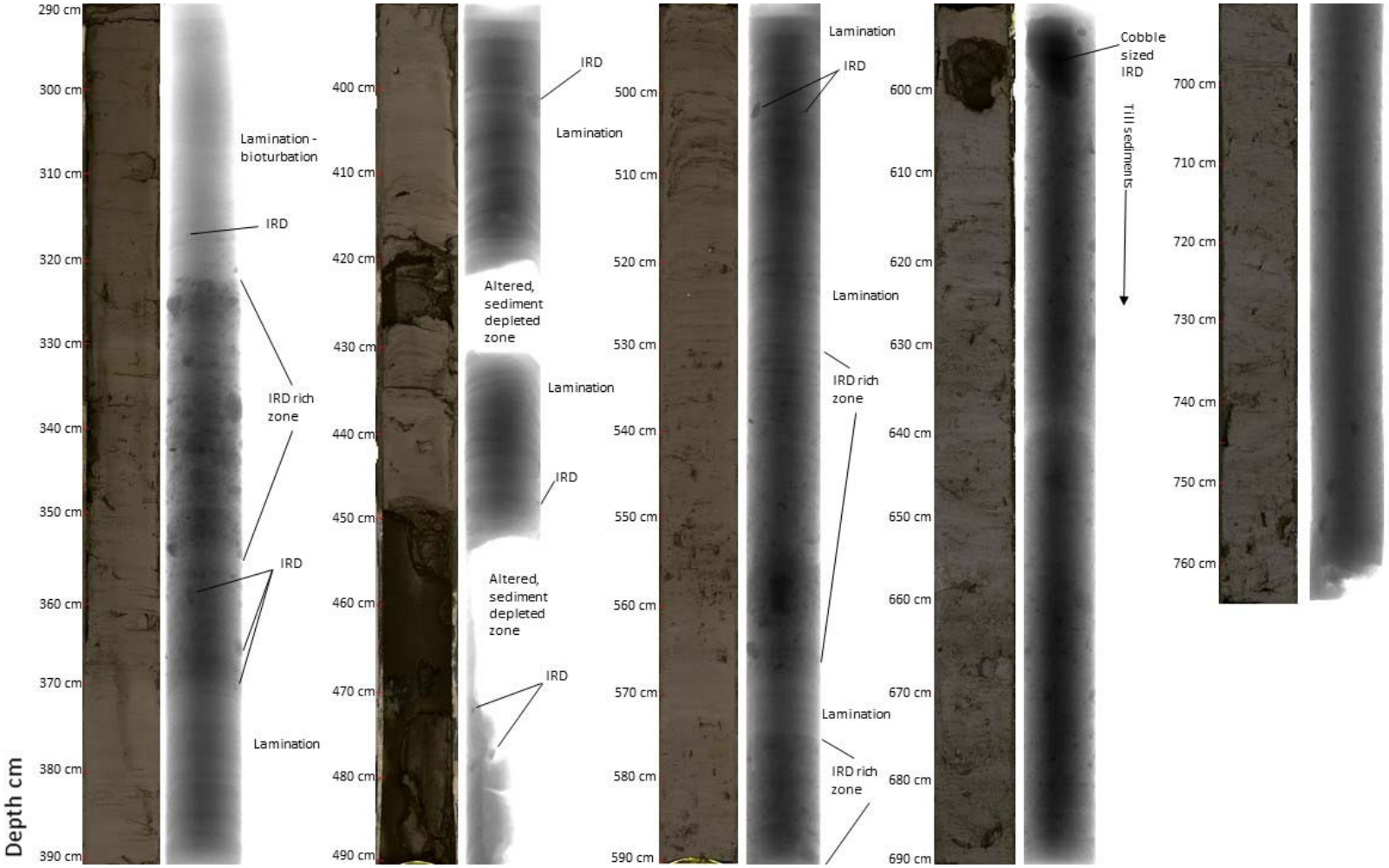

Figure 5.1: Photography and X-ray images of the core sections, plotted against depth (cm).

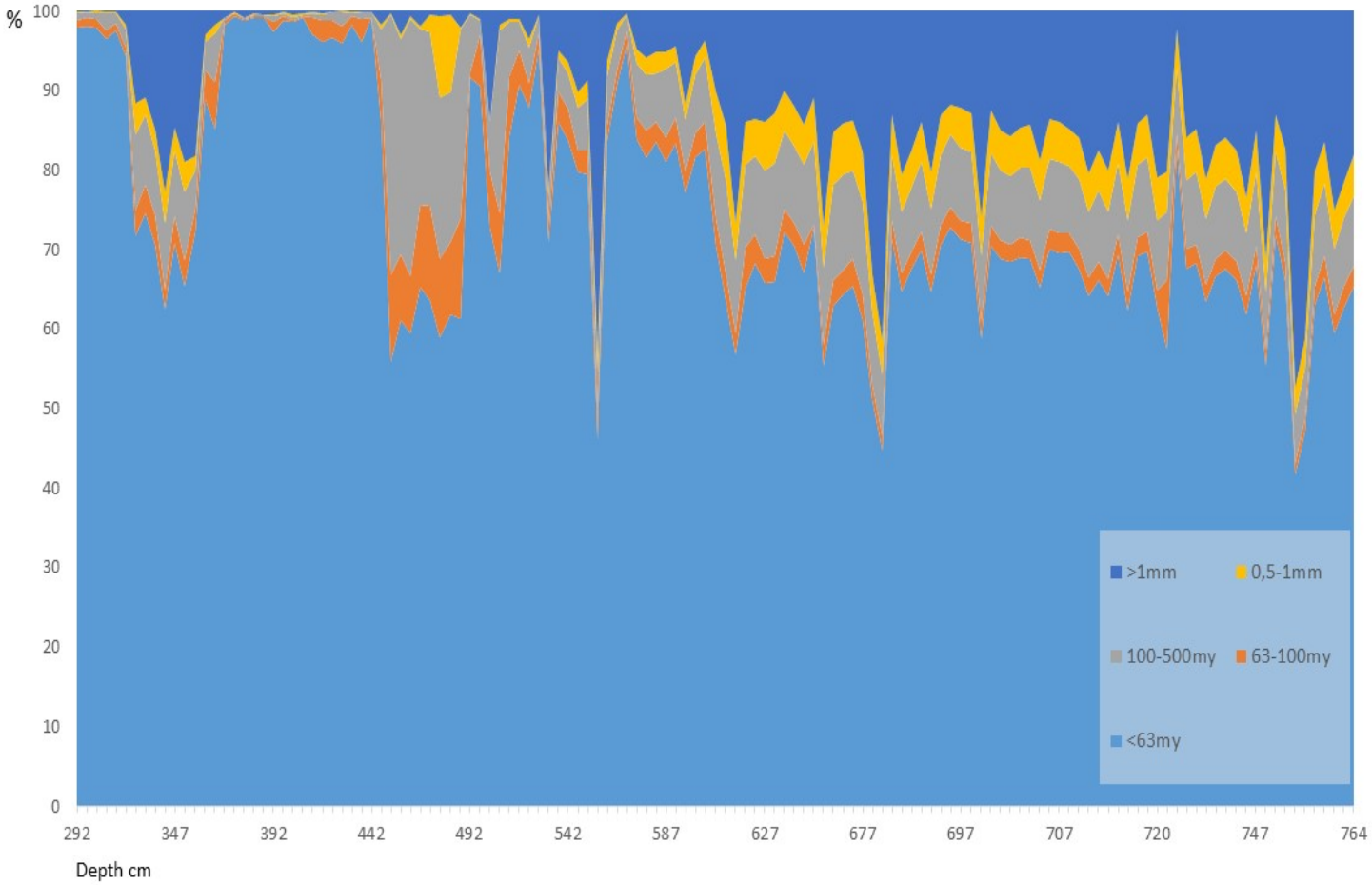

Figure 5.2: Cumulative grain size distribution as weight percentages, plotted against depth (cm).

5.2 Lithological units

The studied part of the HH15-1303 piston corer 290-765 cm (sections 4-8) have been based on visual inspection, grain size distribution, IRD, X-ray images and photographs divided into 7 lithological units that will be presented base-top. Increasing compression down core will naturally affect density and porosity.

5.2.1 Unit 1 (U1) (765-600cm)

The lowermost stiff unit is a massive structureless dense pebbly medium-coarse sandy mud, interpreted as a diamicton (also given the infinite radiocarbon age, see discussion (Fig. 5.3; Fig. 5.4; Fig. 5.5). It was given the Munsell color coding (2,5Y 2,5/1) equivalent of light olive brown. The IRD concentration values are generally continuously high with some minor oscillations in both of the IRD size fractions, with a significant 0.5-1 mm IRD low at 677 cm,

a >1 mm peak at 612 cm and a 0,5-1 mm peak at 607 cm. The magnetic susceptibility- and wet bulk density values are uniformly high throughout the unit. It is the unit with the lowest % water content and porosities.

5.2.2 Unit 2 (U2) (600-575 cm)

Unit 2 shows some resemblance towards Unit 1 (Fig. 5.3; Fig. 5.4; Fig. 5.5).The lower portion of the unit, the top of section 7 is dominated by a cobble with dark grey-olive gray (5Y 2,5/1) structureless (pebbly) medium sandy mud filling the gaps and the upper part of the unit. The wet bulk density values are high, the porosities and % water content relatively low. The IRD concentrations are relatively high throughout the unit, particularly concerning the 0.5-1 mm size fraction. The generally high fluctuating magnetic susceptibility values show a pronounced peak at 600 cm, probably related to the presence of the large cobble.

5.2.3 Unit 3 (U3) (575-565 cm)

Unit 3 only comprises 10 cm forming a sharp interlaminated unit (Fig. 5.3; Fig. 5.4; Fig. 5.5). The unit is composed by dark grey-olive gray (5Y 2,5/1) laminated (sandy) mud devoid of IRD, which is further reflected in the lowered magnetic susceptibility values. The wet bulk density values are moderate, the porosities and % water content slightly enhanced.

5.2.4 Unit 4 (U4) (565-540 cm)

The 25 cm thick unit is mainly structureless (possibly some faint lamination) pebbly medium sandy mud, with higher IRD concentrations in both fractions, particularly in the lower part of the unit, i.e. probably representing a diamicton (Fig. 5.3; Fig. 5.4; Fig. 5.5). The magnetic susceptibility and wet bulk density values are correspondingly high, % water content and porosities correspondingly low. The coloration changes from dark grey-olive grey (5Y 2,5/1) in the lowermost part of the unit into light olive brown (2,5Y 3/1).

5.2.5 Unit 5 (U5) (540-370 cm)

Unit 5 comprise 170 cm and differ in some characteristics compared to the units below (Fig. 5.3; Fig. 5.4; Fig. 5.5). The unit develops from a laminated dark gray (5Y 3/1) to light olive brown (2,5Y 2,5/1) (pebbly) fine-medium sandy mud at the base, into a dark gray (5Y 3/1) laminated fine-medium sandy mud with scattered IRD from 515 cm. A confined distinct sandy mud layer at 507 cm with a considerable high percentage of fine-medium sand is found. Similar grain size distribution containing a considerable amount of fine-medium sand reappears from 490 cm in a greyish olive sandy mud extending to 450 cm. Parts of the interval are clearly altered probably by an implosion caused by suction, clearly seen on the x-ray and pictures (fig. 5.1). A dark gray-olive gray (5Y 2,5/1) laminated mud barren of IRD with a minor fraction of fine-very fine sand follows after 450 cm and extends to the unit top, disrupted by a 10 cm (~428-418 cm) structureless interval also probably altered by suction. The magnetic susceptibility values generally declines from the base of the unit towards the altered interval interrupted by two minor peaks at 534 cm and 506 cm. The two altered intervals are clearly seen as two deviating significant lows, in addition to on the wet bulk density values and porosities. The magnetic susceptibility values subsequently returns to more "normalized" moderate values. The wet bulk density values are high prior to the alternated interval, but are similarly to the magnetic susceptibility lowered as a response to the increasing mud content, the porosity- and % water content values have a corresponding opposing trend.

5.2.6 Unit 6 (U6) (370-~325 cm)

The ~45 cm thick unit develops from a laminated sandy mud at the base, into a massive unsorted pebbly fine-medium sandy mud from 353 cm, i.e. diamicton (Fig. 5.3; Fig. 5.4; Fig. 5.5). Two Munsell color codes were applied, moderate olive brown (2,5Y 3/2) at the base into greyish olive (5Y 2,5/2) for the majority of the unit. The IRD concentration are high, the 0.5-1

mm grain size fraction in particular, increasing towards the top of the section. The moderate magnetic susceptibility values declines towards the top of the unit, while wet bulk density values remains uniformly moderate with a small declining trend upwards. The % water content fluctuates slightly, but are generally moderate, similarly to the porosity values.

5.2.7 Unit 7 (U7) (322-290 cm)

The transition to the 32 cm long uppermost unit is sharp and consist of light olive brown (2,5Y 2,5/1) mud barren of IRD, possibly with some poorly defined lamination and bioturbation (Fig. 5.3; Fig. 5.4; Fig. 5.5). The low magnetic susceptibility- and wet bulk density values decrease towards the top. The water content and porosity values are high, increasing upwards.

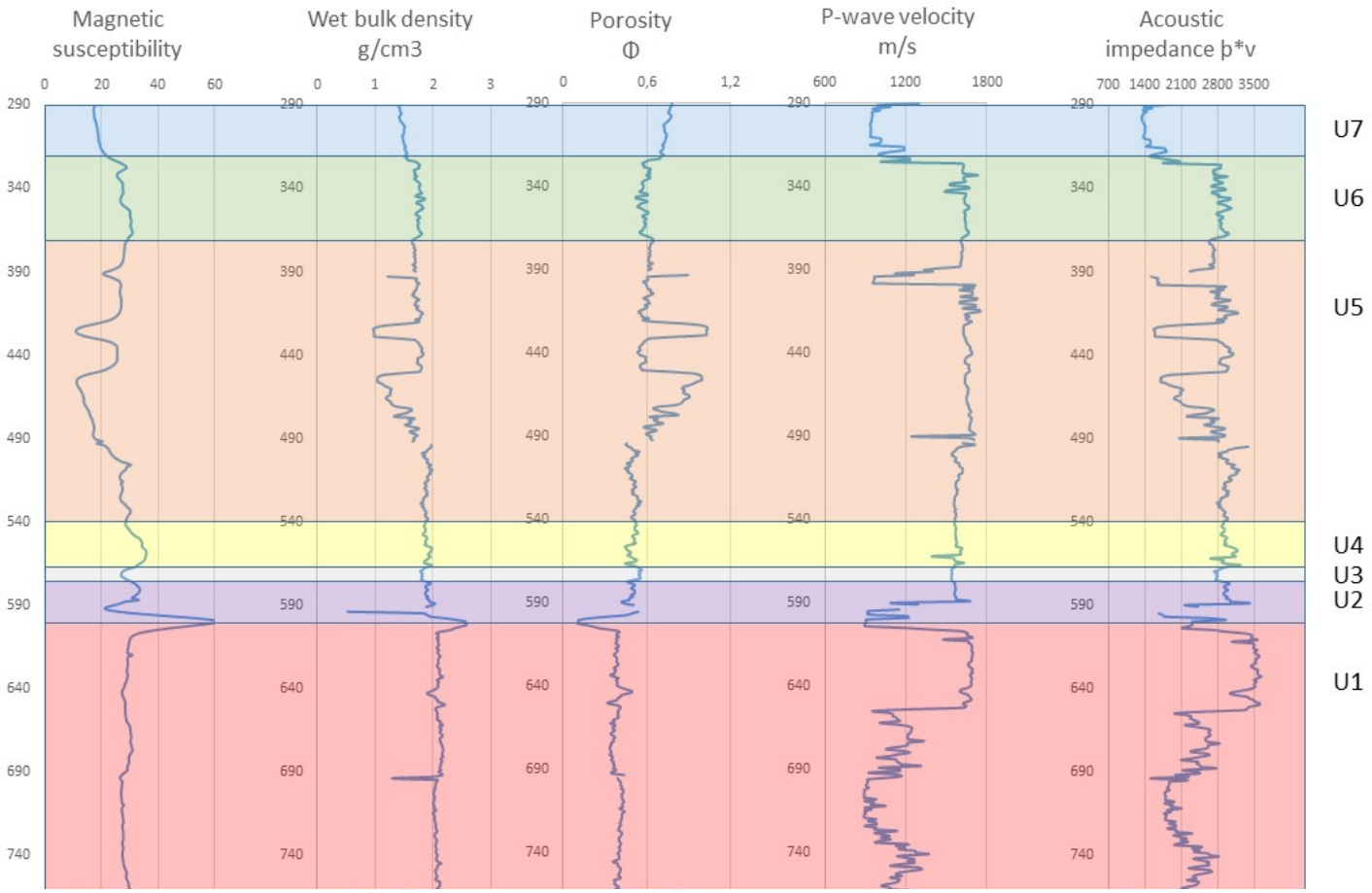

Figure 5.3: Magnetic susceptibility, wet bulk density, porosity, P-wave velocity and acoustic impedance plotted against depth (cm) and their associated lithology unit.

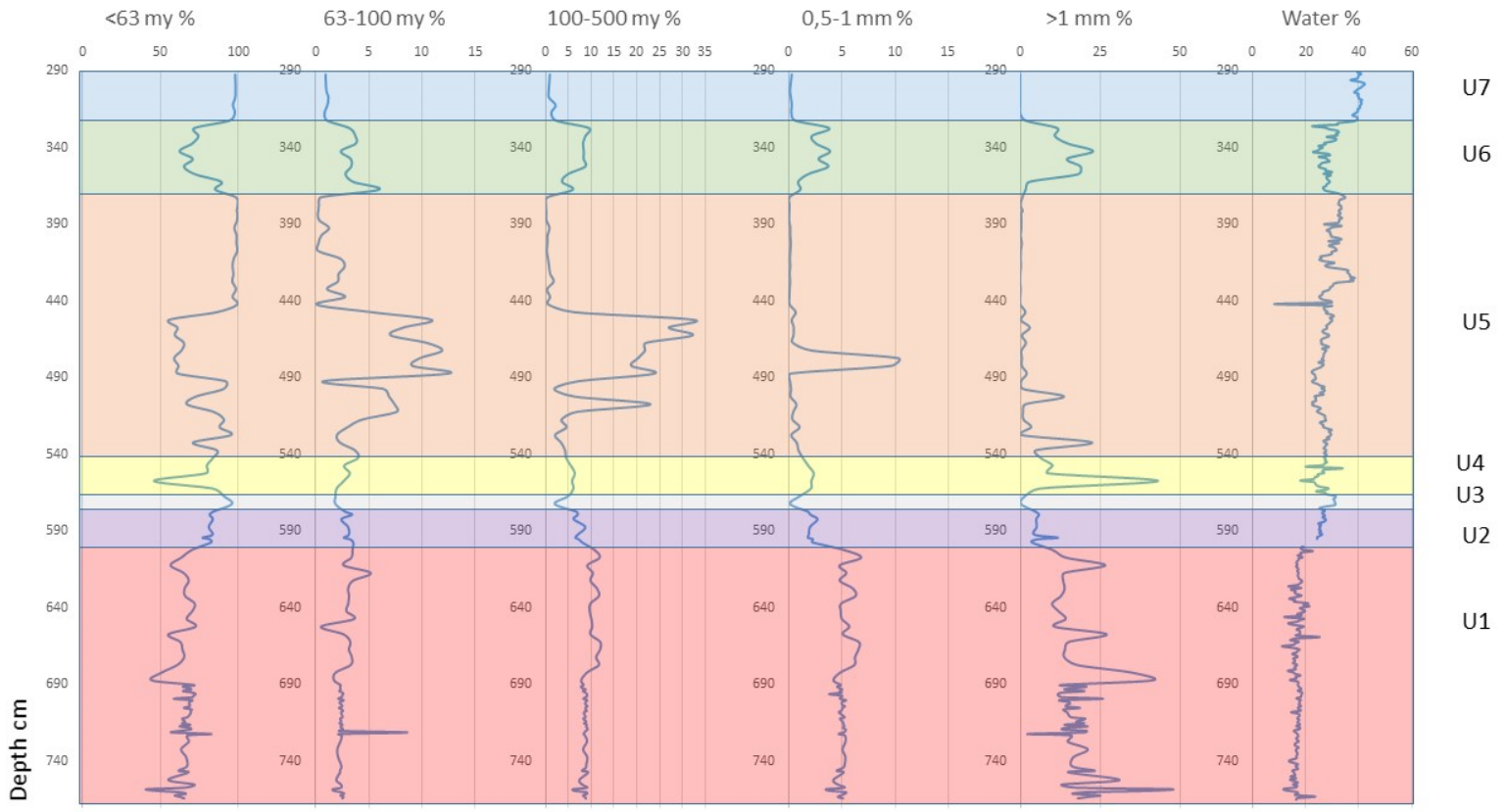

Figure 5.4: Grain size distribution and water content percentage plotted against depth (cm) and their associated lithology unit.

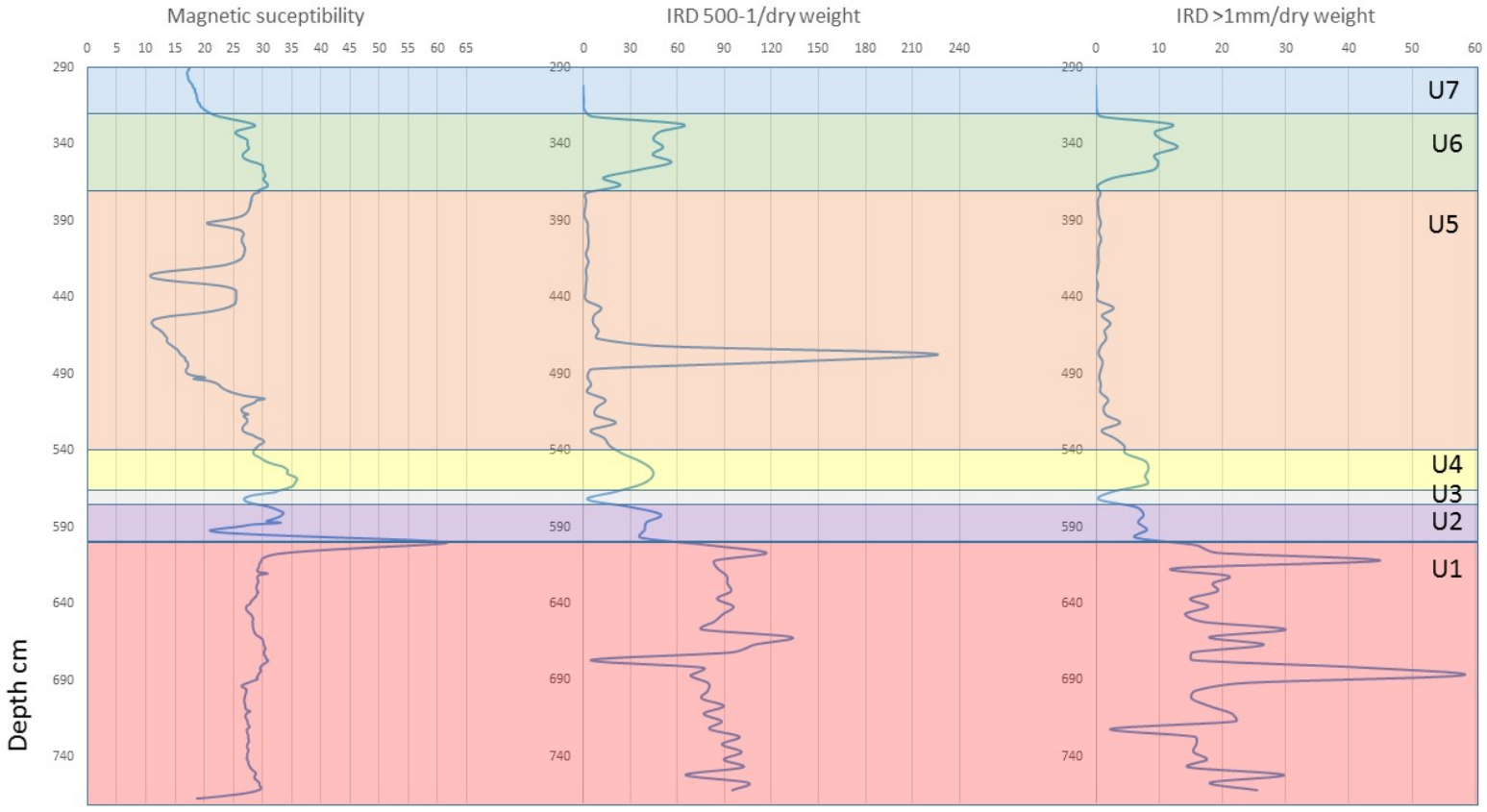

Figure 5.5. Magnetic susceptibility, and IRD 0.5-1 mm concentration and IRD >1 mm concentration, plotted against depth (cm) and their associated lithology unit.

5.3 Foraminiferal results

The studied interval in the foraminiferal study was 302-597 cm. The diamicton starting at 600 cm to core base was barren of foraminifera. Former regional studies on such stiff overconsolidated diamictons have revealed that the preservation state, abundance and taxa often including exotic, older specimens of foraminifera of pre-Quaternary age suggesting reworking (e.g. Hald et al., 1989; Polyak and Mikhailov, 1996). Three samples at depths 377 cm, 382 cm and 392 cm contained fewer than 50 benthic foraminiferal specimens, and were consequently discarded from % species distribution due to statistical uncertainties. Two samples furthermore contained >50-<100 specimens, at 332 cm and 407 cm, but were included. The results presented in this chapter are species %, number of identified benthic species "diversity", and concentration of calcareous-, agglutinated- and planktonic. The interpretation follows in chapter 7. A total of 59 taxa were identified, 37 benthic species were identified to species level, furthermore 22 to genus level "spp.". Four species predominates the assemblage, further 7+1 are considered secondary species (+1 referring to the genus *Buccella*), consequently being the species of main focus in the following foraminiferal description. Neither planktonic nor agglutinated species are included in the results of relative abundances, owing to the low presence. Many agglutinated species are known to have low preservation potential (e.g. Slubowska et al., 2005; Rasmussen and Thomsen, 2015). Low numbers or absence of planktonic species is common for shelf and coastal marine cores, they are more numerous in open ocean settings (e.g. Seidenkrantz, 2013). In addition planktonic foraminifera have been reported to be three times more prone to carbonate dissolution than their benthic counterparts (Steinsund and Hald, 1994).

Seven assemblage zones A-G from the base towards the top were recognized. The percentages of the individual species were calculated relative to the amount of benthic (agglutinated +calcareous) specimens in each respective sample. The diversity is simply

expressed as number of species + genus identified in each respective sample. The concentrations of the benthic-, benthic calcareous-, benthic agglutinated- and planktonic foraminifera are expressed as number/g dry weight sediment.

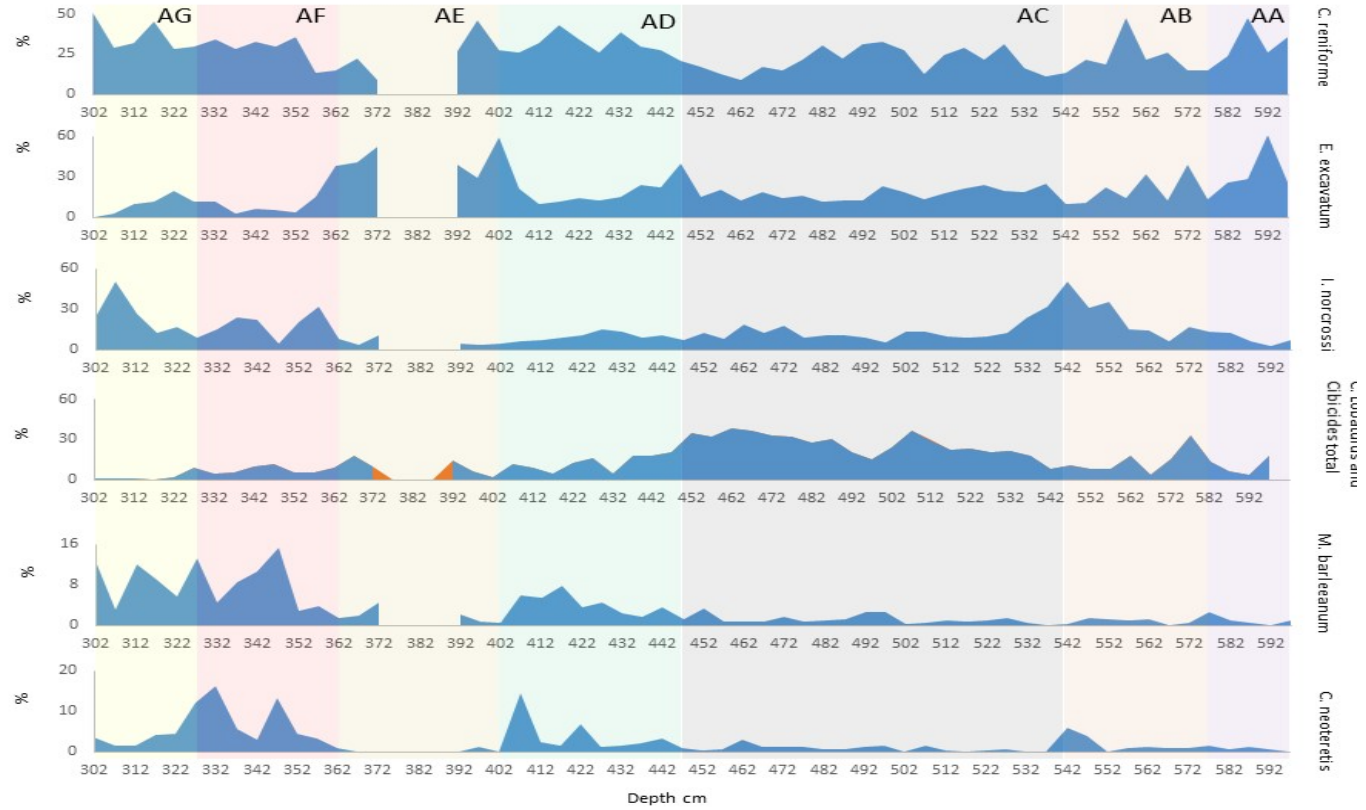

Figure 5.4: Relative abundances of benthic foraminifera species in percentages plotted against depth (cm) and their associated assemblage zones.

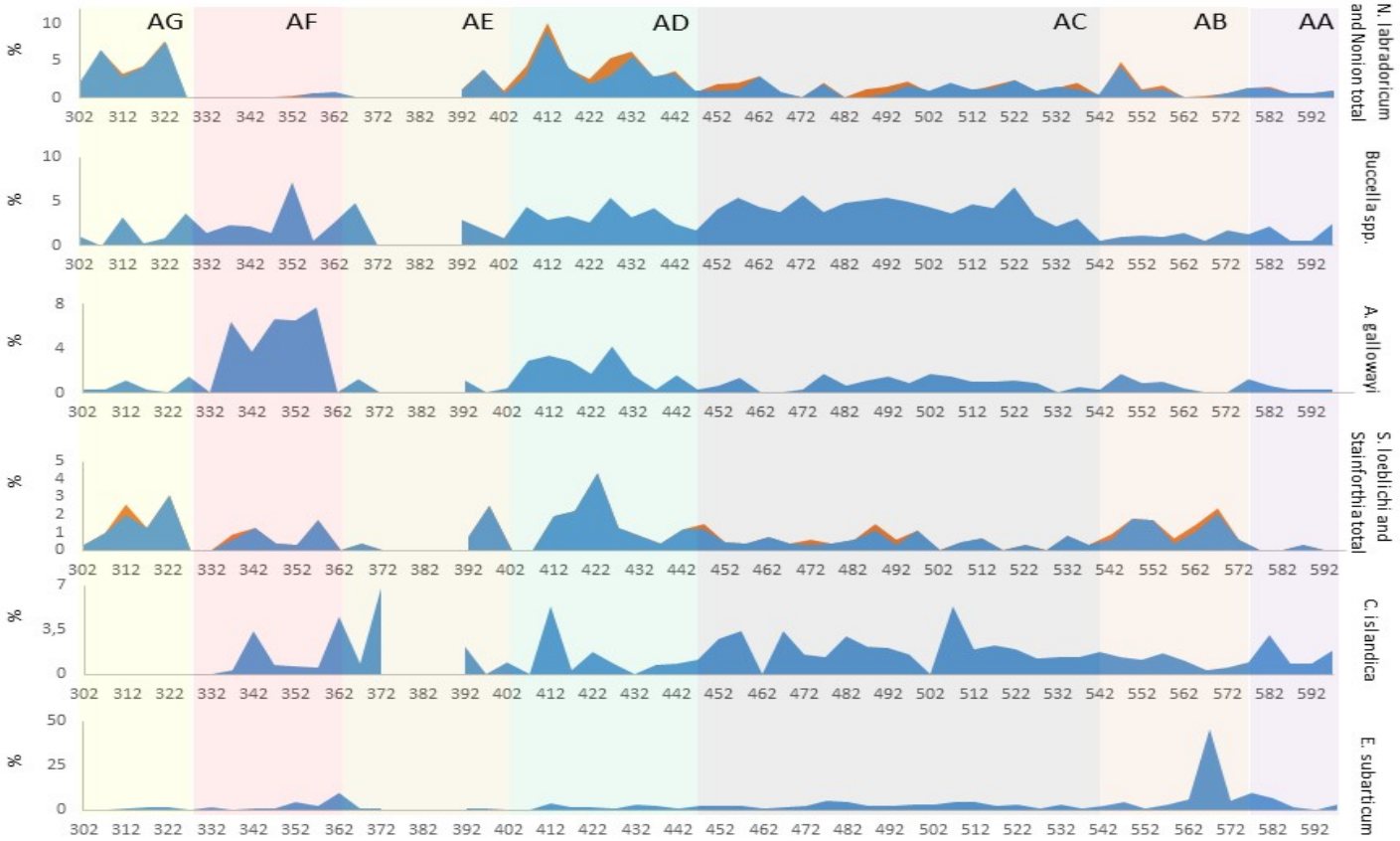

Figure 5.8: Relative abundances of benthic foraminifera species in percentages plotted against depth (cm) and their associated assemblage zones.

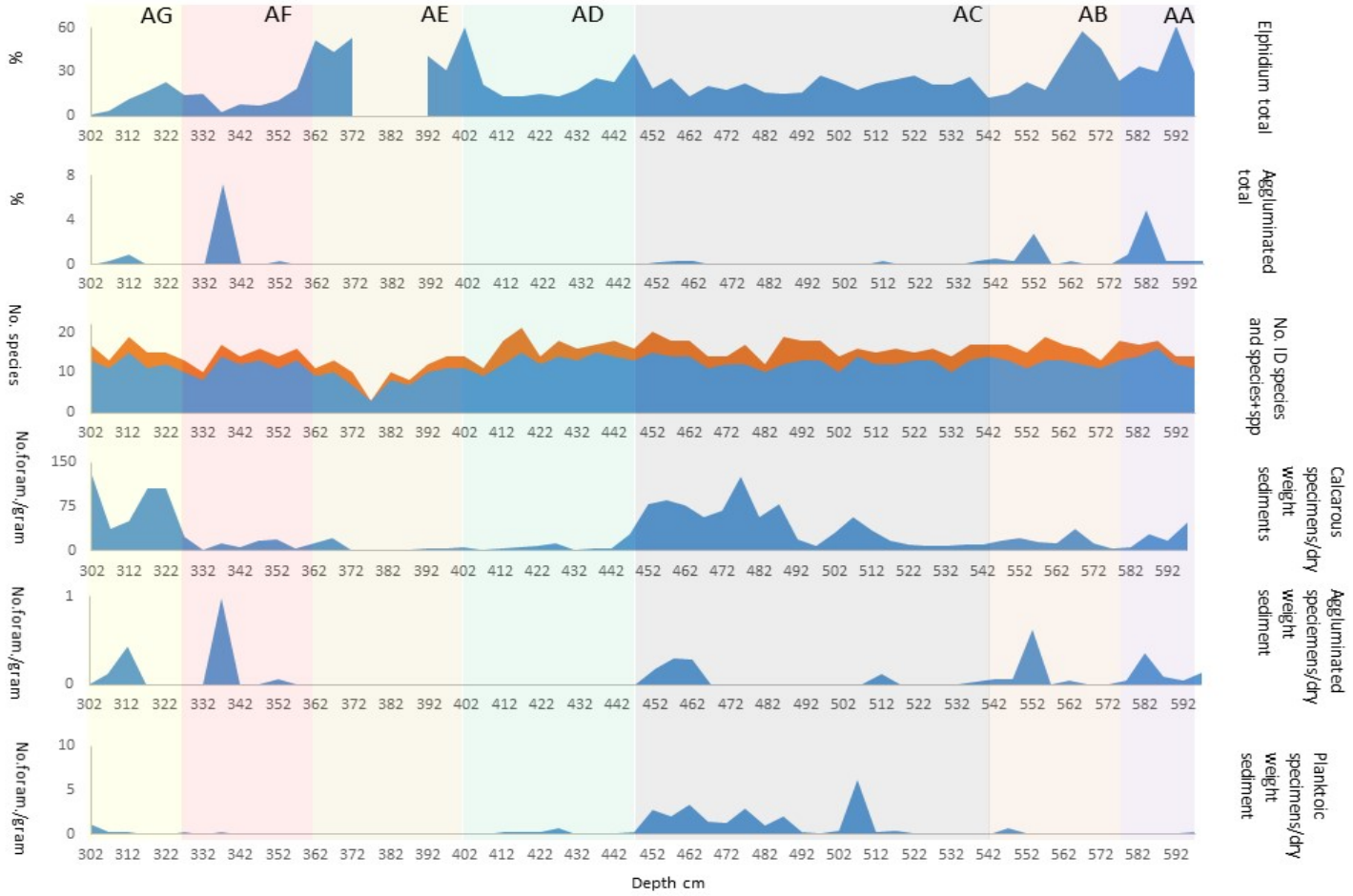

Figure 5.9: Relative abundance Elphidium spp. and agglutinated in percentages. Number of identified species + genus. And concentration of benthic calcareous, agglutinated and planktic specimens pr. gr. sediment. All plotted against depth (cm) and their associated assemblage zones.

5.4 Biozones

5.4.1 Assemblage zone A (AA) (597-575 cm)

The calcareous concentration remains at moderate levels throughout much of the zone, before diminishing to very low levels at top of the zone (Fig. 5.6; Fig. 5.7; Fig. 5.8). The opportunistic duo *C. reniforme* and *E. excavatum* dominates the assemblage particularly in the lower half, their average percentages are 30% and 31% respectively. Both species has one defined peak, *C. reniforme* at 587 cm and *E. excavatum* at 592 cm. *Cibicides lobatulus* and *I. norcrossi* are the two main accessory species increasing in proportions towards the top, in line with the gradually lower domination of C. reniforme and *E. excavatum*, *C. lobatulus* reaching

a 33% peak at 577 cm. The four of them together constitutes about 84% on the average fauna in the zone.

The subspecies are all present at low proportions throughout the zone, whereby *C. islandica* and *E. subarticum* are the more pronounced.

Four specimens (1.66%) of the Atlantic water species *Pyrgo Williamsoni* were found at 587 cm.

The concentration of agglutinated benthic-foraminifera remained moderate-(low), 16 (4.9%) specimens of *C. crassimargo* were found at 582 cm, the highest identified within the samples. The zone was close to devoid of planktonic foraminifera.

5.4.2 Assemblage zone B (AB) (575-542 cm)

The benthic calcareous concentration remains moderate throughout this zone (Fig. 5.6; Fig. 5.7; Fig. 5.8). *Cassidulina reniforme* and *E. excavatum* in addition to *I. norcrossi* dominate the assemblage with 23%, 20% and 24%, respectively. *Islandiella norcrossi* generally increase in proportion towards the top of zone, *E. excavatum* and *C. lobatulus* (10%) gradually decrease.

The zone more peculiar feature is the large *E. subarticum* peak (45.7%) at 567 cm. *Cassidulina neoteretis* is present in low relative abundance with a 5.95% peak at the termination of the zone. Both *N. labradoricum* and *C. neoteretis* gradually increase in proportions in the upper half of the zone. *Cassidulina neoteretis* with a confined peak at 542 cm, *N. labradoricum* with a moderate peak at 547 cm. The remaining subspecies are limitedly present.

The benthic agglutinated foraminiferal concentration is generally low with the exception of 552 cm where 10 (2.8%) specimens of *Cribrostoides crassimargo* were identified. The planktonic foraminiferal concentrations remained very low.

5.4.3 Assemblage zone C (AC) (542-447 cm)

One-third into the zone, the benthic calcareous concentration rapidly increase from the low continuation of the assemblage zone A to a substantially higher concentrations, which further progress into assemblage zone *C. Cibicides* lobatulus rapidly becomes more abundant, increasing throughout the zone, averagely constituting 27% of zone (Fig. 5.6; Fig. 5.7; Fig. 5.8). The relative abundance of *C. reniforme* and *E. excavatum* decrease slightly, averagely 21% and 19%, respectively. *Islandiella norcrossi* steadily decrease in the lowermost part and remains stable around 10%.

One of the zones more characteristic features is the lasting stable presence of *Buccella* spp. (~3-6%). The other subspecies are present in low abundance. On average, the subspecies only constitutes 13% of the fauna.

In addition, it can briefly be mentioned that *Trifarina fluens* and *Fissurina* spp. are present in small numbers in the zone. Warm water species were identified at 462 cm, 492 cm and 507 cm, the former a specimen of *Epistomniella nipponica,* while the two latter ones of *Bulimina marginata*. The zone is almost devoid of agglutinated specimens. The planktonic foraminiferal concentration is initially low, but increases midway through the zone.

5.4.4 Assemblage zone D (AD) (447-402 cm)

The high concentration of calcareous benthic foraminiferas abruptly declines 452cm, to very low levels that persists throughout the zone (Fig. 5.6; Fig. 5.7; Fig. 5.8). *Cassidulina reniforme* dominates the assemblage, averagely accounting for 32% of the assemblage zone.

The three remaining main species are still present, showing an overall small declining trend towards the base of assemblage zone D.

Several of the subspecies becomes more abundant in this zone, combined averagely constituting 20% of the assemblage. This particularly concerns the high biological productivity indicator *N. labradoricum* with one major peak that inclusive *Nonion* spp. constitutes up 11% of the assemblage at 412 cm. *Cassidulina neotertis* peaks at 407 cm constituting ~15% of the assemblage. *Melonis barleeanus, A. gallowavyi* and *S. loeblichi* are moderately present. *Stainforthia loeblichi* is particularly abundant in the zone mid-area, peaking at 422 cm (4.3%) followed by a total absence from 407-402 cm. *Cassidulina islandica* peaks at 412 cm, where it make up 5% of the fauna, but generally low-absent in abundance.

Globobulimina auriculata and the two identified *Pulloides* species *P. bulloides* and *P. osloensis* were found in most of the samples throughout the zone in limited numbers.

The agglutinated and planktonic concentrations were initially moderate-high, but subsequently lowered to low-absent from 447 cm.

5.4.5 Assemblage zone E (AE) (402-362 cm)

This zone is characterized very low foraminiferal concentrations particularly evident from the 387-377 cm interval (Fig. 5.6; Fig. 5.7; Fig. 5.8). The zones was barren for agglutinated specimens and planktonic specimens were scattered. The opportunistic *E. excavatum* in particular, and *C. reniforme* dominates the assemblage and comprise together 66% of the fauna, while *C. lobatulus* averagely constitutes 12%. *Islandiella norcrossi* persist at moderate levels (5.7%).

The subspecies generally constitutes low-moderate percentages of the foraminiferal assemblage, where the most numerous are *Buccella* spp*., E. subarticum, M barleeanus and C. islandica*. *Elphidium subarticum* peaks at 362 where it constitutes 10% of the assemblage.

5.4.6 Assemblage zone F (AF) (362-327 cm)

The low concentration of calcareous benthic species further continues into assemblage zone F (Fig. 5.6; Fig. 5.7; Fig. 5.8). A zone dominated by *C. reniforme* by 29%, while *I. norcrossi* constitutes 18 % of the assemblage. Whereas, the two remaining main species remains relatively moderate-low.

One of the zone characteristics are higher abundance of the bottom current indicator *A. gallowayi* constituting 8% of the fauna at its peak, 5% on average. *Cassidulina neotertis* (8.4%) and *M. barleeanus* (8.4%) both increase in abundance. The trend of the graphs are very similar between the two species during the zone, both with peaks at 347 cm and at 332-327 cm. *Buccella* spp. averagely comprises 2.7% of the assemblage with a distinct peak at 352 cm equivalent to 7%. The remaining subspecies are low.

Six specimens of *Globobulimina auriculata* were collected at 347 cm and one specimen of *Bulimina marginata* was picked at 337 cm.

The agglutinated foraminiferal concentration is low-absent, with the exception of an abrupt higher concentration 337 cm, comprising 7% of the benthic fauna, whereby the predominating species is *Reophax scorpius* subsided by *Reophax difflugiformis*. The assemblage zone is almost barren of planktonic specimens.

5.4.7 Assemblage zone G (AG) (327-302 cm)

One of the defining features of this zone is the sudden increase in concentration of the calcareous benthic foraminiferas (Fig. 5.6; Fig. 5.7; Fig. 5.8). *Cassidulina reniforme* and the

seasonal sea ice indicator *I. norcrossi* dominates the assemblage, together comprising up 63% of the assemblage. *Elphidium excavatum* declines from 19.9% to 0.3% abundance through the assemblage zone. *Cibicides lobatulus* is at its lowest, constituting 1.2% of the assemblage.

The high biological productivity affiliated species *N. labradoricum* rise in abundance after its absence in foraminiferal assemblage zone F, comprising 4.5% on average. It initially peaks at 322 cm and 307 cm accounting for 7% and 6% of the assemblage respectively. *Melonis barleeanus* rises in relative abundance in an oscillating steady fashion similar to in the former zone, accounting for 9% of the assemblage on average. An increasing trend that in general has persisted upwards in the core. *S. loeblichi* is also well represented, but declines towards end top. *Cassidulina neoteretis* constitutes 3%, with lower abundance between 312-307 cm. The remaining secondary species constitutes lower proportions of the assemblage.

One pulse of higher agglutinated concentration is evident at 312 cm, but the agglutinated species only constitutes a fraction of the collected foraminiferas. Planktonic foraminiferal concentration is low.

5.5 Stable isotope analysis:

The stable isotope analysis are based on measurements on the six benthic foraminifera species: *I. norcrossi*, *E. excavatum*, *C. reniforme, N. labradoricum, M. barleeanus and C. lobatulus*.

The $\delta^{18}O$ values corrected for vital effects and ice volume effect (Fig. 5.9). The $\delta^{18}O$ values ranged from 4.297‰ (302 cm) to -0.31‰ (412 cm). Two low $\delta^{18}O$ anomalies of values -0.31‰ and 0.68‰ both obtained on M. *barleeanus* from 417 cm and 412 cm respectively, were considered questionable. Excluding the two anomaly values, the lowest obtained $\delta^{18}O$ value was 2.751‰ from 477 cm, the average $\delta^{18}O$ value is 3.540‰, with an overall increasing trend upwards.

The $\delta^{13}C$ values (Fig. 5.10) obtained from the epifaunal species *C. lobatulus* are confined to the upper half of the record, and shown separate from the other species, that are all infaunal. *Cibicides lobatulus* as an primarily epifaunal species has been reported to provide more reliable values of near bottom water $\delta^{13}C$, than typical infaunal species which probably record the $\delta^{13}C$ of the pore water (e.g. Duplessy et al., 1984; Ivanova et al., 2008; Zajaczkowski et al., 2010).

The phenomena is very evident at 522 cm were 1.26‰ was obtained from *C. lobatulus* and -0.851‰ from *C. reniforme*, and at 572 cm where C. lobatulus $\delta^{13}C$ was 1.292‰, *C. reniforme* -0.738 ‰. The *C. lobatulus* $\delta^{13}C$ values are ~>1‰ while the $\delta^{13}C$ values of *C. reniforme*, *N. labradoricum*, *M. barleeanus*, *E. excavatum* <0‰. The shallow infaunal-epifaunal *I. norcrossi* oscillates between 0.602 to -0.739‰ positive and negative values.

Fig 5.11 combines the uncorrected $\delta^{18}O$ and $\delta^{13}C$ values, illustrating the importance of the application of vital effects, by that each species plots in a specific field, which is related to their habitats (Zajaczkowski et al., 2010).

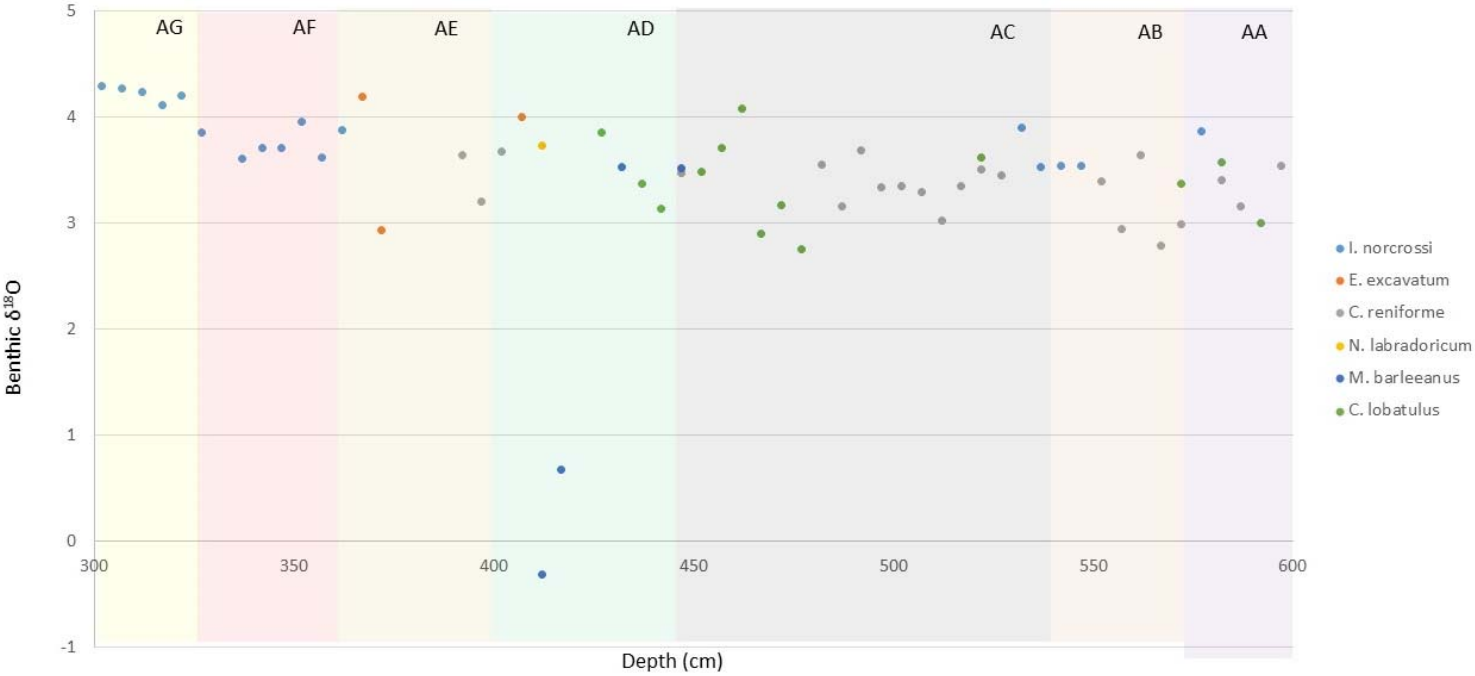

Figure 5.10: Benthic $\delta^{18}O$ values on selected species plotted against depth (cm) and their associated assemblage zones. Values are corrected for ice volumes effects and vital effects.

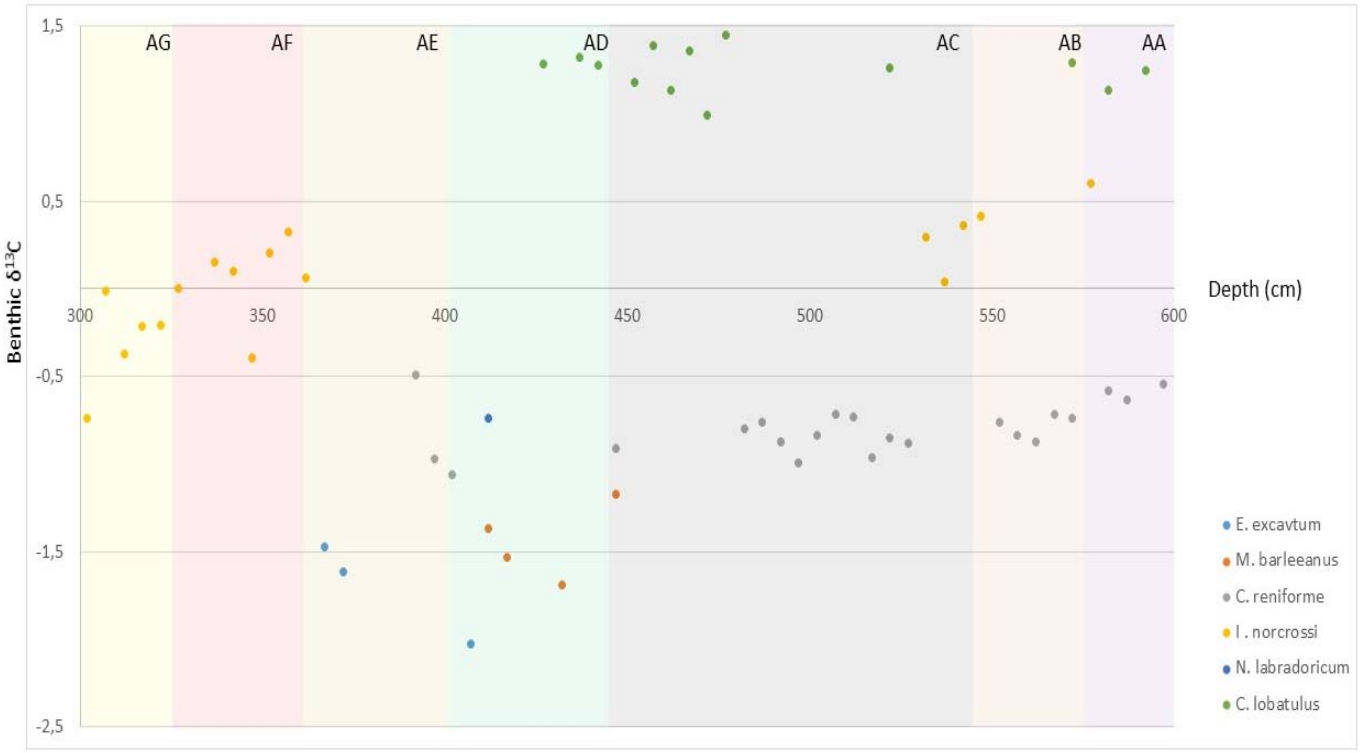

Figure 5.11: Benthic $\delta^{13}C$ values on selected species values plotted against depth (cm) and their associated assemblage zones.

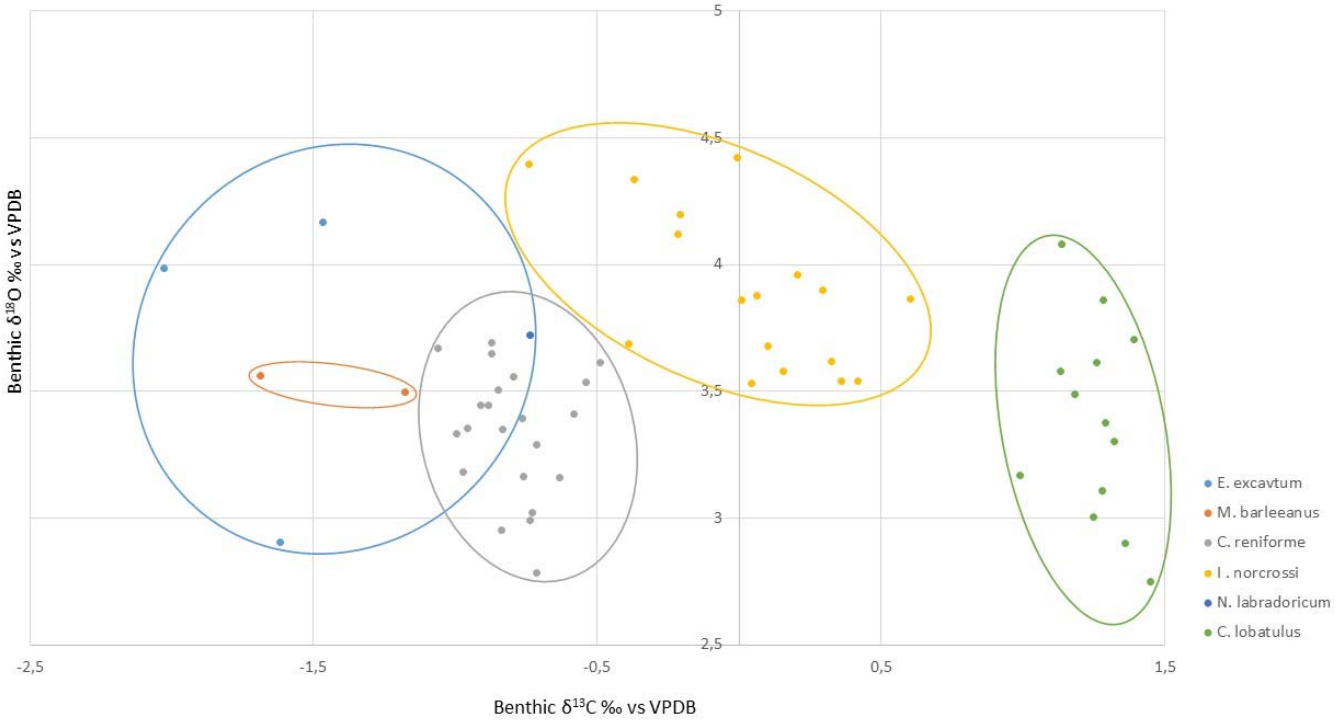

Figure 5.12: Uncorrected $\delta^{18}O$ values plotted against $\delta^{13}C$ values, illustrating the species tendencies to plot within specific fields.

5.6 CTD

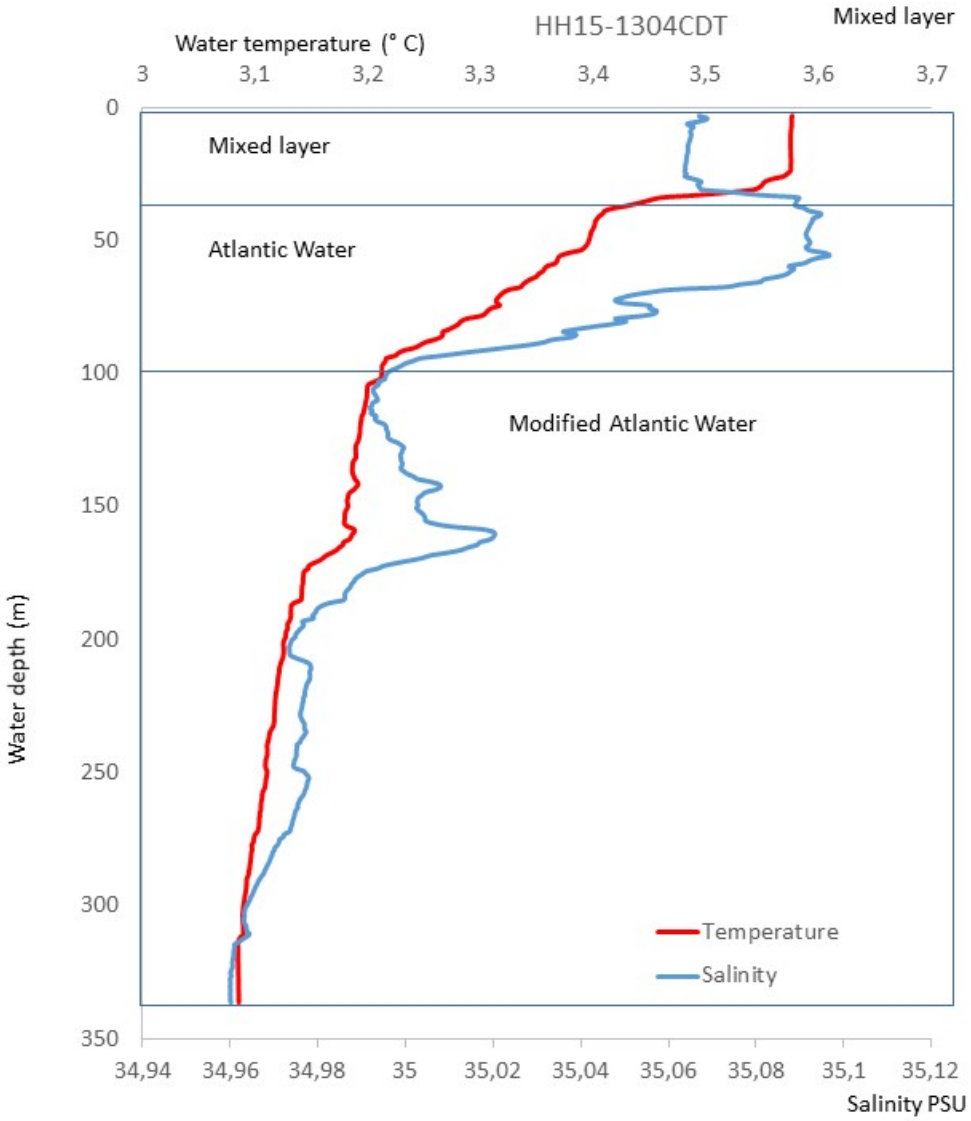

Figure 5.12: HH15-1304CTD from Leirdjupet. 01.08.2015.

6 CHRONOLOGY

Constructing a representative age calibration curve, rely on accurate ages, ages constraining time intervals of different characters. A general lack of reliable obtained ages, made it necessary to adopt additional ages, in order to better constrain the time periods. The following age calibration construction focus on the studied "foraminifera" interval i.e. 302-597 cm, the diamicton interval ~600-765 cm will not be considered in the construction of the age calibration graph due to its till origin.

The youngest obtained age in the core was 12,023 cal yr BP from 330 cm. The base of the study interval was set to 10,700 cal yr BP. Kovalenko (2015) had a dating equivalent to 10,606 cal yr BP from the HH14-012GC core from Leirdjupet, characterized by a large *N. labradoricum* peak (~45%). There was no significant corresponding *N. labradoricum* peaks in the study interval. The bottom of the study interval was thus, probably older than 10,606 cal yr BP.

It was further necessary to constrain the diamicton corresponding to unit 6, which represent Younger Dryas-Holocene transition. In one of the neighboring troughs, Kveithola the transition period appear to have had a short duration time, only 300 years (Groot et al., 2014). 300 years was thus added to the 12,023 cal yr BP, which is situated close to the bottom of the diamicton representing the transition period.

The Younger Dryas termination was therefore estimated to ~12,323 cal yr BP. But, it was further necessary to estimate the onset age, which was presumed to be equivalent to ~402 cm. The onset of the Allerød interstadial presumed starting ~447 cm was set to 14,000 yr BP after Hormes et al. (2013). The onset of the younger Dryas was estimated to 13,057 cal yr BP by linear extrapolation between the Younger Dryas termination ~367 cm and Allerød onset 447 cm.

The onset age 14,693 cal yr BP of the laminated unit 575-565 cm, correlated well to the onset age of a similar unit from Kveithola, which was delimited to ~14,400 cal yr BP (Rüther et al., 2012), and where thus applied to the termination of the unit.

The age of lowermost end of the study interval, was estimated by extrapolation, as a continuation from 14,000 to 14,693 cal yr BP. The boundary to the till was therefore set to 14,828 cal yr BP.

The sedimentation rates were calculated on the assumption of constant linear sedimentation rates, between the calibrated ages (fig. 6.1).

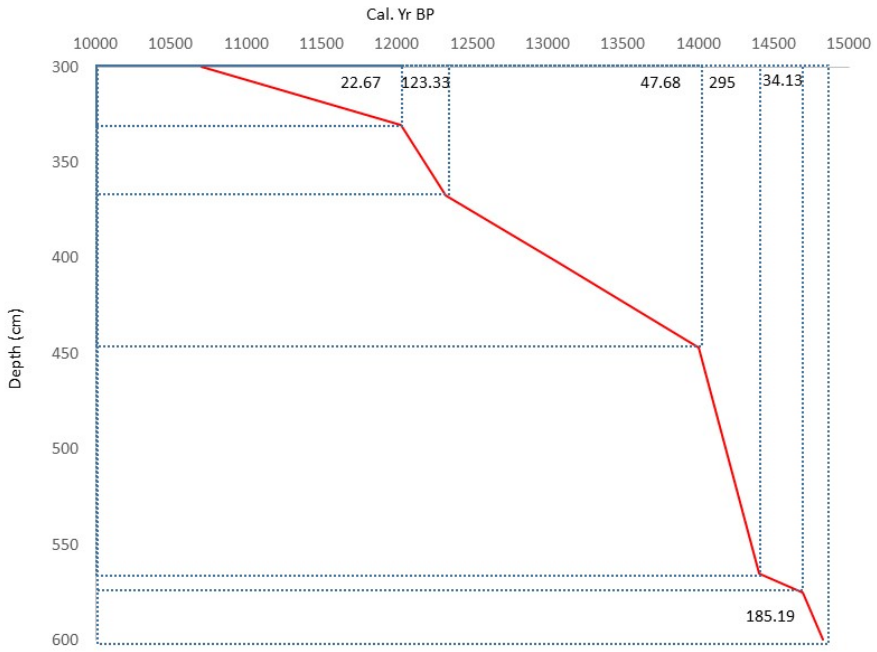

Figure 6.1: Age model, with linear sedimentation rates (cm/ka yr).

Age interval (cm)	Sedimentation rate/1000 yr
600-575	185.19
575-565	34.13
565-447	295
447-367	47.68
367-330	123.33
330-300	22.67

Table 6.1: Linear sedimentation rates as cm/ka yr

7 INTERPRETATION

The following chapter will focus on the obtained results, from the core HH15-1303PC, where the records are plotted against the calibrated age model. The aim is to establish a general interpretation of the prevailing environment at the site by combining the multiple records; lithology, IRD, foraminifera and stable isotopes.

The following five time periods were identified; the time prior to the deglaciation of Leirdjupet >14,800 cal yr BP, Bølling interstadial 14,800-14,000 cal yr BP, Allerød interstadial 14,000-13,000 cal yr BP, Younger Dryas stadial 13,000-12,300 cal yr BP, Younger Dryas-Holocene transition 12,300-11,800 cal yr BP and early Holocene 11,800-10,700 cal yr BP.

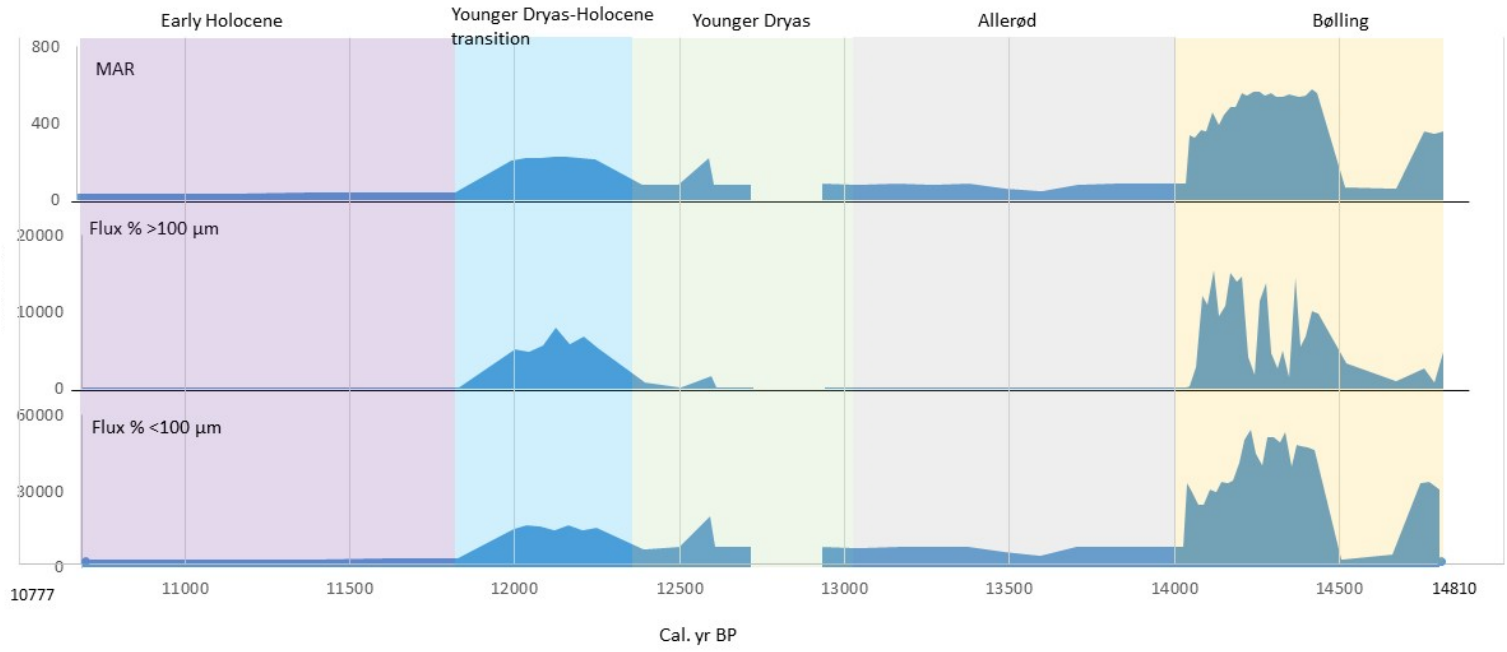

Figure 7.1: Mass accumulation rate (MAR) (g/cm²/ka), flux % >100µm (g/cm²/ka) and flux % <100 µm (g/cm²/ka) plotted against calibrated age BP.

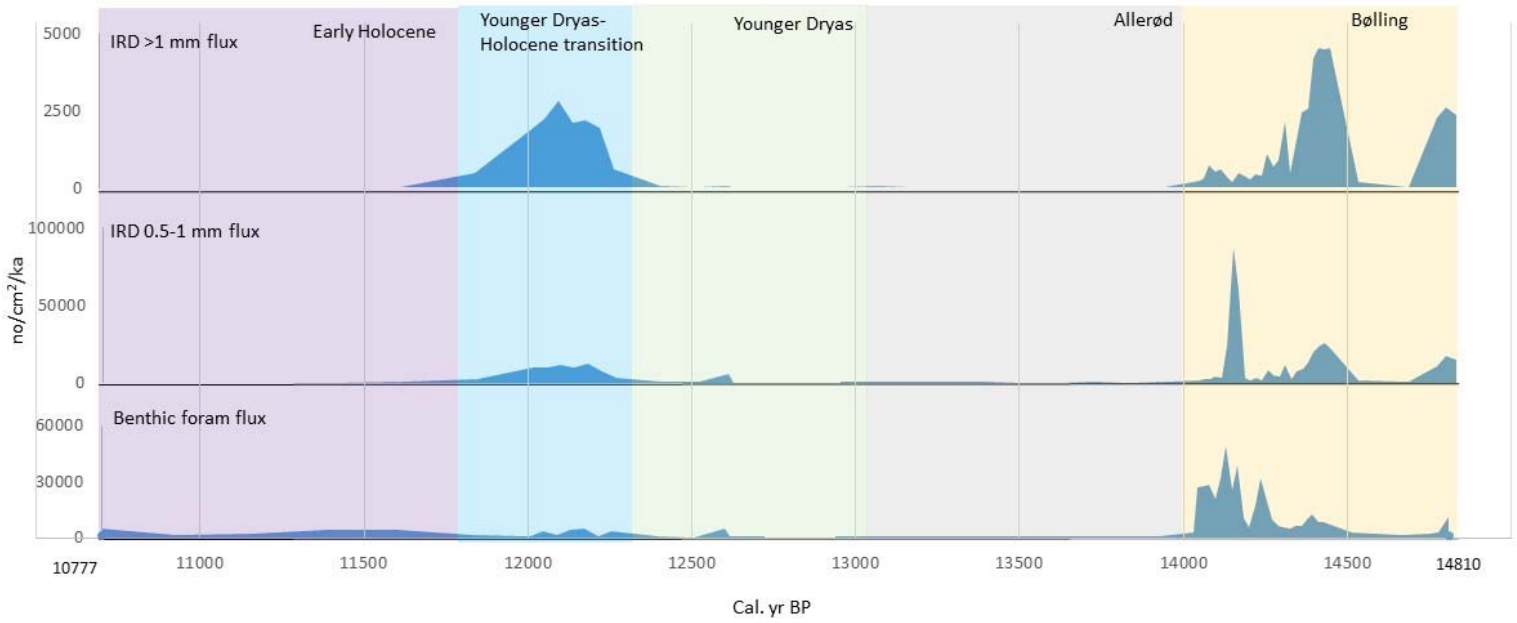

Figure 7.2: IRD flux, IRD flux 0.5-1 mm and benthic foraminifera flux plotted against the calibrated age BP.

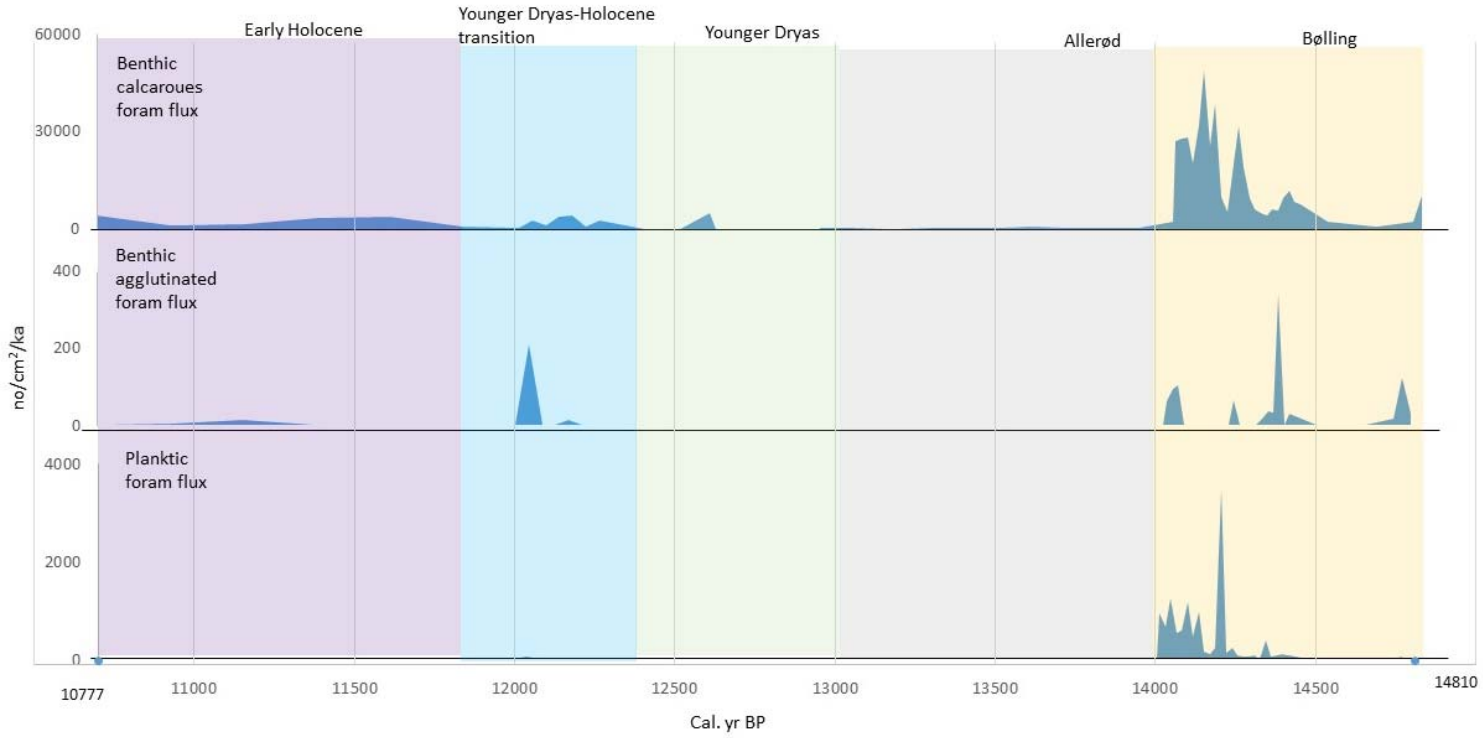

Figure 7.3: Benthic calcareous foraminifera flux, agglutinated foraminifera flux and planktic foraminifera flux plotted against calibrated age BP.

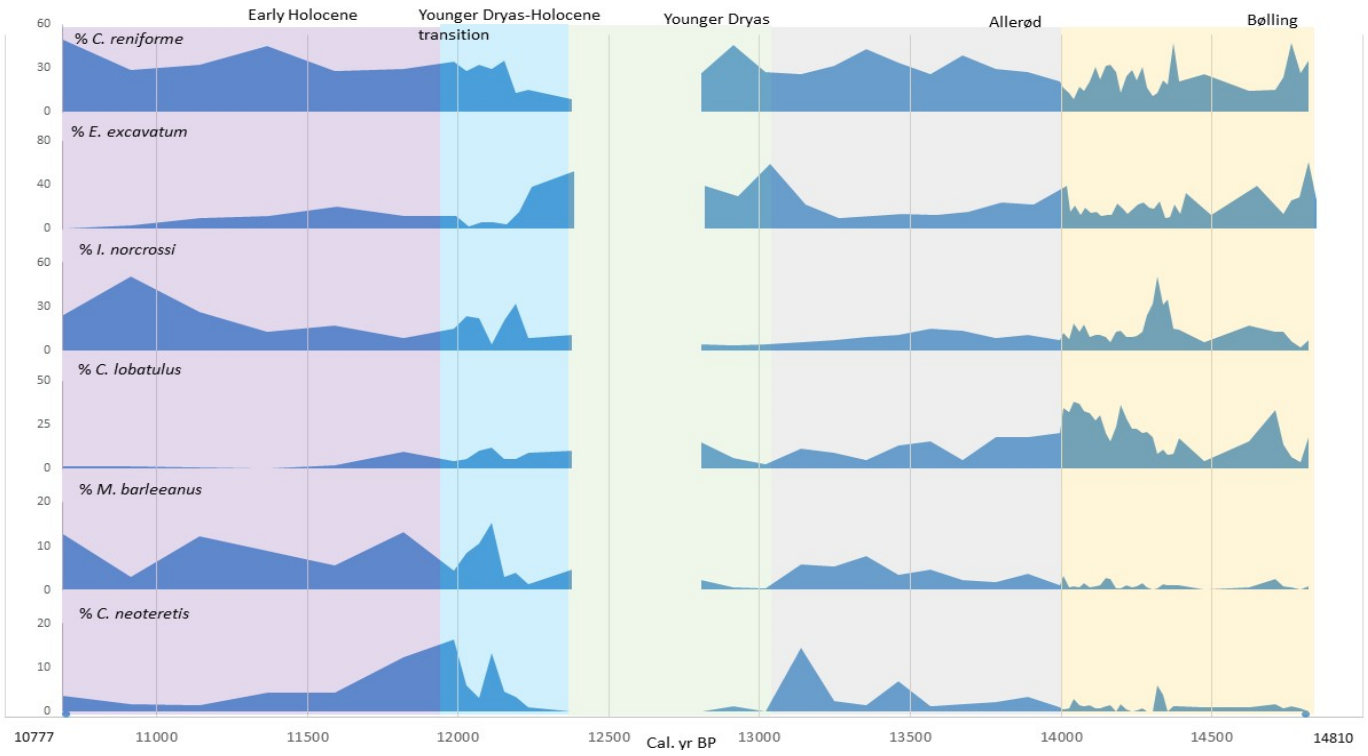

Figure 7.4: Relative % abundances of benthic foraminifera species in percentages plotted against calibrated age BP and associated time zones

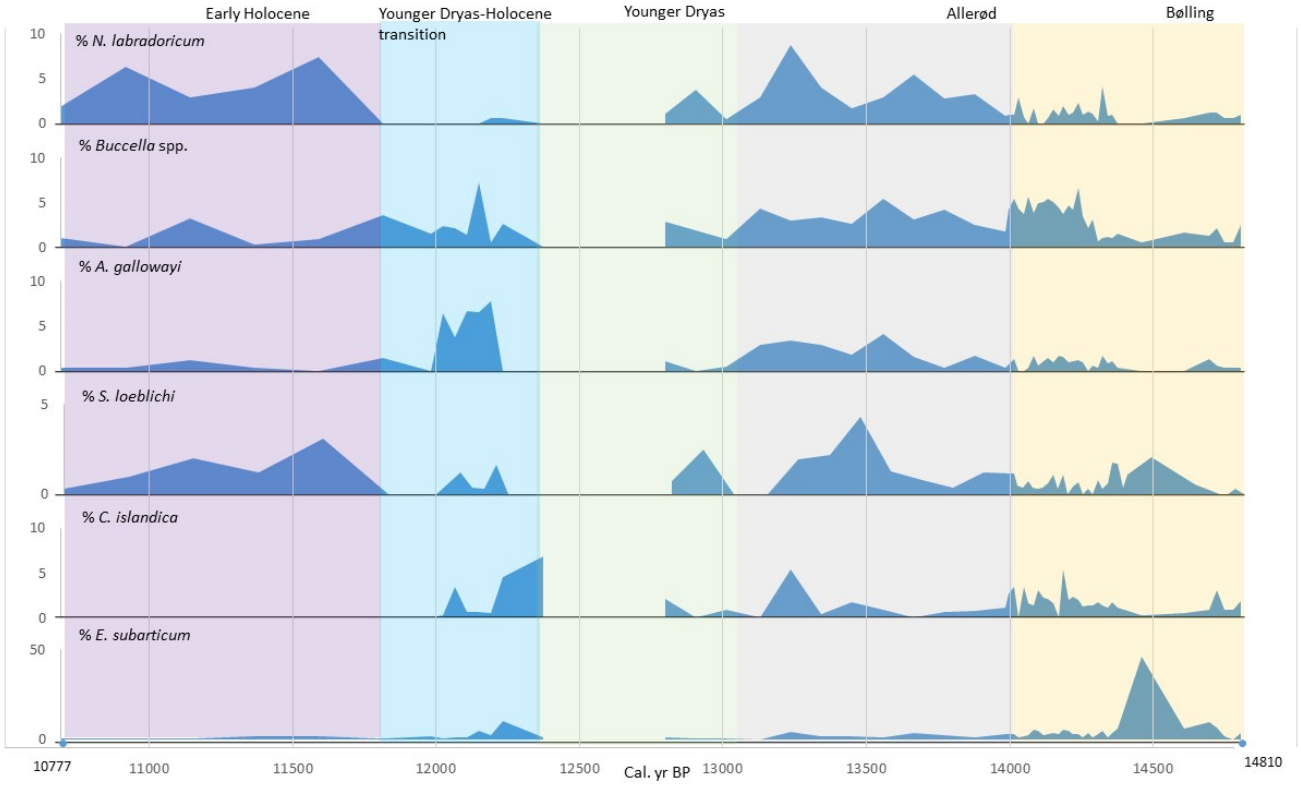

Figure 7.5: Relative abundances of benthic foraminifera species in percentages plotted against calibrated age BP.

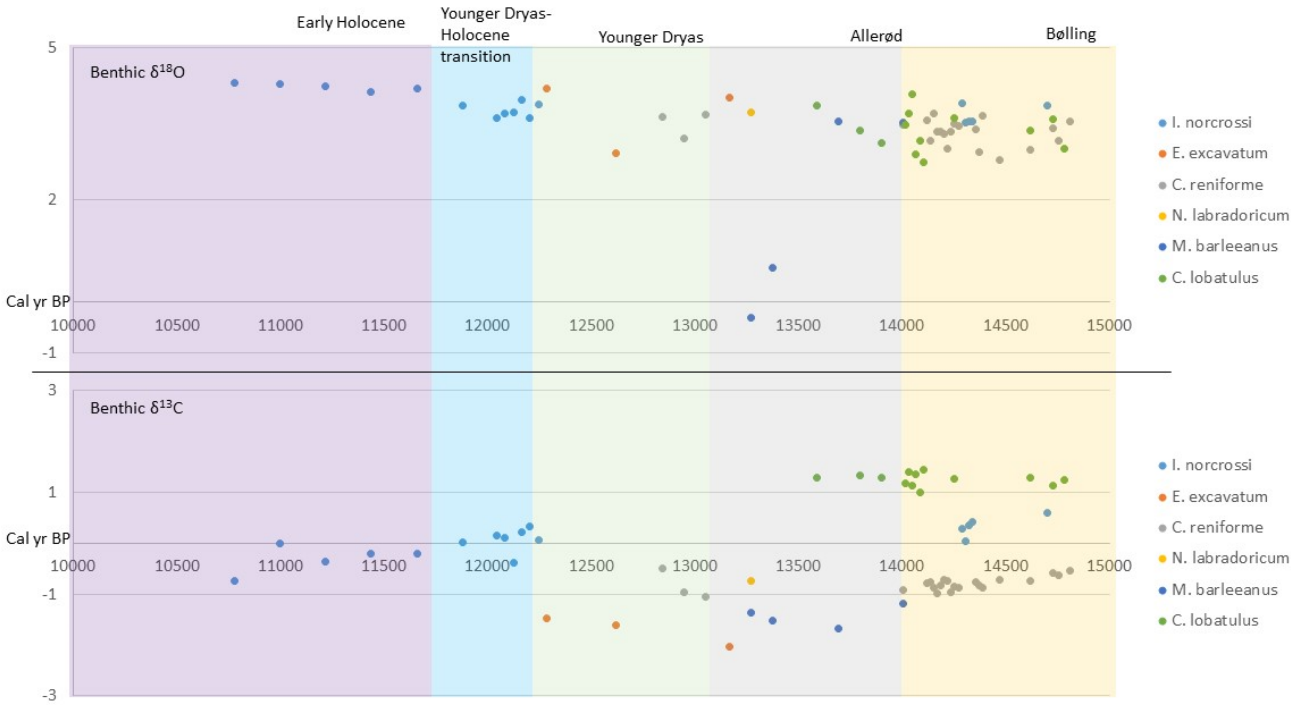

Figure 7.6: Benthic carbon δ13C and benthic oxygen δ18O isotope record, plotted against calibrated age BP.

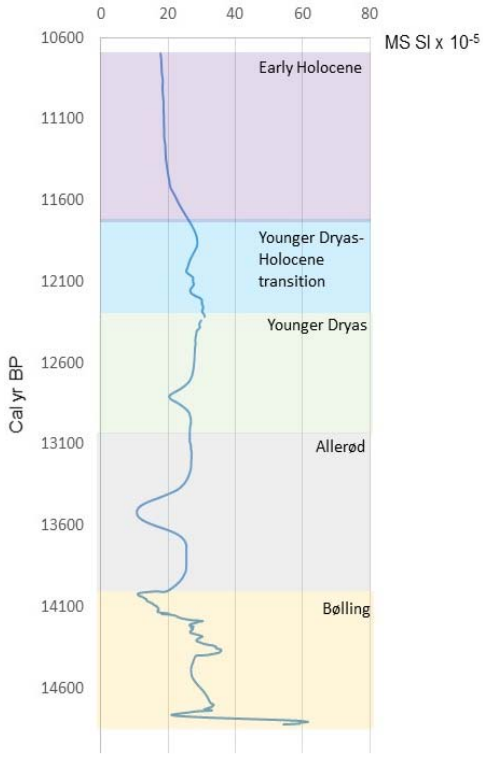

Figure 7.7: Magnetic susceptibility record plotted against calibrated age BP.

7.1 Time prior to the Leirdjupet deglaciation (>14,800 cal yr BP)

The massive compacted unsorted diamicton at the base corresponds to unit 1 extending 765.5-600 cm, show low porosity values and water content. This could suggest exposure to compaction. The magnetic susceptibility and wet bulk density was uniformly high throughout the record, probably related to units massive nature. The diamicton contained some scattered shell fragments, whereby one was dated to 45,040 cal yr BP, suggesting glacial reworking or radiocarbon contamination from older marine deposits. The diamicton is inferred as a till, probably subglacial till inferred from the overconsolidation.

7.2 Bølling interstadial (14,800-14,000 cal yr BP)

Bølling consist of four lithology units, and three foraminifera assemblage zones extending from 600-457 cm. Suggesting that the Bølling interstadial was very dynamic during the duration. Bølling is divided into four phases that will be interpreted separately.

First phase (14,800-14,700 cal yr BP)

The first phase stretching from 600-575 cm is an IRD rich diamicton characterized by high MS and wet bulk density values, which is a typical glaciomarine deposits (Elverhøi and Solheim, 1983). The estimated linear sedimentation rate was 185.19 g/cm^2/ka, which is further reflected in the high <100 μm and moderate >100 μm grain size sediment fluxes, that will be referred to as fine and coarse sediment flux respectively. The two opportunist species *E. excavatum* and *C. reniforme* initially dominates, in a low-moderate benthic foraminifera abundance. The high combined abundance indicates an ice proximal glaciomarine environment with low fluctuating salinities and high turbidity due to high sedimentation rates (Steinsund, 1994). The presence of IRD would suggest seasonally open waters, the absence of planktonic foraminifera are thus, probably related to the low salinities and/or turbidity of the surface waters, inhospitable conditions for planktonic foraminifera (e.g. Polyak et al., 2013).

Cibicides lobatulus and *I. norcrossi* gradually increased in relative abundance from 14,731 cal yr BP, which coincides with declining abundances of *E. excavatum* and *C. reniforme.* Probably reflecting increasing bottom current activity and increased salinities. Low abundances of typical Atlantic Water affiliated species; *Cassidulina neoteretis*, *M. barleeanus* and *P. williamsoni* indicates presence of Atlantic Water at the site (Mackensen et al., 1985; Steinsund, 1994; Wollenburg and Mackensen, 1998). The lowered combined abundance of *E. excavatum* and *C. reniforme* can further be a result of a relative movement in the proximal grounding line position due to the escalating iceberg calving. High positive $\delta^{13}C$ *C. lobatulus* values (1.248-1.132 ‰), further backs ongoing water mass advection at the sea-bottom. The increasing benthic $\delta^{18}O$ values ranging between 3.003-3.886‰, relatively low-moderate values, probably reflects the increased salinity. The moderate benthic infaunal $\delta^{13}C$ values ranging from -0.541‰ to -0.634‰ reflects a poorly ventilated pore waters, related to water mass stratification as a result of high meltwater concentration.

Second phase (14,700-14,400 cal yr BP)

The following phase is marked by a sharp change in the lithology, as rhythmically laminated (sandy) mud succeed the diamicton from 575-565 cm, the MS, wet bulk density drops correspondingly, while porosity and water saturation increase. A significantly lowered linear sedimentation rate equivalent to 34 $g/cm^2/ka$, is further reflected in the reduced low fine and coarse sediment fluxes. The lamination is probably related to deposition by suspension settling, from a meltwater plume with a fluctuating discharge. The thickness of the individual couplets, are not thick enough to imply any immediate proximity to any subglacial grounding line (Cofaight and Dowdeswell, 2001). The high relative abundances of *Excavatum* spp., further support a bottom environment characterized by meltwater influence, causing a freshening in the bottom waters (Steinsund, 1994). *Cibicides lobatulus* (15.5%) with $\delta^{13}C$ value 1.292‰, *I. norcrossi* (17.81%) and *C. reniforme* (14.9%) abundances are moderate in

the early stages of the phase, suggesting presence of moderate strong bottom currents, and moderate salinities. Low presence of typical Atlantic Water associated species e.g. *C. neoteretis*, *M. barleeanus* and *N. labradoricum* possibly reflects a weak Atlantic Water influence at the site (Steinsund, 1994). The subsequent decrease in *C. lobatulus*, *C. reniforme* and *I. norcrossi* abundances are probably related to a bottom current weakening and implications related to the meltwater discharge. The lack of IRD can be related to a semi-permanent extensive sea ice cover, as it would be capable to hamper iceberg drifting, which is further evident by the increasing abundance sea ice associated species *S. loeblichi* (Steinsund, 1994). It would further explain the persistent lack of planktonic foraminifera. The three obtained $\delta^{18}O$ values ranged between 3.375-2.783‰, relatively low values inferred to reflect the cold fresh meltwater. Low benthic $\delta^{13}C$ infaunal values ranging from -0.715 to -0.738‰, can be related to a strong water mass stratification.

Third phase (14,400-14,300cal yr BP)

Bølling interstadials third phase is characterized by the reappearance of the typical glaciomarine deposits composed by IRD rich diamicton, with high MS and wet bulk density values, representing a second pulse of calving iceberg from 565-542 cm (Elverhøi and Solheim, 1983). The linear sedimentation rate was estimated to 295 $g/cm^2/ka$, consequently leading to high corresponding fine and coarse sediment fluxes. In a fauna with moderate benthic foraminifera abundance, *C. reniforme* and *I. norcrossi* are the more prominent species, while the prevalence of *E. excavatum* diminish concordant with the gradually more prominent *I. norcrossi*. Such a shift probably reflect a transition into a more glacier distal environment, with higher salinities originating from a growing influence of cold saline Atlantic Water and proximity to a productive sea ice margin, which is particularly evident by the presence of *N. labradoricum* 14,388 cal yr BP (Steinsund, 1994; Hald and Korsun, 1997). A species thriving in areas with high organic productivity (Steinsund, 1994). The low

planktonic foraminifera abundance probably indicates persisting unfavorable surface water conditions due to presence of cold fresh turbid surface polar water, which were seasonally covered by sea ice. The moderate $\delta^{18}O$ values ranging from 2.951-3.647‰, which are enhanced compared to the laminated unit probably to reflect higher bottom water salinities. The low $\delta^{13}C$ benthic infaunal values ranging from -0.764‰ to -0.872‰ probably reflects a stratified water column, due to the fresh surface waters, hampering ventilation in the pore waters.

Fourth phase (14,300-14,000 cal yr BP)

The diamicton gradually develops into less defined laminated sandy mud with correspondingly lower MS values as the IRD flux decrease, eventually ceased. The interval stretches from 542-447 cm. A peculiar IRD 0.5-1mm IRD flux pulse peak occurs at 14,119-14,102 cal yr BP (Fig. 5.1). However, the peak should be considered as an artifact, disturbed interval caused by suction (chapter 3.3). The samples concerning the interval 14,051-14,014 cal yr BP was neither firm nor intact suggesting that they was affected and should thus be considered ignored. The fine and coarse grain flux remains high, due to the persisting high linear sedimentation rate 295 g/cm^2/ka. The total benthic foraminiferal abundance progressively increased to moderately values, where *C. lobatulus*, *C. reniforme* and *E. excavatum* are the more prominent species. Synchronous to a decreasing eventually stabilizing *I. norcrossi* abundance, are the increasing abundance of *Buccella* spp.. Two species which are very similar in terms of their modern environmental preferences, *I. norcrossi* in comparison to *Buccella* spp., appear to thrive at deeper depths with finer sediments (Steinsund, 1994). *Buccella* spp. is mainly though to respond to the food availably, irrespective origin (Seidenkrantz, 2013), and further shows a lower toleration towards higher sedimentation rates and thrives in colder bottom waters (Zajaczkowski et al., 2010; Chauhan et al., 2015). *Buccella frigida* and *C. lobatulus* often co-appear in glacier distal environments

with stable salinities and is often related to sandy sediments (Kubischta et al., 2010). The fauna is inferred as a glaciomarine, glacier distal environment. The bottom waters were probably cold and saline, under the influence of strong vigorous bottom currents as the Atlantic Water flow became more intense, further complemented by high $\delta^{13}C$ *C. lobatulus* value 1.26‰ 14,254 cal yr BP and low abundances of typical Atlantic Water associated species; *C. neoteretis*, *M. barleeanus* and *N. labradoricum*. The strong bottom currents caused winnowing, which explains the sand higher sand content, favorable conditions for the *C. lobatulus* (Mackensen et al., 1985). The grain size progressively decreased through the sequence, indicating decreasing flow competence, which is typical for more glacier distal settings. A confined planktonic foraminiferal peak 14,203 cal yr BP, in addition to continues presence *of Buccella* spp. and *I. norcrossi* points to seasonally open surface waters. The moderate-low $\delta^{18}O$ values presumably reflect higher bottom water temperatures. Moderate $\delta^{13}C$ benthic infaunal values probably reflect some pore water ventilation, or moderate primary production.

7.3 Allerød interstadial (14,000-13,000 cal yr BP

Allerød is equivalent to 447-402 cm, the transition into Allerød is primarily inferred by the abrupt change to lower benthic foramina abundances, in addition to a predominance of mud. Similarly to Bølling fourth phase, there is an occurrence of an imploded- alternated interval, suspected being caused by suction during the piston coring process, which concerns the interval 13,587-13,419 cal yr BP (Fig. 5.1). The sediments are predominantly mud with high porosities and water content, lowered wet bulk densities, deposited under moderate linear sedimentation rates 47.68 g/cm^2/ka. The MS values are slightly lowered linked to absent flux of coarse sediment, while the fine sediment flux is relatively moderate. Such a shift was probably related to a reduced bottom current intensities. This is further evident from the lower *C. lobatulus* abundance, reflecting reduced bottom current energy regime on the ocean floor

bottom current activity at sea bottom compared to late Bølling (Mackensen et al., 1985). *Cassidulina reniforme* dominates in a low benthic foraminiferal abundance, complemented by *E. excavatum*, *C. lobatulus* and *I. norcrossi* as secondary species (Steinsund, 1994). In addition to the consistent moderate abundances of the accessory species *C. neoteretis*, *M. barleeanus*, *N. labradoricum* and *Buccella* spp., the fauna assemblage is assumed to reflect a higher presence of a chilled saline Atlantic Water advection and extensive sea ice cover (Steinsund, 1994). Allerød interstadial is almost barren of planktic foraminifera, despite food and nutrients appear to be readily available, backed by the combined presence of *Buccella* spp., *N. labradoricum*, *M. barleeanus* and *I. norcrossi,* species affiliated high seasonal productivity, thus influx of food and nutrients (Steinsund, 1994; Seidenkrantz, 2013).

Relatively moderate $\delta^{18}O$ values (3.131-4.004‰) increasing towards Younger Dryas stadial probably reflects decreasing bottom water temperatures. Two low benthic $\delta^{18}O$ anomalies values -0.31‰ and 0.68‰ obtained from *M. barleeanus* between 13,377-13,272 cal yr BP, could suggest episodic downward transport of brine water. The species are often related to cascading brine waters (Polyak et al., 2002). The time interval coincides with a peak in the *N. labradoricum* abundance and a diverse fauna, suggesting that the food availably was good, possibly related to proximity to the marginal ice zone or oceanic front. The benthic infaunal $\delta^{13}C$ values are generally relatively low, suggesting poorly ventilated pore waters.

7.4 Younger Dryas 13,000-12,300 cal yr BP

The Younger Dryas stadial (YD) stretches from 402-367 cm. The transition into the cold stadial is defined by a pronounced *E. excavatum* abundance peak in a fauna assemblage almost barren of foraminifera. The transition is unclear in the lithology and the physical properties records, which remains close to unchanged with a mud predominance. The linear sedimentation rate was the same as during Allerød interstadial 47,68 g/cm^2/ka. *Elphidium excavatum* and *C. reniforme*, in addition to the abnormally low fauna concentration probably

indicate a significant climate deterioration with cold bottom waters with low fluctuating salinities and a general nutrient/food depletion, suited for the two opportunists species (Steinsund, 1994). Their dominance supplemented by the increasing abundance of *S. loeblichi* probably reflects an extensive perennial-semi perennial sea ice, conditions inhospitable for any planktonic foraminifera to persist. The glaciomarine bottom environment appear to undergo an a short term improvement ~12,697 cal yr BP as evident by the combined abundance of *Buccella* spp., *M. barleeanus*, *N. labradoricum* and *C. lobatulus* implying that some food flux became available for consumption possibly related seasonally open surface water (Steinsund, 1994; Seidenkrantz, 2013). The short-term bottom water improvement was subsequently followed by a period barren of foraminifera 12,738-12,529 cal yr BP. It can be interpreted as. the prevalence of exceptionally inhospitable bottom conditions for primary production or as the of result episodic dissolution related to corrosive waters. The depleted benthic $\delta^{18}O$ values can suggest downward transport of brine water, related to sea ice formation, or decreased salinities related to advection of cold fresh Polar Water. While low benthic infaunal $\delta^{13}C$ values suggest poor ventilation or reflects the low primary production. The termination of Younger Dryas appear to have been cold as *E. excavatum* peak once more, moderate abundance of *C. lobatulus*, *I. norcrossi* and accessory species *M. barleeanus* could suggest limited advection of chilled Atlantic Water, as *M. barleeanus* is commonly associated with Atlantic water in the Arctic region (Mackensen et al., 1985; Steinsund, 1994; Polyak et al., 2002).

7.5 Younger Dryas-Holocene transition (12,300-11,800 cal yr BP)

The transition into Holocene happens through a gradual IRD enriched phase, which stretch 367-325 cm. The sediments develops from laminated sandy mud towards a IRD enriched diamicton, with a corresponding small elevated wet bulk density and MS values. Both the fine sediment flux and the coarse sediment flux increase as sand and IRD constitute a greater

portion of the sediments, the linear sedimentation rate remains the estimated 123.33 g/cm^2/ka. *Elphidium excavatum* initially dominates, indicating cold conditions with low fluctuating salinities in a stressed environment, but are replaced 12,319 cal yr BP by a fauna dominated by *C. reniforme* with *I. norcrossi* as descent second, probably suggesting a general improvement in the bottom environments. Probably due to Atlantic Water advection that gradually strengthened, evident by a continues moderate presence of the two Atlantic Water associated species *C. neoteretis* and *M. barleeanus*, in addition to the moderate presence of *C. lobatulus* and *A. gallowavyi* suggesting strong-moderate bottom current advection (Mackensen et al., 1985; Steinsund, 1994; Polyak et al., 2002). The presence of IRD implies that icebergs passed the site, as the surface waters was seasonally open. The low planktonic abundance is thus probably a result of cold turbid surface waters. *Astronion gallowavyi* shows a similar distribution to that of *C. lobatulus*, but relies on a steadier food supply (Rasmussen et al., 2007), which also applies for *I. norcrossi* and *Buccella* spp. (Steinsund, 1994; Seidenkrantz, 2013), two species commonly associated with lower sedimentation rates (Steinsund, 1994; Zajaczkowski et al., 2002). The food supply was probably high, related to the ice margin, but the benthic foraminifera flux remained low, probably as an effect of turbid bottom waters, as a result of high sedimentation rates. The moderate decreasing benthic $\delta^{18}O$ probably reflects initial cold bottom temperatures, that later warmed as evident from the correlation to *E. excavatum.* Alternatively presence of fresh meltwater.

7.6 Early Holocene 11,300-10,200 cal yr BP

Early Holocene covers the depth interval 325-300 cm. The sediments are predominantly mud as the IRD flux ceases, further reflected by sudden absence of the coarse sediment flux, lowered MS and wet bulk densities with correspondingly higher porosities and water saturation levels as compared to the transition phase. The fine sediment flux is low, as an effect of low mass accumulation rates, despite moderate linear accumulation rates 22.67

g/cm^2/ka. The foraminifera fauna is dominated by *C. reniforme* with an increasingly more abundant *I. norcrossi* and gradually decreasing *E. excavatum* as the two more prominent species after *C. reniforme,* indicating that the early stages of the time period was cold with low fluctuating salinities (Steinsund, 1994). Continues presence of *C. neoteretis*, *M. barleeanus* and *N. labradoricum* reflects a strong continues inflow of saline Atlantic Water at the site, which gradually improved the bottom water environment (Steinsund, 1994; Hald and Korsun. 1997). *Melonis barleeanus* is the more abundant of the Atlantic Water associated species, a species showing a preference towards high salinities, fine sediment with high organic detritus (Steinsund, 1994). The sea ice cover was probably seasonal, inferred by the higher presence of *I. norcrossi* and presence of *S loeblichi* (Steinsund, 1994). Planktonic foraminiferas remained close to absent despite the seasonally opened waters, possibly as consequence of surface waters still occupied by cold fresh waters that further forced the weak Atlantic Water advection to flow subsurface. Compiled with the lack of IRD, this probably indicate a shift from a glaciomarine to a more stable marine environment. Increasing $\delta^{18}O$ values probably reflects Atlantic Water derived by the North Cape Current, which is known for higher $\delta^{18}O$ values and lower abundance of *C. neoteretis* (Lubinski et al., 2001).

8 DISCUSSION

Prior to the deglaciation >14,800 cal yr BP

The firm massive diamicton could possibly be of glaciomarine origin having been formed as iceberg keel ploughing the seafloor through reworking and eroding the sediments as its been dragged by wind and currents, which is common feature in front of modern Antarctic marine glaciers (Barnes and Lien, 1987; Svendsen et al., 1996). Coarse and unsorted in character are furthermore debris flow deposits which is known to leave a unrespondent magnetic susceptibility record similar to the case, but debris flows are more confined to the slope systems encircling the Barents Sea (Rasmussen et al., 2007; Jessen et al., 2010). Although plausible, the diamicton was interpreted as a till. It can be difficult to differentiate between icebergs and till in particular; icebergs will often tend to leave diamictons, which is less homogenous (Svendsen et al., 1996; Hald et al., 1990). The stiffness grade and compaction presumably due to overconsolidation of the till deposit probably hindered the piston corer from any deeper penetration, and the force upon impact in contact with the till could be responsible for the two collapsed water enriched intervals in section 5, further adding to subglacial origin. The till would have originated from a time the coring site were over-run by a grounded ice stream draining the Svalbard Barents Sea Ice Sheet forming and deforming the diamicton (Elverhøi and Solheim, 1983; Elverhøi et al., 1993) i.e. a subglacial till deposit. One age was obtained from a shelf fragment within the till, yielding ~45 ka cal yr BP. Svendsen et al. (1996) dated similar shell fragments in diamicton inferred as a till with similar high results, suggesting reworking of older marine sediments. Similar tills overlaying glaciomarine sediments is widely distributed around the Barents Sea (e.g. Elverhøi and Bomstad, 1980; Elverhøi and Solheim, 1983; Hald et al., 1989; Vassmyr and Vorren, 1990; Elverhøi et al., 1993; Svendsen et al., 1996), reflecting the LGM where the BSIS grounded in the troughs (Lubinski et al., 1996; Lubinski et al., 2001). In comparison have studies shown

that the Fram Strait and the western Svalbard margin experienced seasonally open water with inflow of cooled Atlantic surface water from the West Spitsbergen Current (e.g. Hebbeln et al., 1994; Rasmussen et al.,2007).

The transverse ridge at 300-360 m water depth (fig 2.3) separating Leirdjupet trough from Bjørnøyrenna at the distal end of Leirdjupet has been interpreted as a moraine ridge based on the positioning at the termination of the trough, the unsorted sediment composition (boulder-clay) and the morphology including the asymmetric pattern with steepest slop facing southwards/distal to the ice stream (Elverhøi and Kristoffersen, 1977; Elverhøi and Solheim, 1983). The preservation level led Elverhøi and Kristoffersen (1977b) to suggest a relation to the youngest major glacial stage where ice streams drained down Leirdjupet terminating in contact with Bjørnøyrenna ice stream, acting as conveyor belts transferring ice and sediments from an ice dome located over Spitsbergenbanken (Elverhøi and Solheim, 1983).

Constraining the timing of the Leirdjupet deglaciation

A collection of foraminifera in glaciomarine sediments above the till was dated to 20,908 cal yr BP, a minimum Leirdjupet deglaciation onset age. The age almost correspond to the first of at least two late Weichsel advances (22 ka cal yr BP and after 19 ka cal yr BP) (Laberg and Vorren, 1996). Minimum ages constraining the deglaciation in the Barents Sea is sparse due to limited datable material, consequently resulting in poor retreat chronologies (Jackobsson et al., 2014; Patton et al., 2015). The initial deglaciation of Bjørnøyrenna appear to coincide with a slow rising global eustatic sea level that probably initiated the Bjørnøyrenna deglaciation (Landvik et al., 1998; Winsborrow 2010). Bjørnøyrenna deglaciation ages are sparse, but appear to have initiated sometime prior to 17,6-17 cal yr based on a meltwater pulse (Bischof, 1994), the first and oldest retreat stage has been dated to 17,1 cal yr BP (Rüther et al., 2011). Earlier deglaciation onset ages have been suggested for the western Svalbard margin 20,5 +/- 500 ka cal yr BP soon after the LGM (Jessen et al., 2010), possibly >19 ka cal yr BP in the

outermost Storfjorden and more uncertain Kveithola (Rasmussen et al., 2007; Bjarnadottir et al., 2013) and > 18,7 ka cal yr BP for northern Ingøydjupet (Junttila et al., 2010). A complex deglaciation pattern. BSIS splitted into several ice domes during the deglaciation (Hughes et al., 2016). The Storfjorden-Kveithola system was comparably smaller than Bjørnøyrenna with different basin configurations, with a considerable smaller catchment area (Elverhøi et al., 1998; Rebesco et al., 2011), thus shorter distance from source to ice margin i.e. potentially shorter ice residence time, responding quicker to climatic changes (Cofaight et al., 2008; Rebesco et al., 2011). Storfjordens vicinity to the Fram Strait and its throughput of the West Spitsbergen Current and the climatic complications it entails are factors that could explain the time differences between the two systems (Rebesco et al., 2011). Although Storfjorden glaciation onset were earlier, the retreat was slower, possibly due to shallower bathymetry and proximity to terrestrial ice centers (Patton et al., 2015). While the deglaciation onset age of Ingøydjupet reflects the Fennoscandian ice system deglaciation (Vorren and Kristoffersen, 1986; Junttila et al., 2010; Patton et al., 2015). The Barents Sea Ice Sheet and the Fennoscandian Ice Sheets were confluent during the late Weichel (Andreassen et al., 2008; Winsborrow et al., 2010). The separation occurred approaching the deglaciation, inflicted large-scale ice flow reorganization (Andreassen et al., 2008; Winsborrow et al., 2010). Bjarnadottir et al. (2012) speculated whether the small and confined Kveithola was more susceptible to external forcing in terms of glaciodynamics than neighboring systems (Cofaight et al., 2008). If analogues with Leirdjupet, it could imply that ice margin responses are fast in Leirdjupet. Another age was obtained 25 cm further up, dated 14,693 cal yr BP. Unless presence of a hiatus is present, 25 cm accumulated sediments in ~6000 years seems doubtful. The credibility of the 20,908 cal yr BP age could therefore be questioned, suggesting that the sample were contaminated with older radiocarbon or some of the foraminifera were redeposited from the underlying till. A minimum age of 14,800 cal yr BP was adapted by

linear extrapolation of the Bølling 14,000-14,693 by the assumption of a constant sedimentation rate.

Bølling Allerød interstadial (14,800-13,000cal yr BP)

The transition from the subglacial till into the IRD enriched diamicton marks the minimum transition time into the initial deglaciation and the correspondent environmental shift at the coring site from a subglacial into a glaciomarine setting. The IRD are inferred to derive from melting icebergs passing the site indicating the destabilization of ice sheets. The disintegration was probably a consequence of sea level rise and increasing solar radiation causing enhancing calving rates (e.g. Aagaard-Sørensen et al., 2010). Similar IRD sediment sequences have been reported from e.g. Bjørnøyrenna (Elverhøi and Bomstad, 1980), Storfjorden slope (Lucchi et al., 2013), western Svalbard slope (Jessen et al., 2010), Ingøydjupet (Junttila et al., 2010; Aagaard-Sørensen et al., 2010; Pau et al., 2014) and Isfjorden (Svendsen et al., 1996). The environment during the transition into Bølling is interpreted as a polar environment where the bottom conditions were turbid, cold and of variable salinity due suspension settling from buoyant subglacial meltwater due to proximity to glaciers, dominated by a fauna *E. excavatum* and *C. reniforme* fauna. Low abundances of *C. neoteretis*, *M barleeanus* and *P williamsoni* indicates that some Atlantic Water advection was taking place at the site. The reestablishment of the North Cape Current required a deglaciation of the deep trough Bjørnøyrenna and the shallower central parts of the Barents Sea in order for it to pass through (Hald et al., 1999; Lubinski et al., 2001). According to Lubinski et al. (2001) could the initiation have taken place between 15-13 ka ^{14}C.

Glaciomarine diamictons on top of till deposits have been associated with floating ice shelfs, where deposition of the glaciomarine diamictons occurs beneath the floating margin (ice shelf) of ice streams by basal melting (Anderson et al., 1991). Elverhøi and Kristoffersen (1977) and Elverhøi and Solheim (1983) suggested that the moraine ridge at the termination

of Leirdjupet was formed by an ice stream under influence of buoyancy and speculated whether the moraine ridge and the glaciomarine sediments where deposited synchronously.

The short lasting event with fine grained rhythmically laminated sediments with low magnetic susceptibility starting 14,693 cal yr BP in Leirdjupet are widespread around the Barents Sea region, e.g. southwestern Svalbard (Rasmussen et al., 2007), western Svalbard slope (Jessen et al., 2010), northern Svalbard (Klitgaard-Kristensen et al., 2013), Ingøydjupet (Aagaard-Sørensen et al., 2010), Kveithola (Rüther et al., 2012; Lucchi et al., 2013) and Isfjorden (Svendsen et al., 1996) and corresponds to Older Dryas (Stanford et al., 2006). Despite some minor time discrepancies between the areas/sites, they appear to be close to synchronous (Jessen et al., 2010). Which have put them association with the meltwater pulse mwp-1a that raised global sea levels by ~20 m in a matter of 500 years (Deschamps et al., 2012; Lucchi et al., 2013; Lucchi et al., 2015). Loss of ice mass from BSIS, by lift up/floatation with escalating ice calving and subsequent grounding line retreat on some of the shallower marine grounded ice streams (e.g. Storfjorden, Kveithola) has been suggested to have contributed significantly to the progressing sea level rise (Lucchi et al., 2013). The general interpretation are fairly consistent, inferred as a glaciomarine environment characterized by high sedimentation rates by a turbulent buoyant seasonal/cyclic fluctuating subglacial meltwater (e.g. Elverhøi et al., 1995; Svendsen et al., 1996; Rasmussen et al., 2007; Jessen et al., 2010; Aagard-Sørensen et al., 2010; Klitgaard-Kristensen et al., 2013), as a response to rapid ice melting and ice margin retreat towards more distal settings (Jessen et al., 2010; Klitgaard-Kristensen et al., 2013). As a consequence the bottom waters at the site experienced a freshening as evident in the stable oxygen isotopes record as a low $\delta^{18}O$ and the dominance of *Elphidium* species indicating low fluctuating salinities (Steinsund, 1994). The thickness of the regional stratigraphic laminated unit are more varied, the 10 cm thickness in Leirdjupet could be considered limited in that respect. The thickness could reflect the relative

proximity between the site and a possibly distal ice margin (Cofaight and Dowdeswell, 2001; Pau and Hammer, 2016). An alternative solution is presence of a hiatus, it can further be speculated whether the meltwater periodically was funneled trough Leirdjupet under high discharge, causing erosion. Ruther et al. 2012 observed that every 12th couplet in Kveithola was thicker, and speculated whether the meltwater under tidal influence under extensive sea ice could have had an amplifying effect in such a narrow trough. The lack-reduced presence of IRD has been speculated to be associated with extensive seasonal-(semi) perennial sea ice, hampering iceberg drift (Aagaard-Sørensen et al., 2010; Junttila et al., 2010; Lucchi et al., 2013). Whereby the subsequent melting of the earlier icebergs episode exposed the sea surface for cooled surface water promoting sea ice formation (Kleiber et al., 2000).

The following IRD rich diamicton starting 14,400 cal yr BP represent a second pulse of enhanced calving from a destabilizing ice sheet in seasonally open water and a persistent subglacial meltwater in a glaciomarine environment. Similar units have been identified e.g. Ingøydjupet (Junttila et al., 2010; Aagaard-Sørensen et al., 2010, northern Barents Sea (Kleiber et al., 2000; Klitgaard-Kristensen et al., 2013), Kveithola (Rüther et al., 2012). Such conditions is inferred to represent destabilization of a nearby ice sheet as a response to the cumulating net sea level rise, enhanced solar insolation and increasing surface water temperatures (e.g. Kleiber et al., 2000; Aagaard-Sørensen et al., 2010). Despite the lithological similarities between the two IRD rich diamictons separated by the laminated unit are the foraminifera assemblage composition different. Increasing abundance of *I. norcrossi* concurrent with declining abundance of *E. excavatum* reflects the transition into more glacier distal environments, suggesting that the fresh cold bottom waters were gradually becoming more saline, as the meltwater influence decreased. Possibly indicating that Leirdjupet similar to Kveithola was fully by deglaciated by the end of laminated mwp-1a unit or during the early stages in the deposition of the diamicton unit sometime prior to ~14,350 cal yr BP (Rüther et

al., 2012; Bjarnadottir et al., 2013; Lucchi et al., 2013). The increasing abundance of *I. norcrossi* probably further reflects increasing inflow of chilled saline Atlantic Water.

As the IRD flux ceased ~14,315 cal yr BP, the Atlantic Water advection intensified leading to a higher benthic foraminifera flux from 14,315 cal yr BP. The faunal composition with high abundances of low temperature thriving species that includes *I. norcrossi*, *Buccella* spp., *E. excavatum* and *C. reniforme* probably reflects a cold Atlantic Water inflow (Steinsund, 1994). Rasmussen et al. (2007) suggested that the cold Atlantic Water advection in Storfjorden during Bølling-Allerød was a result of heat loss to the atmosphere and outpouring of the cold meltwater.

The bottom currents than weakened during the Allerød interstadial 14,00 cal yr BP, reflected in the predominance of mud and the gradually lower abundances of *C. lobatulus,* which further appear to have negatively affected the benthic foraminifera flux (Mackensen et al., 1985).

Younger Dryas (13,000-12,300 cal yr BP)

YD stadial was characterized by a rapid short term atmospheric temperature decrease, a halt in the deglaciation as evident from Greenland ice cores (Johnsen et al., 2001; Slubowska-Woldengen et al., 2007). High abundances of *E. excavatum* and *C. reniforme,* and increasing *S. loeblichi* abundance in a very scarce to almost barren foraminifera assemblage indicate that the bottom waters were cold, marking a return towards polar conditions, with an expanding sea ice cover, favorable conditions for the three opportunist species (Steinsund, 1994; Slubowska-Woldengen et al., 2008). The low flux of benthic foraminifera during the Younger Dryas are commonly related to a low primary production and dense brine water formation as an affect of the intensifying sea ice conditions (Rasmussen and Thomsen, 2015; Aagaard-Sørensen et al., 2010).

Similar peak in *E. excavatum* at the beginning of Younger appear to be widespread around the Barents Sea region in e.g.; Kveithola (Groot et al., 2014), Storfjorden (Rasmussen et al., 2007) and northern Svalbard (Slubowska et al., 2005).

The Atlantic Water advection abruptly ceased at the Younger Dryas inception, suggesting that the cold shift was related to the water masses, as the lithology remained unaffected. The low $\delta^{18}O$ values seen in the core (fig 7.6) during Younger Dryas has been associated with freshwater input (Rasmussen et al., 2007).

The abnormally low foraminifera flux during the period could be an effect of episodic dissolution due to presence of corrosive bottom waters (Rasmussen and Thomsen, 2015).

Enhanced sea ice covers during colder periods such as the Younger Dryas stadial, has been related higher corrosive brine water production, which could explain the three highly benthic foraminifera barren samples between 12,738-12,529 cal yr BP (Rasmussen and Thomsen, 2015). Occasional short term bottom water improvement, related to a reduced Atlantic Water advection appeared prior to and after the foraminifera barren interval ~12,738-12,529 cal yr BP, indicating that the Younger Dryas was not uniformly cold. The Younger Dryas characterized by an early stable cold period and a later period with alterations between Atlantic Water and sea ice (Rasmussen et al., 2007; Groot et al., 2014, Lacka et al. 2015). Similar faunas has also reported from e.g. Ingøydjupet (Aagaard-Sørensen et al., 2010), south eastern Barents Sea (Polyak and Mikhailov, 1996). The cause of the climate deterioration is still a topic of debate (e.g. Slubowska-Woldengen et al., 2007). The event is often linked up to the Lake Agassiz freshwater outburst, infiltrating e.g. Barents and Kara Sea, further instigated enhanced sea ice formation additionally to more locally meltwater (e.g. Patton et al., 2015; Lacka et al., 2015). The Atlantic thermohaline circulation underwent a weakening, consequently leading to a general cooling in the North Atlantic region (e.g. Ebbesen et al., 2007; Patton et al., 2015). Rasmussen et al., (2007) speculated whether the initiation of the

East Spitsbergen Current following the Barents Sea Ice Sheet retreat, was a contributing factor to the polar conditions in Storfjorden during the Younger Dryas.

Younger Dryas-Holocene transition: (12,300-11,800 cal yr BP)

The transition from the mud rich sediments into the reappearance of a glaciomarine IRD rich diamicton marks the transition phase from Younger Dryas into the Holocene, and the melting of the remaining ice sheet. Which coincides with increased influence of Atlantic Water as *C. neoteretis* and *M. barleeanus* reestablished during this period (Steinsund, 1994). The benthic foraminifera flux remained low, possibly as a consequence of turbid water.

Early Holocene (11,800-10,700 cal yr BP)

During the Early Holocene the Atlantic Water advection strengthened, which particularly evident by the higher *M. barleeanus* abundance (Steinsund, 1994).

9 SUMMARY

The early stages of Bølling were characterized high sedimentation rates by subglacial meltwater and melting calving icebergs. Large Atlantic Water Advection followed the period.

During the Younger Dryas stadial climate deterioration, polar bottom environment prevailed at the site. Characterized by low bottom water temperatures and salinities, with an extensive perennial- semi perennial sea ice cover.

The Younger Dryas-Holocene transition was characterized by a turbid environment, wit

10 REFRENCES

Aagaard, K., Foldvik, A., & Hillman, S. R. (1987). The West Spitsbergen Current: disposition and water mass transformation. *Journal of Geophysical Research: Oceans*, *92*(C4), 3778 3784.

Aagaard-Sørensen, S., Husum, K., Hald, M., & Knies, J. (2010). Paleoceanographic development in the SW Barents Sea during the late Weichselian–Early Holocene transition. *Quaternary Science Reviews*, *29*(25), 3442-3456.

Aagaard-Sørensen, S., Husum, K., Hald, M., Marchitto, T., & Godtliebsen, F. (2011). Atlantic Water influx in the Nordic Seas over the past 14.000 cal yr BP: Mg/Ca paleo temperature reconstructions

Anderson, J. B., Kennedy, D. S., Smith, M. J., & Domack, E. W. (1991). Sedimentary facies associated with Antarctica's floating ice masses.*Geological Society of America Special Papers*, *261*, 1-26.

Andreassen, K., Nilssen, L. C., Rafaelsen, B., & Kuilman, L. (2004). Three-dimensional seismic data from the Barents Sea margin reveal evidence of past ice streams and their dynamics. *Geology*, *32*(8), 729-732.

Andreassen, K., Ødegaard, C. M., & Rafaelsen, B. (2007). Imprints of former ice streams, imaged and interpreted using industry three-dimensional seismic data from the south-western Barents Sea. *Geological Society, London, Special Publications*, *277*(1), 151-169.

Andreassen, K., Laberg, J. S., & Vorren, T. O. (2008). Seafloor geomorphology of the SW

Barents Sea and its glaci-dynamic implications. *Geomorphology*,*97*(1), 157-177.

Armstrong, H. A., & Brasier, M. D. (2005). Foraminifera. *Microfossils, Second Edition*, 142-187.

Bard, E., Arnold, M., Mangerud, J., Paterne, M., Labeyrie, L., Duprat, J., ... & Duplessy, J. C. (1994). The North Atlantic atmosphere-sea surface 14 C gradient during the Younger Dryas climatic event. *Earth and Planetary Science Letters*, *126*(4), 275-287.

Barnes, P. W., & Lien, R. (1987). Icebergs rework sediments on Antarctic shelf.*Antarctic Journal of the United States*, *22*(5), 130-131..

Batchelor, C. L., & Dowdeswell, J. A. (2014). The physiography of High Arctic cross-shelf troughs. *Quaternary Science Reviews*, *92*, 68-96.

Bennett, M. R. (2003). Ice streams as the arteries of an ice sheet: their mechanics, stability and significance. *Earth-Science Reviews*, *61*(3), 309-339.

Berger, W. H., & Vincent, E. (1986). Deep-sea carbonates: reading the carbon-isotope signal. *Geologische Rundschau*, *75*(1), 249-269

Berben, S. M. P., Husum, K., Cabedo-Sanz, P., & Belt, S. T. (2014). Holocene sub-centennial evolution of Atlantic water inflow and sea ice distribution in the western Barents Sea. *Climate of the Past*, *10*(1), 181-198.

Bischof, J. F. (1994). The decay of the Barents ice sheet as documented in Nordic Seas icerafted debris. *Marine Geology*, *117*(1), 35-55.

Bjarnadóttir, L. R., Rüther, D. C., Winsborrow, M., & Andreassen, K. (2013). Grounding-line

dynamics during the last deglaciation of Kveithola, W Barents Sea, as revealed by seabed geomorphology and shallow seismic stratigraphy.*Boreas*, *42*(1), 84-107.

Bond, G., Broecker, W., Johnsen, S., McManus, J., Labeyrie, L., Jouzel, J., & Bonani, G. (1993). Correlations between climate records from North Atlantic sediments and Greenland ice. *Nature*, *365*(6442), 143-147.

Bondevik, S., Mangerud, J., Birks, H. H., Gulliksen, S., & Reimer, P. (2006). Changes in North Atlantic radiocarbon reservoir ages during the Allerød and Younger Dryas. *Science*, *312*(5779), 1514-1517.

Bowman, S. (1990). *Radiocarbon dating* (Vol. 1). Univ of California Press.

Buckley, D. E., MacKinnon, W. G., Cranston, R. E., & Christian, H. A. (1994). Problems with piston core sampling: Mechanical and geochemical diagnosis.*Marine Geology*, *117*(1), 95-106.

Butt, F. A., Drange, H., Elverhøi, A., Otterå, O. H., & Solheim, A. (2002). Modelling Late Cenozoic isostatic elevation changes in the Barents Sea and their implications for oceanic and climatic regimes: preliminary results.*Quaternary Science Reviews*, *21*(14), 1643-1660.

Caralp, M. H. (1989). Abundance ofBulimina exilis andMelonis barleeanum: Relationship to the quality of marine organic matter. *Geo-Marine Letters*, *9*(1), 37-43.

Chauhan, T., Noormets, R., & Rasmussen, T. L. (2016). Glaciomarine sedimentation and bottom current activity on the north-western and northern continental margins of Svalbard during the late Quaternary. *Geo-Marine Letters*,*36*(2), 81-99.

Chistyakova, N. O., Ivanova, E. V., Risebrobakken, B., Ovsepyan, E. A., & Ovsepyan, Y. S. (2010). Reconstruction of the postglacial environments in the southwestern Barents Sea based on foraminiferal assemblages. *Oceanology*,*50*(4), 573-581.

Cofaigh, C. Ó., & Dowdeswell, J. A. (2001). Laminated sediments in glacimarine environments: diagnostic criteria for their interpretation. *Quaternary Science Reviews*, *20*(13), 1411-1436.

Cofaigh, C. Ó., Dowdeswell, J. A., Evans, J., & Larter, R. D. (2008). Geological constraints on Antarctic palaeo-ice-stream retreat. *Earth Surface Processes and Landforms*, *33*(4), 513-525.

Deschamps, P., Durand, N., Bard, E., Hamelin, B., Camoin, G., Thomas, A. L., ... & Yokoyama, Y. (2012). Ice-sheet collapse and sea-level rise at the Bolling warming 14,600 [thinsp] years ago. *Nature*, *483*(7391), 559-564.

Duplessy, J. C., Moyes, J., & Pujol, C. (1980). Deep water formation in the North Atlantic Ocean during the last ice age.

Duplessy, J. C., Shackleton, N. J., Matthews, R. K., Prell, W., Ruddiman, W. F., Caralp, M., & Hendy, C. H. (1984). 13C record of benthic foraminifera in the last interglacial ocean: implications for the carbon cycle and the global deep water circulation. *Quaternary Research*, *21*(2), 225-243.

Duplessy, J. C., Cortijo, E., Ivanova, E., Khusid, T., Labeyrie, L., Levitan, M., & Paterne, M. (2005). Paleoceanography of the Barents Sea during the Holocene. *Paleoceanography*, *20*(4).

Ebbesen, H., Hald, M., & Eplet, T. H. (2007). Lateglacial and early Holocene climatic oscillations on the western Svalbard margin, European Arctic.*Quaternary Science Reviews*, *26*(15), 1999-2011.

Eldevik, T., Risebrobakken, B., Bjune, A. E., Andersson, C., Birks, H. J. B., Dokken, T. M., & Otterå, O. H. (2014). A brief history of climate–the northern seas from the Last Glacial Maximum to global warming. *Quaternary Science Reviews*, *106*, 225-246.

Elverhøi, A., and Kristoffersen, Y. (1978a). Holocene sedimentation on the shelf around Bjørnøya, north-western part of the Barents Sea. *Nor. Polarinst., Årbok, 1977, pp. 200-207*

Elverhøi, A., and Kristoffersen, Y., (1978b). Glacial deposits southeast of Bjørnøya, NW Barents Sea. Nor. Polarinst. Årbok 1977, pp. 209-215.

Elverhøi, A., & Solheim, A. (1983). The Barents Sea ice sheet-a sedimentological discussion. *Polar Research*, *1*(1), 23-42.

Elverhøi, A., Fjeldskaar, W., Solheim, A., Nyland-Berg, M., & Russwurm, L. (1993). The Barents Sea Ice Sheet—a model of its growth and decay during the last ice maximum. *Quaternary Science Reviews*, *12*(10), 863-873.¨

Elverhøi, A., Hooke, R. L., & Solheim, A. (1998). Late Cenozoic erosion and sediment yield from the Svalbard–Barents Sea region: Implications for understanding erosion of glacierized basins. *Quaternary Science Reviews*,*17*(1), 209-241.

Fairbanks, R. G. (1989). A 17, 000-year glacio-eustatic sea level record: influence of glacial melting rates on the Younger Dryas event and deep-ocean circulation. *Nature*, *342*(6250),

637-642.

Feyling-Hanssen, R. W. (1971). Weichselian interstadial Foraminifera from the Sandnes-Jaeren area. *Bulletin of the Geological Society of Denmark*, *21*, 72-116.

Faleide, J. I., Vågnes, E., & Gudlaugsson, S. T. (1993). Late Mesozoic-Cenozoic evolution of the south-western Barents Sea in a regional rift-shear tectonic setting. *Marine and Petroleum Geology*, *10*(3), 186-214.

Feyling-Hanssen, R. W. (1972). The foraminifer Elphidium excavatum (Terquem) and its variant forms. *Micropaleontology*, 337-354

Flückiger, J., Knutti, R., & White, J. W. (2006). Oceanic processes as potential trigger and amplifying mechanisms for Heinrich events. *Paleoceanography*,*21*(2).

Godwin, H. (1962). Half-life of radiocarbon. *Nature*, *195*.

Grossman, E. L. (1987). Stable isotopes in modern benthic foraminifera; a study of vital effect. *The Journal of Foraminiferal Research*, *17*(1), 48-61.

Gawarkiewicz, G., & Plueddemann, A. J. (1995). Topographic control of thermohaline frontal structure in the Barents Sea Polar Front on the south flank of Spitsbergen Bank. *Journal of Geophysical Research: Oceans*, *100*(C3), 4509-4524.

Hald, M., Ebbesen, H., Forwick, M., Godtliebsen, F., Khomenko, L., Korsun, S., & Vorren, T. O. (2004). Holocene paleoceanography and glacial history of the West Spitsbergen area, Euro-Arctic margin. *Quaternary Science Reviews*,*23*(20), 2075-2088.

Hald, M., & Vorren, T. O. (1987). Foraminiferal stratigraphy and environment of Late

Weichselian deposits on the continental shelf off Troms, Northern Norway.*Marine Micropaleontology*, *12*, 129-160.

Hald, M., Danielsen, T. K., & Lorentzen, S. (1989). Late Pleistocene-Holocene benthic foraminiferal distribution in the southwestern Barents Sea: Paleoenvironmental implications. *Boreas*, *18*(4), 367-388.

Hald, M., Sættem, J., & Nesse, E. (1990). Middle and Late Weichselian stratigraphy in shallow drillings from the southwestern Barents Sea: foraminiferal, amino acid and radiocarbon evidence.*Norsk Geologisk Tidsskrift*, *70*(4), 241-257.

Hald, M., & Steinsund, P. I. (1992). Distribution of surface sediment benthic foraminifera in the southwestern Barents Sea. *The Journal of Foraminiferal Research*, *22*(4), 347-362.

HALD, M., & ASPELI, R. (1997). Rapid climatic shifts of the northern Norwegian Sea during the last deglaciation and the Holocene. *Boreas*, *26*(1), 15-28.

Hald, M., & Korsun, S. (1997). Distribution of modern benthic foraminifera from fjords of Svalhard, European Arctic. *Journal of Foraminiferal Research*, *27*, 101-122.

Hald, M., Andersson, C., Ebbesen, H., Jansen, E., Klitgaard-Kristensen, D., Risebrobakken, B., ... & Telford, R. J. (2007). Variations in temperature and extent of Atlantic Water in the northern North Atlantic during the Holocene.*Quaternary Science Reviews*, *26*(25), 3423-3440.

Harris, C. L., Plueddemann, A. J., & Gawarkiewicz, G. G. (1998). Water mass distribution and polar front structure in the western Barents Sea. *Journal of Geophysical Research:*

Oceans, *103*(C2), 2905-2917.

Hebbeln, D., Dokken, T., Andersen, E. S., Hald, M., & Elverhøi, A. (1994). Moisture supply for northern ice-sheet growth during the Last Glacial Maximum.

Henrich, R. (1997). Evolution of an Arctic open-shelf carbonate platform, Spitsbergen Bank (Barent Sea)

Holtedahl, H., & Bjerkli, K. (1982). Late Quaternary sediments and stratigraphy on the continental shelf off Møre-Trøndelag, W. Norway. *Marine Geology*, *45*(3-4), 179205-202226.

Hormes, A., Gjermundsen, E. F., & Rasmussen, T. L. (2013). From mountain top to the deep sea–Deglaciation in 4D of the northwestern Barents Sea ice sheet. *Quaternary Science Reviews*, *75*, 78-99.

Jakobsson, M., Mayer, L., Coakley, B., Dowdeswell, J. A., Forbes, S., Fridman, B., ... & Schenke, H. W. (2012). The international bathymetric chart of the Arctic Ocean (IBCAO) version 3.0. *Geophysical Research Letters*,*39*(12).

Ingvaldsen, R. B., Asplin, L., & Loeng, H. (2004). The seasonal cycle in the Atlantic transport to the Barents Sea during the years 1997–2001. *Continental Shelf Research*, *24*(9), 1015-1032.

Ingvaldsen, R. B. (2005). Width of the North Cape Current and location of the Polar Front in the western Barents Sea. *Geophysical Research Letters*, *32*(16).

Ivanova, E. V., Ovsepyan, E. A., Risebrobakken, B., & Vetrov, A. A. (2008). Downcore distribution of living calcareous foraminifera and stable isotopes in

the western Barents Sea. *The Journal of Foraminiferal Research*, *38*(4), 337-356.

Jennings, A. E., Weiner, N. J., Helgadottir, G., & Andrews, J. T. (2004). Modern foraminiferal faunas of the southwestern to northern Iceland shelf: oceanographic and environmental controls. *The Journal of Foraminiferal Research*, *34*(3), 180-207.

Jessen, S. P., Rasmussen, T. L., Nielsen, T., & Solheim, A. (2010). A new Late Weichselian and Holocene marine chronology for the western Svalbard slope 30,000–0 cal years BP. *Quaternary Science Reviews*, *29*(9), 1301-1312.

Johnsen, S. J., Dahl-Jensen, D., Gundestrup, N., Steffensen, J. P., Clausen, H. B., Miller, H., & White, J. (2001). Oxygen isotope and palaeotemperature records from six Greenland icecore stations: Camp Century, Dye-3, GRIP, GISP2, Renland and NorthGRIP. *Journal of Quaternary Science*, *16*(4), 299-307.

Jorissen, F. J., de Stigter, H. C., & Widmark, J. G. (1995). A conceptual model explaining benthic foraminiferal microhabitats. *Marine Micropaleontology*, *26*(1), 3-15.

Junttila, J., Aagaard-Sørensen, S., Husum, K., & Hald, M. (2010). Late Glacial–Holocene clay minerals elucidating glacial history in the SW Barents Sea. *Marine Geology*, *276*(1), 71-85.

Kleiber, H. P., Knies, J., & Niessen, F. (2000). The Late Weichselian glaciation of the Franz

Victoria Trough, northern Barents Sea: ice sheet extent and timing. *Marine Geology*, *168*(1), 25-44.

Kovalenko, B. (2015). Palaeoceanographic development in Leirdjupet Trough, western Barents Sea, during the Holocene: evidence from foraminiferal, isotopic and sedimentological records. Unpublished MSc thesis, University of Tromsø.

Korsun, S. A., Pogodina, I. A., Forman, S. L., & Lubinski, D. J. (1995). Recent foraminifera in glaciomarine sediments from three arctic fjords of Novaja Zemlja and Svalbard. *Polar Research*, *14*(1), 15-32.

Korsun, S., & Hald, M. (2000). Seasonal dynamics of benthic foraminifera in a glacially fed fjord of Svalbard, European Arctic. *The Journal of Foraminiferal Research*, *30*(4), 251-271.

Kristensen, D. K., Rasmussen, T. L., & Koç, N. (2013). Palaeoceanographic changes in the northern Barents Sea during the last 16 000 years–new constraints on the last deglaciation of the Svalbard–Barents Sea Ice Sheet.*Boreas*, *42*(3), 798-813.

Kubischta, F., Knudsen, K. L., & Salonen, V. P. (2010). Late Quaternary foraminiferal assemblages as a tool to reconstruct the fjord environment of Murchisonfjorden, Nordaustlandet, Svalbard. In *FORAMS 2010, International Symposium on Foraminifera*.

Laberg, J. S., & Vorren, T. O. (1996). The middle and late pleistocence evolution and the bear island trough mouth fan. *Global and Planetary Change*,*12*(1), 309-330.

Laberg, J. S., Andreassen, K., & Vorren, T. O. (2012). Late Cenozoic erosion of the highlatitude southwestern Barents Sea shelf revisited. *Geological Society of America Bulletin*, *124*(1-2), 77-88.

Łącka, M., Zajączkowski, M., Forwick, M., & Szczuciński, W. (2015). Late Weichselian and Holocene palaeoceanography of Storfjordrenna, southern Svalbard.

Landvik, J. Y., Bondevik, S., Elverhøi, A., Fjeldskaar, W., Mangerud, J. A. N., Salvigsen, O., & Vorren, T. O. (1998). The last glacial maximum of Svalbard and the Barents Sea area: ice sheet extent and configuration. *Quaternary Science Reviews*, *17*(1), 43-75.

Linke, P., & Lutze, G. F. (1993). Microhabitat preferences of benthic foraminifera—a static concept or a dynamic adaptation to optimize food acquisition?. *Marine Micropaleontology*, *20*(3-4), 215-234.

Knies, J., Matthiessen, J., Vogt, C., Laberg, J. S., Hjelstuen, B. O., Smelror, M., ... & Vorren, T. O. (2009). The Plio-Pleistocene glaciation of the Barents Sea–Svalbard region: a new model based on revised chronostratigraphy.*Quaternary Science Reviews*, *28*(9), 812-829.

Lucchi, R. G., Camerlenghi, A., Rebesco, M., Colmenero-Hidalgo, E., Sierro, F. J., Sagnotti, L., & Giorgetti, G. (2013). Postglacial sedimentary processes on the Storfjorden and Kveithola trough mouth fans: Significance of extreme glacimarine sedimentation. *Global and planetary change*, *111*, 309-326.

Larsen, E., Andreassen, K., Nilssen, L., & Raundalen, S. (2003). The prospectivity of the Barents Sea: ice ages, erosion and tilting of traps. *NGU Report*, *102*.

Loeng, H. (1991). Features of the physical oceanographic conditions of the Barents Sea. *Polar research*, *10*(1), 5-18.

Lowe, D., & Walker, M. (1997). Reconstructing Quaternary Enviroment. 2rd ed. Oxon: Routledge.

Lubinski, D. J., Polyak, L., & Forman, S. L. (2001). Freshwater and Atlantic water inflows to the deep northern Barents and Kara seas since ca 13 14 Cka:: foraminifera and stable isotopes. *Quaternary Science Reviews*, *20*(18), 1851-1879.

Lucchi, R. G., Camerlenghi, A., Rebesco, M., Colmenero-Hidalgo, E., Sierro, F. J., Sagnotti, L., & Giorgetti, G. (2013). Postglacial sedimentary processes on the Storfjorden and Kveithola trough mouth fans: Significance of extreme glacimarine sedimentation. *Global and planetary change*, *111*, 309-326.

Lucchi, R. G., Sagnotti, L., Camerlenghi, A., Macrì, P., Rebesco, M., Pedrosa, M. T., & Giorgetti, G. (2015). Marine sedimentary record of Meltwater Pulse 1a along the NW Barents Sea continental margin. *arktos*, *1*(1), 1-14.

Lunne, T., & Long, M. (2006). Review of long seabed samplers and criteria for new sampler design. *Marine Geology*, *226*(1), 145-165.

Mackensen, A., Sejrup, H. P., & Jansen, E. (1985). The distribution of living benthic foraminifera on the continental slope and rise off southwest Norway.*Marine Micropaleontology*, *9*(4), 275-306.

Mangerud, J., Bondevik, S., Gulliksen, S., Hufthammer, A. K., & Høisæter, T. (2006). Marine

14 C reservoir ages for 19th century whales and molluscs from the North Atlantic. *Quaternary Science Reviews*, *25*(23), 3228-3245.

Maslowski, W., Marble, D., Walczowski, W., Schauer, U., Clement, J. L., & Semtner, A. J. (2004). On climatological mass, heat, and salt transports through the Barents Sea and Fram Strait from a pan-Arctic coupled ice-ocean model simulation. *Journal of Geophysical Research: Oceans*, *109*(C3).

Midttun, L. (1989). Climatic fluctuations in the Barents Sea. *Rapports et Proces-Verbaux des Reunions du Conseil International pour*, *1*, 23-35.

Ottesen, D., & Dowdeswell, J. A. (2009). An inter–ice-stream glaciated margin: Submarine landforms and a geomorphic model based on marine-geophysical data from Svalbard. *Geological Society of America Bulletin*, *121*(11-12), 1647-1665.

Parsons, A. R., Bourke, R. H., Muench, R. D., Chiu, C. S., Lynch, J. F., Miller, J. H., & Pawlowicz, R. (1996). The Barents Sea polar front in summer.*Journal of Geophysical Research: Oceans*, *101*(C6), 14201-14221.

Patton, H., Andreassen, K., Bjarnadóttir, L. R., Dowdeswell, J. A., Winsborrow, M., Noormets, R., ... & Hubbard, A. (2015). Geophysical constraints on the dynamics and retreat of the Barents Sea ice sheet as a paleobenchmark for models of marine ice sheet deglaciation. *Reviews of Geophysics*, *53*(4), 1051-1098.

Pau, M., Hammer, Ø., & Chand, S. (2014). Constraints on the dynamics of pockmarks in the SW Barents Sea: evidence from gravity coring and high-resolution, shallow seismic

profiles. *Marine Geology*, *355*, 330-345.

Pau, M., & Hammer, Ø. (2016). Sedimentary environments in the south-western Barents Sea during the last deglaciation and the Holocene: a case study outside the Ingøydjupet trough. *Polar Research*, *35*.

Pfirman, S. L., Bauch, D., & Gammelsrød, T. (1994). The northern Barents Sea: water mass distribution and modification. *The polar oceans and their role in shaping the global environment*, 77-94.

Polyak, L., & Mikhailov, V. (1996). Post-glacial environments of the southeastern Barents Sea: foraminiferal evidence. *Geological Society, London, Special Publications*, *111*(1), 323-337.

Polyak, L., Korsun, S., Febo, L. A., Stanovoy, V., Khusid, T., Hald, M., ... & Lubinski, D. (2002). Benthic foraminiferal assemblages from the southern Kara Sea, a river-influenced Arctic marine environment. *The Journal of Foraminiferal Research*, *32*(3), 252-273.

Polyak, L., Best, K. M., Crawford, K. A., Council, E. A., & St-Onge, G. (2013). Quaternary history of sea ice in the western Arctic Ocean based on foraminifera. *Quaternary Science Reviews*, *79*, 145-156.

Rasmussen, T. L., Thomsen, E., Ślubowska, M. A., Jessen, S., Solheim, A., & Koç, N. (2007). Paleoceanographic evolution of the SW Svalbard margin (76 N) since 20,000 14 C yr BP. *Quaternary Research*, *67*(1), 100-114.

Rasmussen, T. L., & Thomsen, E. (2015). Palaeoceanographic development in Storfjorden, Svalbard, during the deglaciation and Holocene: evidence from benthic foraminiferal records. *Boreas*, *44*(1), 24-44.

Rebesco, M., Liu, Y., Camerlenghi, A., Winsborrow, M., Laberg, J. S., Caburlotto, A., ... & Tomini, I. (2011). Deglaciation of the western margin of the Barents Sea Ice Sheet—a swath bathymetric and sub-bottom seismic study from the Kveithola Trough. *Marine Geology*, *279*(1), 141-147.

Reimer, P. J. et al., 2013. Intcall113 and MARINE13 radiocarbon age calibration curves 0-50000 years calBP. Radiocarbon, Volume 55 (4), p. DOI:10.2458/azy_js_rc.55.16947.

Risebrobakken, B., Moros, M., Ivanova, E. V., Chistyakova, N., & Rosenberg, R. (2010). Climate and oceanographic variability in the SW Barents Sea during the Holocene. *The Holocene*.

Robinson, S. G. (1986). The late Pleistocene palaeoclimatic record of North Atlantic deep-sea sediments revealed by mineral-magnetic measurements.*Physics of the Earth and Planetary Interiors*, *42*(1), 22-47.

Rodrigues, C. G., Hooper, K., & Jones, P. C. (1980). The apertural structures of Islandiella and Cassidulina. *The Journal of Foraminiferal Research*, *10*(1), 48-60.

Rüther, D. C., Bjarnadóttir, L. R., Junttila, J., Husum, K., Rasmussen, T. L., Lucchi, R. G., & Andreassen, K. (2012). Pattern and timing of the northwestern Barents Sea Ice Sheet deglaciation and indications of episodic Holocene

deposition. *Boreas*, *41*(3), 494-512.

Sarnthein, M. (2011). Northern meltwater pulses, CO2, and changes in Atlantic convection. *Science*, *331*(6014), 156-158.

Seidenkrantz, M. S. (2013). Benthic foraminifera as palaeo sea-ice indicators in the subarctic realm–examples from the Labrador Sea–Baffin Bay region.*Quaternary Science Reviews*, *79*, 135-144.

Sejrup, H. P., Birks, H. J. B., Kristensen, D. K., & Madsen, H. (2004). Benthonic foraminiferal distributions and quantitative transfer functions for the northwest European continental margin. *Marine Micropaleontology*, *53*(1), 197-226.

Sejrup, H. P., Fjaeran, T., Hald, M., Beck, L., Hagen, J., Miljeteig, I., ... & Norvik, O. (1981). Benthonic foraminifera in surface samples from the Norwegian continental margin between 62 degrees N and 65 degrees N. *The Journal of Foraminiferal Research*, *11*(4), 277-295.

Shackleton, N. J., & Pisias, N. G. (1985). Atmospheric carbon dioxide, orbital forcing, and climate. *The Carbon Cycle and Atmospheric CO: Natural variations Archean to Present*, 303-317.

Siegert, M. J., & Dowdeswell, J. A. (2004). Numerical reconstructions of the Eurasian Ice Sheet and climate during the Late Weichselian. *Quaternary Science Reviews*, *23*(11), 1273-1283.

Ślubowska, M. A., Koç, N., Rasmussen, T. L., & Klitgaard-Kristensen, D.

(2005). Changes in the flow of Atlantic water into the Arctic Ocean since the last deglaciation: evidence from the northern Svalbard continental margin, 80 N. *Paleoceanography*, *20*(4).

Ślubowska-Woldengen, M., Rasmussen, T. L., Koc, N., Klitgaard-Kristensen, D., Nilsen, F., & Solheim, A. (2007). Advection of Atlantic Water to the western and northern Svalbard shelf since 17,500 calyr BP. *Quaternary Science Reviews*, *26*(3), 463-478.

Ślubowska-Woldengen, M., Koç, N., Rasmussen, T. L., Klitgaard-Kristensen, D., Hald, M., & Jennings, A. E. (2008). Time-slice reconstructions of ocean circulation changes on the continental shelf in the Nordic and Barents Seas during the last 16,000 cal yr BP. *Quaternary Science Reviews*, *27*(15), 1476-1492.

Smedsrud, L. H., Esau, I., Ingvaldsen, R. B., Eldevik, T., Haugan, P. M., Li, C., & Risebrobakken, B. (2013). The role of the Barents Sea in the Arctic climate system. *Reviews of Geophysics*, *51*(3), 415-449.

Spielhagen, R. F., Bonani, G., Eisenhauer, A., Frank, M., Frederichs, T., Kassens, H., & Schäper, S. (1997). Arctic Ocean evidence for late Quaternary initiation of northern Eurasian ice sheets. *Geology*, *25*(9), 783-786.

Steinsund, P. I. (1994). Benthic foraminifera in surface sediments of the Barents and Kara seas: modern and late Quaternary applications. *Unpublished PhD Thesis, University of Tromsø*.

Stuvier, M. & Reimer, P. J., 1993. Radiocarbon. Volume 35, pp. 215-230.

Svendsen, J. I., Elverhøi, A., & Mangerud, J. (1996). The retreat of the Barents Sea Ice Sheet on the western Svalbard margin. *Boreas*, *25*(4), 244-256.

Van der Zwaan, G. J., Duijnstee, I. A. P., Den Dulk, M., Ernst, S. R., Jannink, N. T., & Kouwenhoven, T. J. (1999). Benthic foraminifers: proxies or problems?: a review of paleocological concepts. *Earth-Science Reviews*, *46*(1), 213-236.

Vassmyr, S. T. I. G., & Vorren, T. O. (1990). Clast petrography and stratigraphy in Late Quaternary sediments in the southwestern Barents Sea. *Norsk Geologisk Tidsskrift*, *70*(2), 95-110.

Vogt, C., & Knies, J. (2009). Sediment pathways in the western Barents Sea inferred from clay mineral assemblages in surface sediments. *Norwegian Journal of Geology*, *89*, 41-55.

Vorren, T. O., & Kristoffersen, Y. (1986). Late Quaternary glaciation in the south-western Barents Sea. *Boreas*, *15*(1), 51-59.

Vorren, T. O., & Laberg, J. S. (1997). Trough mouth fans—palaeoclimate and ice-sheet monitors. *Quaternary Science Reviews*, *16*(8), 865-881.

Weaver, A. J., Saenko, O. A., Clark, P. U., & Mitrovica, J. X. (2003). Meltwater pulse 1A from Antarctica as a trigger of the Bølling-Allerød warm interval.*Science*, *299*(5613), 1709 1713.

Winsborrow, M. C., Andreassen, K., Corner, G. D., & Laberg, J. S. (2010). Deglaciation of a marine-based ice sheet: Late Weichselian palaeo-ice dynamics and retreat in the southern

Barents Sea reconstructed from onshore and offshore glacial geomorphology. *Quaternary Science Reviews*, *29*(3), 424-442.

Williamson, M. A., Keen, C. E., & Mudie, P. J. (1984). Foraminiferal distribution on the continental margin off Nova Scotia. *Marine Micropaleontology*, *9*(3), 219-239.

Wilson, L. J., Hald, M., & Godtliebsen, F. (2011). Foraminiferal faunal evidence of twentiethcentury Barents Sea warming. *The Holocene*, *21*(4), 527-537.

Wollenburg, J. E., & Mackensen, A. (1998). Living benthic foraminifers from the central Arctic Ocean: faunal composition, standing stock and diversity.*Marine Micropaleontology*, *34*(3), 153-185.

Wright, P. L. (1974). Recent sediments of the southwestern Barents Sea.*Marine Geology*, *16*(2), 51-81.

Zajączkowski, M., Szczuciński, W., Plessen, B., & Jernas, P. (2010). Benthic foraminifera in Hornsund, Svalbard: Implications for paleoenvironmental reconstructions. *Polish Polar Research*, *31*(4), 349-375.

Zwally, H. J., Abdalati, W., Herring, T., Larson, K., Saba, J., & Steffen, K. (2002). Surface melt-induced acceleration of Greenland ice-sheet flow.*Science*, *297*(5579), 218-222.

Ådlandsvik, B., & Loeng, H. (1991). A study of the climatic system in the Barents Sea. *Polar Research*, *10*(1), 45-50.